5-1-2009

Sliding mode control applied to an underactuated fuel cell system

Daniel C. DiFiore

Sliding Mode Control Applied to an Underactuated Fuel Cell System

By

Daniel C. DiFiore

A Thesis Submitted in Partial Fulfillment of the Requirements
for Master of Science in Mechanical Engineering

Approved by:

Dr. Agamemnon Crassidis - *Thesis Advisor* _____
Department of Mechanical Engineering

Dr. Jason Kolodziej _____
Department of Mechanical Engineering

Dr. Tuhin Das _____
Department of Mechanical Engineering

Dr. Edward Hensel _____
Department Head of Mechanical Engineering

Department of Mechanical Engineering
Rochester Institute of Technology
Rochester, New York 14623

May 2009

PERMISSION TO REPRODUCE THE THESIS

Sliding Mode Control Applied to an Underactuated Fuel Cell System

I, Daniel DiFiore, hereby grant permission to the Wallace Memorial Library of Rochester Institute of Technology to reproduce my thesis in the whole or part. Any reproduction will not be for commercial use or profit.

Date: _____ Signature: _____

May 2009

Acknowledgements

I would like to thank Dr. Agamemnon Crassidis for his advice and guidance throughout this research process. Also, I would like to thank Dr. Jason Kolodziej and Dr. Tuhin Das for their support and questions. Finally, I would like to thank my family and particularly my wife, Kate, for her continued support and encouragement.

Abstract

In this work, a method for controlling a nonlinear underactuated system using augmented sliding mode control (SMC) is proposed. SMC requires inversion of the input influence matrix to derive the desired control law. In under or over actuated systems this matrix is nonsquare therefore a true inverse does not exist. The proposed control approach demonstrated in this work involves introducing a transformation matrix mapping the systems input influence matrix to a transformed system that is square and thus invertible. The proposed approach is shown to control selectable states with proper choice of the transformation matrix yielding good control performance. The methodology is applied to an underactuated nonlinear fuel cell system to show its viability in a real world application. A sliding mode controller is derived for the full nonlinear system with a switching gain accounting for modeling errors and uncertainties. Simulation results indicate the viability of the proposed control law and demonstrate the robust nature of the control law in the presence of significant modeling errors while maintaining tracking stability. Finally, the augmented SMC is compared to a traditional linear control architecture illustrating the effectiveness and advantages in tracking performance and control effort over traditional methods.

Contents

Acknowledgements **ii**

Abstract **iii**

Table of Contents **v**

List of Figures **vii**

List of Tables **viii**

Nomenclature **ix**

1 Introduction **1**
1.1 Background 1
1.2 Current Work 2
1.3 Overview 3

2 Theoretical Development **5**
Preface 5
2.1 Lyapunov's Direct Method 5
2.2 Scalar Sliding Mode Control 9
2.3 Multiple Input, Multiple Output Sliding Mode Control 11

3 Anode Fuel Cell Model **18**
Preface 18
3.1 Pressure Model 19
3.2 Nitrogen Model 23
3.3 Matrix Form 25

4 SMC Applied to the Fuel Cell Model **26**
Preface 26
4.1 Applied Sliding Mode Controller 26
4.2 Handling Modeling Uncertainties 27

5 Results **32**
5.1 Choice of Transformation Matrix 32
5.2 SMC with Sign Function 34
5.2.1 Varying **T** with a Perfect Plant Model 34
5.2.2 Varying Plant Parameters 41
5.3 SMC with Saturation Function 48
5.3.1 Tracking Comparision 49
5.3.2 Control Effort Comparison 55
5.3.3 Evaluating Discrete Effects 56
5.3.4 Robustness to Sensor Noise 63
5.4 Comparing SMC and PI Control 66

6 Conclusion **73**
6.1 Conclusion 73
6.2 Recommendations 74

Bibliography **77**

A Matlab Code **78**

B Simulink Diagrams **83**

List of Figures

2.1 Concept of Nonlinear System Stability 6
2.2 Example of a Positive Definite Function 8
2.3 MIMO SMC Algorithm Structure 11

3.1 Anode System Mechanization 19
3.2 Lumped System Flow Diagram 20
3.3 Saturation Pressure Curve Fit using Equation 3.4 21

4.1 Example of Local Maximum 29

5.1 Tracking Performance for $\mathbf{T} = [1 \quad -1]$ and $\Delta_p = 0.5$ 35
5.2 K Term for $\mathbf{T} = [1 \quad -1]$ and $\Delta_p = 0.5$ 36
5.3 y Tracking for $\mathbf{T} = [1 \quad -1]$ and $\Delta_p = 0.5$ 37
5.4 Tracking Performance for $\mathbf{T} = [1 \quad -1000000]$ and $\Delta_p = 0.5$ 38
5.5 K Term for $\mathbf{T} = [1 \quad -1000000]$ and $\Delta_p = 0.5$ 39
5.6 Tracking Performance for $\mathbf{T} = [1 \quad -6000]$ and $\Delta_p = 0.5$ 40
5.7 Effect of Varying $\mathbf{T}$ on System Response 42
5.8 Tracking Performance for $\mathbf{T} = [1 \quad -1]$ and $\Delta_p = 0$ 44
5.9 Tracking Performance for $\mathbf{T} = [1 \quad -1000000]$ and $\Delta_p = 0$ 45
5.10 Tracking Performance for $\mathbf{T} = [1 \quad -1]$ and $\Delta_p = 1$ 46
5.11 Tracking Performance for $\mathbf{T} = [1 \quad -1000000]$ and $\Delta_p = 1$ 47
5.12 Effect of Varying $\mathbf{T}$ on System Response 48
5.13 Saturation Tracking Performance for $\mathbf{T} = [1 \quad -1]$ and $\Delta_p = 0$ 50
5.14 Saturation Tracking Performance for $\mathbf{T} = [1 \quad -1000000]$ and $\Delta_p = 0$ . . 51
5.15 Saturation Tracking Performance for $\mathbf{T} = [1 \quad -1]$ and $\Delta_p = 1$ 52
5.16 Saturation Tracking Performance for $\mathbf{T} = [1 \quad -1000000]$ and $\Delta_p = 1$ . . 53
5.17 Effect of Varying $\mathbf{T}$ on System Response With Saturation Function . . . 54
5.18 K Term with Sat Function $\mathbf{T} = [1 \quad -1000000]$ and $\Delta_p = 0.5$ 55
5.19 K Term with Sat Function $\mathbf{T} = [1 \quad -1000000]$ and $\Delta_p = 0$ 56
5.20 K Term with Sat Function $\mathbf{T} = [1 \quad -1000000]$ and $\Delta_p = 1$ 57
5.21 K Term with Sat Function $\mathbf{T} = [1 \quad -1]$ and $\Delta_p = 0$ 57
5.22 Tracking Performance for $\mathbf{T} = [1 \quad -1]$, $\Delta_p = 1$ and a 10ms Zero Order Hold 58

5.23 Tracking Performance for $\mathbf{T} = [1 \quad -1]$, $\Delta_p = 1$ and a 50ms Zero Order Hold 59
5.24 Tracking Performance for $\mathbf{T} = [1 \quad -1000000]$, $\Delta_p = 1$ and a 50ms Zero Order Hold 60
5.25 Tracking Performance for $\mathbf{T} = [1 \quad -1]$, $\Delta_p = 1$ and a 20ms Zero Order Hold 61
5.26 Tracking Performance for $\mathbf{T} = [1 \quad -1000000]$, $\Delta_p = 1$ and a 10ms Zero Order Hold 62
5.27 Tracking Performance for $\mathbf{T} = [1 \quad -1]$, $\Delta_p = 1$ and Sensor Noise 63
5.28 Tracking Performance for $\mathbf{T} = [1 \quad -1000000]$, $\Delta_p = 1$ and Sensor Noise 64
5.29 Tracking Performance for $\mathbf{T} = [1 \quad -1]$, $\Delta_p = 0$ and Sensor Noise 65
5.30 Pressure Control Comparision 68
5.31 Nitrogen Control Comparision 69
5.32 Tracking Performance for $\mathbf{T} = [1 \quad -1]$, $\Delta_p = 0$ and a Step Input 70
5.33 Pressure Control Comparision with Step Input 71
5.34 Nitrogen Control Comparision with Step Input 72

B.1 PI Block Diagram 83
B.2 Top Level Model 84
B.3 Desired Tracking Block 85
B.4 Simulink Representation of Nonlinear Terms 86
B.5 Plant Model Block Diagram 86
B.6 SMC Block Diagram 87
B.7 Robustness Term Block Diagram 87

List of Tables

5.1 Tested Operating Points 34
5.2 Tested Operating Points with Modeling Error 43
5.3 Upper and Lower Bounds 67
5.4 Tested Cases with Gains 67

Nomenclature

t	Time
$\mathbf{x}$	System State
λ	Positive Constant
$\mathbf{V}$	Lyapunov Function
$\mathbf{B}$	Input Influence Matrix
$\mathbf{u}$	Control Inputs
$\mathbf{f}$	Nonlinear System Dynamics
$\hat{}$	Best Approximation
$\mathbf{s}$	Sliding Surface
$\tilde{\mathbf{x}}$	Tracking Error
$\mathbf{y}$	Mapping Function
$\mathbf{x_d}$	Desired State Value
$\mathbf{T}$	Transformation Matrix
$\mathbf{K}$	SMC Robustness Term
sgn	Signum Function
η	Small Positive Constant
$\mathbf{I}$	Idenitiy Matrix and Current in Amps
$\tilde{\mathbf{f}}$	Modeling Error in System Dynamics
$\mathbf{\Delta}$	Upper Bound Limit of the Uncertainties in $\mathbf{B}$
sat	Saturation Function
ϕ	Boundary Layer
n	Number of moles
P	Pressure in kPa
$_{AN}$	Anode Subsystem
$_{Ca}$	Cathode Subsystem

T	Temperature
V	Volume
N_2	Nitrogen
H_2	Hydrogen
H_2O	Water
R	Universal Gas Constant
H	Nitrogen Permeation Rate
pp	Partial Pressure
$\dot{m}_{max}$	Maximum Mass Flow Through the Injector
DC	Injector Duty Cycle
M_W	Molecular Weight
RH	Relative Humidity
A_{eff}	Injector Effective Area
K	Ratio of Specific Heats
N_{cell}	Number of Cells in the Fuel Cell Stack
F	Faraday's Constant
A_{or}	Orifice Area
C_d	Coefficient of Discharge
ρ	Density
P_1	Upstream Pressure
P_2	Downstream Pressure
A_{pipe}	Pipe Area
x_{xx}	Molar Fraction of Gas Stream
P_{supply}	Hydrogen Supply Pressure
Δ_p	Plant Model Deviation
y_{error}	Simulation Error for Tracking
P_{error}	Simulation Error for Pressure Tracking
n_{N_2error}	Simulation Error for Nitrogen Tracking
RER	System Response Error Ratio
Kp_p	Proportional Gain for Pressure Control
Ki_p	Integral Gain for Pressure Control
Kp_N	Proportional Gain for Nitrogen Control
Ki_N	Integral Gain for Nitrogen Control

J Cost Function

R Pressure Control Weighting

Q Nitrogen Control Weighting

S Control Effort Weighting

Typical matrix notation is employed. A lowercase italic variable indicates a scalar, a lowercase bold variable indicates a vector, and an uppercase bold variable indicates a matrix.

Chapter 1

Introduction

1.1 Background

Linear control theory and its applications have been used successfully for many years in practical control systems. Typical applications of this theory include, proportional, proportional-integral (PI), and proportional-integral-derivative (PID) control. For linear systems a robust mathematical theory has been developed. With this theory engineers can quickly determine if a set of gains will be stable and predict the tracking performance for the closed loop linear system.

As systems have become more complex researchers have looked to new methods to determine system stability particularly for nonlinear systems. The most useful methods were derived by a Russian mathematician Alexandr Lyapunov in the early 1890's. Lyapunov created two methods for evaluating stability of nonlinear systems, the most relevant was the "direct method". The "direct method" determines the stability properties of nonlinear systems by using an "energy function". This theory has become the backbone for all nonlinear stability analysis and will be discussed in detail in this work.

A number of different control strategies have been proposed for nonlinear systems. An attractive method is sliding mode control, which guarantees stability for both linear and nonlinear systems in the presence of modeling errors and uncertainties by applying Lyapunov's "direct method". SMC uses a form of feedback linearization. Feedback linearization is another form of nonlinear control which attempts to map a nonlinear system to a linear system by feeding back and therefore canceling the nonlinear terms. The major shortcoming of this type of control is that it relies heavily on the system models accuracy. In practical systems this is a major shortcoming since all models are

based on assumptions which cause inaccuracy. Sliding mode control has overcome this shortcoming by adding a robustness term to the feedback linearization. For this reason sliding mode control is the main focus of this research.

1.2 Current Work

In recent years there has been a number of different papers dealing with applying sliding mode control to an underactuated system. One of these papers by Schokoda [12] considered different methods of squaring the system to properly develop the sliding surface. The research focused on linear systems represented in state space form. When developing a sliding mode controller for these systems the inverse of the input influence matrix is required for the control law to function properly. For underactuated systems the input influence matrix is not square therefore the inverse does not exist. By using a transformation matrix the controller was flexible enough to choose which state to control. The pseudo inverse method only controlled the state that is directly impacted by that actuator. In the research, optimal control theory was used to determine the values of the transformation matrix that will give the desired system response. Schokoda's research provides the building blocks for this work.

A paper by Hao et al [15], tackles a similar problem in a much different manner. Hao looked at a class of underactuated systems with mismatched uncertainties and tried to apply sliding mode control. The method they derive for guaranteeing stability for this type of system involves generating n-1 sliding mode controllers where the output of the previous controller is one of the inputs to the next controller along with the next state variable. This method allows for exceptional control of each state and guarantees stability for the system. To deal with the mismatched uncertainties a second compensator was added to each layer of the incremental sliding mode controller. The method showed good tracking but the choice of values for the second compensator appeared arbitrarily chosen and the system was tedious to implement due to the large number of controllers that needed to be designed.

Wang et al [14] implemented a slightly different approach for the same type of inverted pendulum problem. They attempted to use an adaptive sliding mode controller to handle the underactuated system. The split the controller into two subsystems and designed a sliding mode controller for each. Wang then applied a form of adaptive control to the sliding mode controller and tested the controller with a number of different

disturbances. The research found that the controller was robust and fairly insensitive to external disturbances. The approach has the same limitations as the previous approach in that there are a number of controllers in series that all need to be tuned.

Park et al [10] applied a very similar controls approach to Wang, exploring the inverted pendulum problem as their underactuated system. The system was broken up into two subsystems and SMC was applied to each subsystem. The two resulting controllers were then summed and a new sliding surface was developed which was a function of the two initial controllers. Gains were added to each of the controllers to allow flexibility in the final sliding surface and to increase its reliability. The final controller was tested at a number of conditions and met expectations in all simulations.

Nikkhah et al [9] took the controller one step further than the previous two and applied optimal control theory to determine the optimal sliding surfaces to minimize energy and transient time. The inverted pendulum problem was used to show the validity of this method. The results demonstrated improved transient response over the initial sliding surfaces.

The problem with applying a sliding mode controller to a fuel cell system has been approached by several researchers in the last few years. In a paper by Kunusch et al [3], sliding mode control is proposed to regulate the cathode air compressor of a PEM fuel cell. A second order sliding mode controller was chosen to modify air flow. The controller demonstrated expected stability and fairly quick response to load disturbances. The system developed by Kunusch is similar to the fuel cell system that will be introduced and applied in this work. However, while Kunusch focused mainly on integrating the cathode system, this work will introduce a method for anode control.

1.3 Overview

In this work, a new augmented sliding mode control law is proposed for applications in multiple input multiple output nonlinear underactuated systems. "Square systems", or systems with the same number of inputs and control variables, are not the primary focus of this work. These types of systems can be dealt with using more traditional methods of sliding mode control. The intent of this work will be to implement under and overactuated systems, which are, systems with a different number of inputs than control variables. A similar approach to the one taken by Schokoda to deal with a linear underactuated system will be utilized and applied to a fuel cell system using SMC. A

number of new problems need to be solved to successfully accomplish this task. First, the approach has to be implemented on a nonlinear system. As a result, state space models cannot be used. Second, a robustness term must be derived to account for modeling uncertainties. The robustness term is what separates sliding mode control from most other controllers because it is able to guarantee stability of nonlinear systems. This research extends the work conducted Schokoda with the inclusion of nonlinear systems and the SMC method for guaranteeing stability in the presence of modeling uncertainties.

In Chapter 2, the required theory of nonlinear stability is presented. The theory is then applied to derive a scalar sliding mode controller. Finally, a nonlinear multiple input multiple output system is introduced and an augmented sliding mode controller is derived.

In Chapter 3, a fuel cell system is presented. The system states are then specified and there dependant equations are derived. Finally, the nonlinear system model is manipulated into matrix from to utilized the controller developed in Chapter 2. In Chapter 4, the system model is applied to the sliding mode controller and the parameter uncertainties are specified. The robustness term is then developed to handle the given error.

In Chapter 5, the control law is simulated and the results are analyzed. The controller is then exposed to real world conditions and implementation suggestions are proposed. Finally, SMC is compared to a traditional PI control law to examine the benefits of SMC. In Chapter 6, conclusions are drawn based on the results displayed in Chapter 5. Finally, next steps are proposed to further enhance this work.

Chapter 2

Theoretical Development

Preface

Sliding mode control is a form of robust feedback linearization. In this chapter the fundamentals of sliding mode control will be developed as well as an extension of the basic principals to accommodate a nonsquare system. Sliding mode control is capable of guaranteeing stability of a nonlinear system given a set of unknown but bounded parameters. This is possible due to stability criteria created by Lyapunov. This stability criteria known as Lyapunov's direct method will be discussed in the first part of this chapter. The second part of this chapter will derive a sliding mode controller for a SISO nonlinear system. The final section will rederive a sliding mode controller for a nonsquare MIMO system.

2.1 Lyapunov's Direct Method

Stability in a linear system is a simple concept. Is the system response to a given input bounded? If the answer is yes then the system is stable. Stability for this type of system can be found from the system roots. If all the system roots lie on the left half of a root locus plot then the system is stable. The concept of stability for a nonlinear system is not as straight forward. To understand the concept of stability one must examine the phase portrait of the system. The phase portrait is a plot of the system states and their interactions. An example of a phase portrait is given by Figure 2.1. The following theory developed by Aleksandr Mikhailovich Lyapunov is the basis that allows sliding mode control to ensure stability and perfect error tracking.

Nonlinear systems have three types of stability; asymptotically stable, marginally stable, or unstable. A detailed description of nonlinear stability theory is given by Slotine [13] and the main concepts are introduced in this section. The concept of stability is vitally important in the understanding of sliding mode control therefore the basic concepts will be reviewed here. The following definitions are used to introduce the basic theory used to derive sliding mode control.

Definition 2.1. *The equilibrium state* $\mathbf{x} = 0$ *is said to be stable if, for any* $R > 0$*, there exists* $r > 0$*, such that if* $\| \mathbf{x}(0) \| < r$*, then* $\| \mathbf{x}(t) \| < R$ *for all* $t > 0$*. Otherwise, the equilibrium point is unstable.*

The definition is illustrated by Figure 2.1. A state trajectory starts in the phase plane inside a circle with radius r. For that state trajectory to be considered stable it must stay within some larger circle with radius R as $t \to \infty$. Inversely, if the state trajectories do not remain arbitrarily close to the origin then the system is unstable.

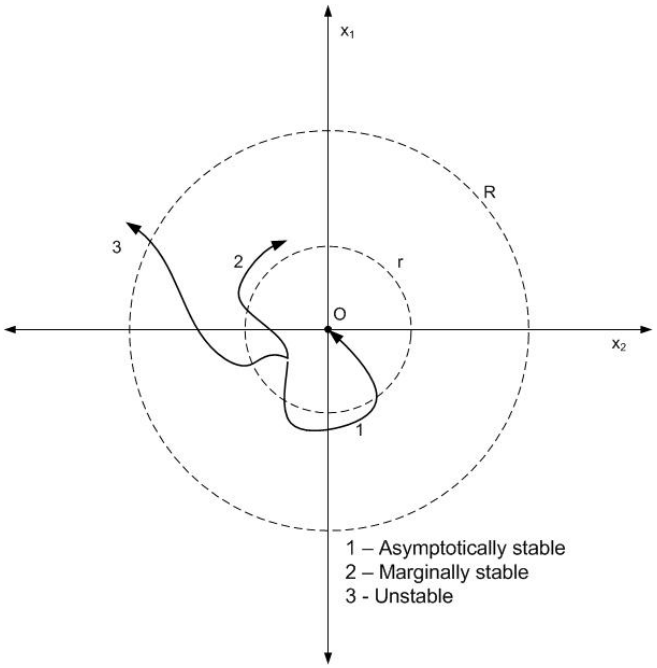

Figure 2.1: Concept of Nonlinear System Stability

Instability in a nonlinear system is not necessarily the same as instability in a linear system. In linear system the concept of instability means the state trajectories approach infinity as time approaches infinity. The concept of instability is not the same for nonlinear systems. While an unstable nonlinear system can tend to infinity as time increases

some unstable system tend to a constant.

By the same logic, the concept of stability between linear and nonlinear system is not the same. All stable linear systems demonstrate asymptotic stability and tend towards zero as time increases for the regulator problem. This is not the case for nonlinear systems, stable nonlinear system can show the same behavior but this is only a special case. Some stable nonlinear systems stay marginally close to the origin as time increase but do not ever reach the origin. These systems are called marginally stable.

Definition 2.2. *The equilibrium point 0 is asymptotically stable if it is stable, and if in addition there exists some* $r > 0$ *such that* $\| \mathbf{x}(0) \| < r$ *implies that* $\mathbf{x}(t) \to 0$ *as* $t \to \infty$.

This definition says that for a system to be asymptotically stable the origin must be stable and that states starting close to zero actually reach zero as time goes to infinity. The idea of exponential stability is a form of asymptotic stability only the system approaches the equilibrium point in an exponential manner.

Definition 2.3. *An equalibrium point 0 is exponentially stable if there exists two strictly positive numbers* α *and* λ *such that*

$$\forall t > 0, \| \mathbf{x}(t) \| \leq \alpha \| \mathbf{x}(0) \| e^{-\lambda t}$$

in some region $\mathbf{B_r}$ *around the origin.*

This definition says that for a system to be exponentially stable it must approach the origin as fast as or faster than an exponential function. λ is this case is the rate of exponential convergence and will be seen latter in the derivation of sliding mode control. Exponential stability is the most desirable form of stability for a nonlinear system.

Lyapunov developed a theory for guaranteeing stability for nonlinear systems it is called Lyapunov's direct method. The motivation for this work has origins from energy concepts. Energy concepts have two main properties. For a stable system the energy is always positive unless the state variable is zero. Second the energy is always decreasing as the state variables are varied. The first property can be satisfied with the concept of positive definite functions.

Definition 2.4. *A scalar continuous function* $V(\mathbf{x})$ *is said to be locally positive definite if* $V(\mathbf{0}) = 0$ *and, in a ball* $\mathbf{B_{R_0}}$

$$\mathbf{x} \neq \mathbf{0} \Rightarrow V(\mathbf{x}) > 0$$

If $V(\mathbf{0}) = 0$ and the above property hold over the whole state space, then $V(\mathbf{x})$ is said to be globally positive definite.

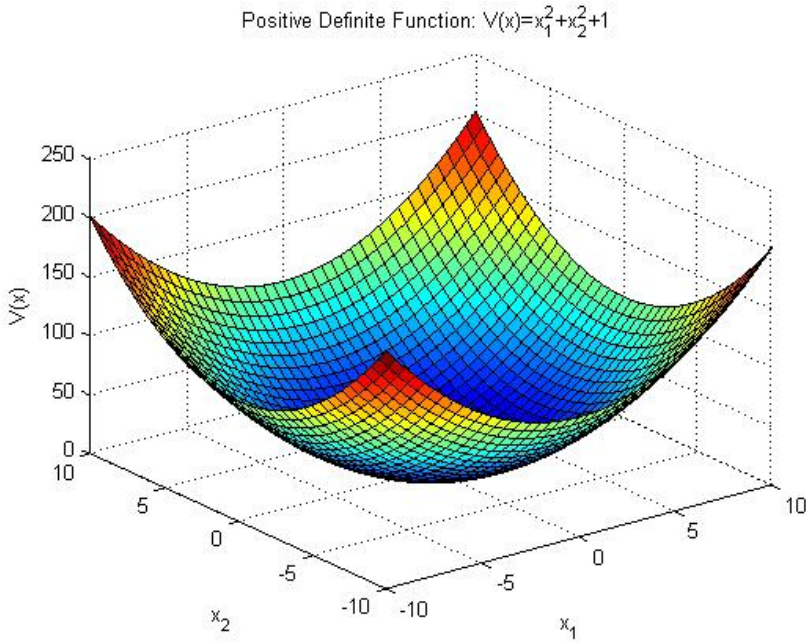

Figure 2.2: Example of a Positive Definite Function

The definition states that a function is considered positive definite if that function, $V(\mathbf{x})$, is greater than zero for all values of $\mathbf{x}$ and $\dot{\mathbf{x}}$. A simple example is given by Figure 2.2. The second property can be satisfied with the concept of negative definite functions. A negative definite function is the opposite of a positive definite function.

Definition 2.5. *If, in a region $\mathbf{B_{R_0}}$, the function $V(\mathbf{x})$ is positive definite and has continuous partial derivatives, and if its time derivative along any state trajectory is negative semi-definite,*

$$\dot{V}(\mathbf{x}) \leq 0$$

then $V(\mathbf{x})$ is said to be a Lyapunov function for the system.

A Lyapunov function is guaranteed to be stable because the functions derivative is always moving toward the origin. The concept is similar to an energy equation always dissipating energy and eventually coming to rest with no motion.

2.2 Scalar Sliding Mode Control

Sliding mode control is a robust form of feedback linearization. It relys on the inverse of the plant model to track the desired states with a defined control effort. In this section a sliding mode controller will be developed for a general scalar nonlinear case where the system has one input and output. This derivation can be found in Slotine [13]. The general form of the SISO nonlinear system is given by

$$\dot{x} = f(x, \dot{x}, t) + Bu \tag{2.1}$$

where x is the output of the system, u is the control input, and f are the system dynamics. To allow the system to track a desired state, x_d, a sliding surface must be defined. The sliding surface is defined as

$$s = \tilde{x} + \lambda \int_0^{t=\infty} \tilde{x} dr \tag{2.2}$$

where $\tilde{x} = x - x_d$ and λ is a positive constant. From Section 2.1, λ is shown to be inversely proportional to the reaching phase time constant. Therefore, as λ increase the controller becomes faster responding. Differentiating s and applying equation 2.1 leads to

$$\dot{s} = \dot{x} - \dot{x}_d + \lambda\tilde{x} = f + Bu - \dot{x}_d + \lambda\tilde{x} \tag{2.3}$$

By setting $\dot{s} = 0$ the resulting control law will, once on the sliding surface, remain on the sliding surface. Our best approximation of such a control law given equation 2.3 is given by

$$\hat{u} = \frac{\dot{x}_d - \lambda\tilde{x} - \hat{f}}{\hat{B}} \tag{2.4}$$

where the $\hat{}$ symbol denotes the best estimate of the system parameters. The result is important since all system models have some level of error associated with them. Sliding mode control accounts for those error within the control law guaranteeing stability. A discontinuous term is added to account for modeling uncertainties. The resulting control equation becomes

$$u = \hat{u} - Ksgn(s) \tag{2.5}$$

where sgn is the signum function and K is always positive. By properly choosing K to be large enough to overcome any modeling errors system stability will be ensured. Using Lyapunov stability criteria a positive definite function in s is chosen. A candidate function is given by

$$V = \frac{1}{2}s^2$$

The derivative must be negative definite to satisfy Lyapunov's criteria therefore

$$\dot{V} = \frac{1}{2}\frac{d}{dt}s^2 = s\dot{s} \geq -\eta|s| \tag{2.6}$$

Equation 2.6 is known as the sliding condition. Inserting equations 2.3 and 2.5

$$\left(\frac{B}{\hat{B}} - 1\right)(\dot{x}_d - \lambda\tilde{x} - \hat{f})s + \frac{\tilde{f}s}{B} - BK|s| \leq \eta|s|$$

where $\tilde{f} = |f - \hat{f}|$ and η is a small positive constant. Solving for K results in

$$K|s| \geq \frac{\tilde{f}s}{B} + \frac{\eta|s|}{B} + \left(\frac{1}{B} - \frac{1}{\hat{B}}\right)(\hat{f} + \lambda\tilde{x} - \dot{x}_d)s \tag{2.7}$$

To satisfy the inequality in equation 2.7 the following must be true

$$K \geq \frac{\tilde{f}}{|B|} + \frac{\eta}{|B|} + \left|\frac{1}{B} - \frac{1}{\hat{B}}\right||\hat{f} + \lambda\tilde{x} - \dot{x}_d| \tag{2.8}$$

Based on Lyapunov's direct method perfect tracking and stability are guaranteed by defining f and B conservatively. Therefore f and B should be chosen to be the extremes of the system model. The final form of the nonlinear SISO control law is given by

$$u = \frac{\dot{x}_d - \lambda\tilde{x} - \hat{f}}{\hat{B}} - Ksgn(s) \tag{2.9}$$

The next section will show how the sliding mode control derivation differs when applied to a multiple input multiple output system.

2.3 Multiple Input, Multiple Output Sliding Mode Control

The scalar case presented in Section 2.2 is an illustrative example of sliding mode control method. However, in reality most systems are not single input single output type system they consist of multiple inputs and outputs. This section expands the definition of the sliding mode controller to incorporate multiple variable systems. Figure 2.3 shows a schematic diagram of a typical MIMO sliding mode controller.

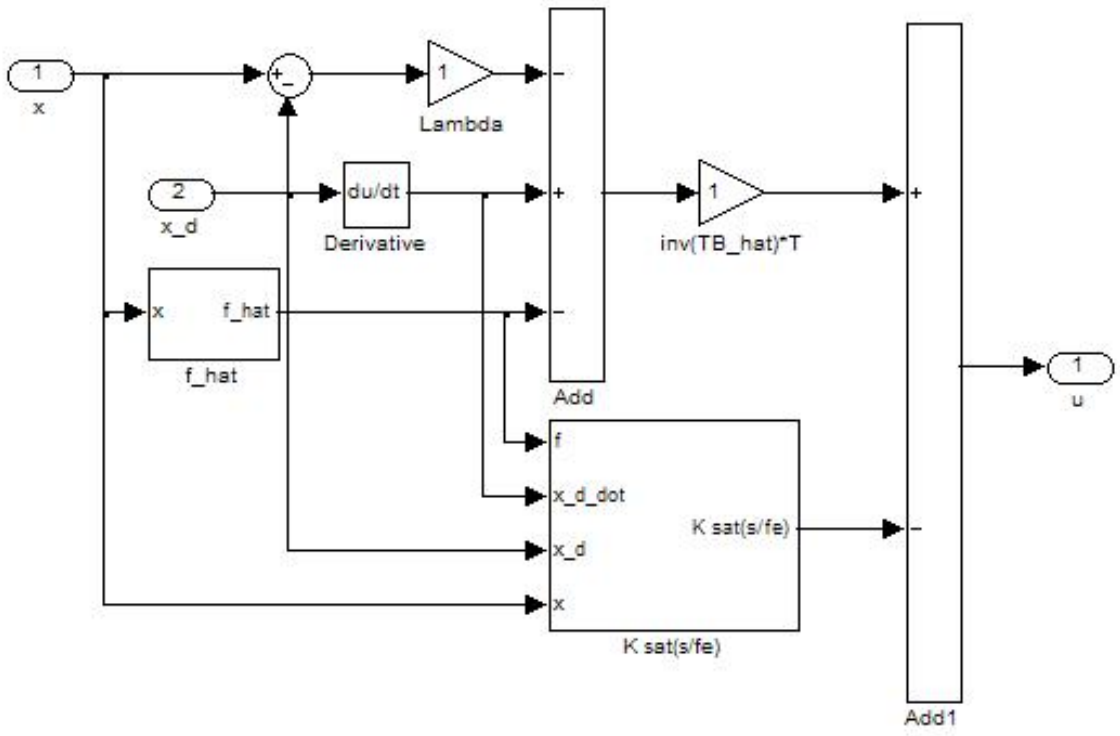

Figure 2.3: MIMO SMC Algorithm Structure

A general form for a nonlinear MIMO system is

$$\dot{\mathbf{x}} = \mathbf{f}(\mathbf{x}, \dot{\mathbf{x}}, \mathbf{t}) + \mathbf{Bu} \tag{2.10}$$

where $\dot{\mathbf{x}}$ is a nx1 vector of the system states, $\mathbf{f}$ is a nx1 vector of the nonlinear terms in

the system, $\mathbf{B}$ is the nxm input influence matrix, and $\mathbf{u}$ is a mx1 vector of control inputs. The form of the $\mathbf{f}$ vector is unknown and may be a function of the system state, $\mathbf{x}$, the state derivatives, $\dot{\mathbf{x}}$, and time. Sliding mode control is attempting to allow the system to achieve perfect tracking assuming the system model is inaccurate but the inaccuracies are bounded. In other words, $\mathbf{f}$ and $\mathbf{B}$ are not known exactly but bounded by some function in $\mathbf{x}$ and time. The modeled system takes the form

$$\dot{\mathbf{x}} = \hat{\mathbf{f}}(\mathbf{x}, \dot{\mathbf{x}}, \mathbf{t}) + \hat{\mathbf{B}}\mathbf{u} \tag{2.11}$$

Where the $\hat{}$ symbol represents the best estimate for the system parameters.

Choose a candidate sliding surface as

$$\mathbf{s} = \tilde{\mathbf{x}} + \lambda \int_0^\infty \tilde{\mathbf{x}} dt \tag{2.12}$$

where $\tilde{\mathbf{x}} = \mathbf{x} - \mathbf{x_d}$ and λ is a strictly positive constant. By defining $\mathbf{s}$ in this manner the problem now becomes one of reducing s to zero and maintaining a zero condition. The sliding surface $\mathbf{s}$ has now become a direct measure of the tracking error $\tilde{\mathbf{x}}$. To force $\mathbf{s} \to 0$, a Lyapunov function needs to be defined in $\mathbf{s}$.

$$V_i = \frac{1}{2} s_i^2 \tag{2.13}$$

Equation 2.13 is a Lyapunov function because it is positive semi-definite, when $s_i = 0$ then $V_i = 0$. To satisfy Lyapunov's direct method and ensure the origin is globally asymptotically stable the derivative of 2.13 must be negative definite.

$$\dot{V}_i = \dot{s}_i s_i \leq 0 \tag{2.14}$$

When $\mathbf{s} \neq 0$ the system state trajectories are not on the sliding surface and must tend toward the surface to maintain stability. In other words, the trajectories must "reach" the sliding surface. The sliding mode control law must ensure that during the "reaching phase" that the state trajectories remain asymptotically stable.

For now, assume the state trajectories are on the sliding surface. The controller should be designed such that once this state is reached no movement is allowed off the sliding surface. This implies that $\dot{\mathbf{s}} = 0$. Lets force this condition to be true by setting

$\dot{\mathbf{s}} = 0$ and solving for $\hat{\mathbf{u}}$.

$$\dot{\mathbf{s}} = \dot{\mathbf{x}} - \dot{\mathbf{x}}_\mathbf{d} + \lambda\tilde{\mathbf{x}} = 0 \tag{2.15}$$

Substituting in 2.11 into 2.15 and solving for $\hat{\mathbf{u}}$

$$\hat{\mathbf{u}} = \hat{\mathbf{B}}^{-1}(\dot{\mathbf{x}}_\mathbf{d} - \hat{\mathbf{f}} - \lambda\tilde{\mathbf{x}}) \tag{2.16}$$

From this equation the issue arises that if $\hat{\mathbf{B}}$ is not constrained to a square matrix then the inverse of $\hat{\mathbf{B}}$ does not exist. In other words, if $n \neq m$ then there is no solution for $\hat{\mathbf{u}}$. One option is to take the pseudo-inverse of the $\hat{\mathbf{B}}$ matrix but this could lead to the control law ignoring dynamics if the $\hat{\mathbf{B}}$ matrix is not fully populated. Is there a solution that would account for all the system dynamics and allow for the solution of $\hat{\mathbf{u}}$? A solution is proposed by Schkoda using a squaring transformation matrix to map the input influence matrix to a square system. The research demonstrated the technique worked well for dynamic inversion. Expanding on that understanding, a sliding mode controller can be derived using a similar approach.

Define a mapping function that will force the system to act like a square system. To accomplish the objective an intermediate variable is defined as follows

$$\mathbf{y} = \mathbf{T}\mathbf{x} \tag{2.17}$$

Where $\mathbf{T}$ is the mxn mapping matrix and is assumed to be fully populated and $\mathbf{y}$ is then a mx1 vector. Substituting 2.11 into 2.17 and taking the derivative gives

$$\dot{\mathbf{y}} = \mathbf{T}\hat{\mathbf{f}} + \mathbf{T}\hat{\mathbf{B}}\mathbf{u} \tag{2.18}$$

From the previous definition of $\hat{\mathbf{B}}$ as a nxm matrix and given that $\mathbf{T}$ is a mxn matrix the resulting matrix multiplication will result in a square matrix of size mxm. With proper choice of $\mathbf{T}$ the resulting augmented input influence matrix will be invertible and allows the control law to be developed. Redefine the sliding surface in terms of the new control states $\mathbf{y}$

$$\mathbf{s} = \mathbf{y} - \mathbf{y}_\mathbf{d} + \lambda \int_0^\infty (\mathbf{y} - \mathbf{y}_\mathbf{d})dt$$

Again, to ensure no movement off the sliding surface once the state trajectories have reached that surface set $\dot{\mathbf{s}} = 0$.

$$\dot{\mathbf{s}} = \dot{\mathbf{y}} - \dot{\mathbf{y}}_\mathbf{d} + \lambda\tilde{\mathbf{y}} = 0 \tag{2.19}$$

where

$$\tilde{\mathbf{y}} = \mathbf{y} - \mathbf{y_d}$$

Substitute 2.18 into 2.19 and solving for $\mathbf{u}$ results in

$$\hat{\mathbf{u}} = (\mathbf{T}\hat{\mathbf{B}})^{-1}\mathbf{T}[\dot{\mathbf{x}}_\mathbf{d} - \lambda\tilde{\mathbf{x}} - \hat{\mathbf{f}}] \tag{2.20}$$

From this result the desired effect of adding a mapping term is confirmed. The matrix to be inversed in the control law is square. However, the sliding mode controller is now trying to obtain perfect tracking of $\mathbf{y}$ not $\mathbf{x}$ an important point and will be expanded on later. Equation 2.20 is our best guess at the desired controller dynamics. If the model was perfectly accurate the controller proposed in equation 2.20 ensures perfect tracking of all of the system states. However, it is more desirable to have a control law that will ensure stability even with a less than perfect model. To push the state trajectories back to the sliding surface in the face of modeling uncertainties a discontinuous term is added to the control law.

$$\mathbf{u} = (\mathbf{T}\hat{\mathbf{B}})^{-1}\mathbf{T}[\dot{\mathbf{x}}_\mathbf{d} - \lambda\tilde{\mathbf{x}} - \hat{\mathbf{f}}] - \mathbf{K}\mathbf{sgn}(\mathbf{s}) \tag{2.21}$$

To ensure stability using Lyapunov's direct method, $\mathbf{K}$ must satisfy the sliding condition therefore

$$\dot{s}_i s_i \leq -\eta_i \left|s_i\right| \tag{2.22}$$

where η is a mx1 vector of small positive constants. This term is needed to ensure that $\dot{\mathbf{V}}(\mathbf{y})$ is negative definite and not just negative semi-definite. Defining $\dot{\mathbf{s}}$ in terms of $\mathbf{x}$ by combining 2.18 with 2.19 and applying 2.17 results in:

$$\dot{\mathbf{s}} = \mathbf{T}\mathbf{f} + \mathbf{T}\mathbf{B}\mathbf{u} - \mathbf{T}\dot{\mathbf{x}}_\mathbf{d} + \mathbf{T}\lambda\tilde{\mathbf{x}} \tag{2.23}$$

Insert the definition for the control law $\mathbf{u}$ equation 2.21 into 2.23. Yields

$$\dot{\mathbf{s}} = \mathbf{T}\mathbf{f} + \mathbf{T}\mathbf{B}(\mathbf{T}\hat{\mathbf{B}})^{-1}\mathbf{T}[\dot{\mathbf{x}}_\mathbf{d} - \lambda\tilde{\mathbf{x}} - \hat{\mathbf{f}}] - \mathbf{T}\mathbf{B}\mathbf{K}\mathbf{sgn}(\mathbf{s}) - \mathbf{T}\dot{\mathbf{x}}_\mathbf{d} + \mathbf{T}\lambda\tilde{\mathbf{x}}$$

Before going any further it is important that care is taken when manipulating matrix equations. Since not all of the properties of scalar equations apply to matrix equations.

A short list of useful properties of matrices is given by [6] and shown here

$$\begin{aligned}
\mathbf{AB} &\neq \mathbf{BA} \\
\mathbf{AC} &= \mathbf{AD} \nrightarrow \quad \mathbf{C} = \mathbf{D} \\
(\mathbf{A}+\mathbf{B})\mathbf{C} &= \mathbf{AC}+\mathbf{BC} \\
\mathbf{A}(\mathbf{B}+\mathbf{C}) &= \mathbf{AB}+\mathbf{AC} \\
(\mathbf{AB})^{-1} &= \mathbf{B}^{-1}\mathbf{A}^{-1} \\
\mathbf{AI} &= \mathbf{IA} = \mathbf{A}
\end{aligned}$$

The first two properties of matrix algebra are not intuitive and are very different from scalar algebra. The first property states that order matters with matrix multiplication. The second property is a very interesting result in that from the relation $\mathbf{AC} = \mathbf{AD}$ it should follow that $\mathbf{C} = \mathbf{D}$, however, this is not always the case and because so care must be taken when canceling matrices. The last property of interest is the inverse of a matrix product is equal to the inverse of each matrix multiplied in reverse order.

Continuing with the derivation, collecting like terms results in

$$\dot{\mathbf{s}} = [\mathbf{Tf} - \mathbf{TB}(\mathbf{T}\hat{\mathbf{B}})^{-1}\mathbf{T}\hat{\mathbf{f}}] + [\mathbf{T} - \mathbf{TB}(\mathbf{T}\hat{\mathbf{B}})^{-1}\mathbf{T}](\lambda\tilde{\mathbf{x}} - \dot{\mathbf{x}}_{\mathbf{d}}) - \mathbf{TBKsgn}(\mathbf{s})$$

Multiplying both sided of the previous equation by $\mathbf{s}$ and applying the sliding condition given by 2.22

$$\dot{\mathbf{s}}\mathbf{s} = [\mathbf{Tf} - \mathbf{TB}(\mathbf{T}\hat{\mathbf{B}})^{-1}\mathbf{T}\hat{\mathbf{f}}]\mathbf{s} + [\mathbf{T} - \mathbf{TB}(\mathbf{T}\hat{\mathbf{B}})^{-1}\mathbf{T}](\lambda\tilde{\mathbf{x}} - \dot{\mathbf{x}}_{\mathbf{d}})\mathbf{s} - \mathbf{TBK}|\mathbf{s}| \leq -\eta|\mathbf{s}|$$

Rewritting the previous equation in terms of a vector of scalars leads to

$$\begin{aligned}
\dot{s}_i s_i = &\sum_{j=1}^{m} T_{ij} f_j s_i - \sum_{j=1}^{m} \Delta_{ij} \hat{f}_j s_i - \sum_{j=1}^{m} \Delta_{ij}(\lambda_{jj}\tilde{x}_j - \dot{x}_{dj}) s_i + \sum_{j=1}^{m} T_{ij}(\lambda_{jj}\tilde{x}_j - \dot{x}_{dj}) s_i \\
&- \left[\sum_{j=1}^{m} T_{ij} B_{ji}\right] K_i |s_i| \leq -\eta_i |s_i|
\end{aligned}$$

where $\Delta = \mathbf{TB}(\mathbf{T}\hat{\mathbf{B}})^{-1}\mathbf{T}$. Solving for K results in

$$\left[\sum_{j=1}^{m} T_{ij} B_{ji}\right] K_i \geq \left|\sum_{j=1}^{m} T_{ij}\tilde{f}_j\right| - \left|\sum_{j=1}^{m} \Delta_{ij}(\hat{f}_j + \lambda_{jj}\tilde{x}_j - \dot{x}_{dj})\right| + \left|\sum_{j=1}^{m} T_{ij}(\hat{f}_j + \lambda_{jj}\tilde{x}_j - \dot{x}_{dj})\right| + \eta_i$$

where $\tilde{\mathbf{f}} = |\mathbf{f} - \hat{\mathbf{f}}|$. The above result must be true in order to satisfy the inequality constraint. The final constraint is that K_i must be positive at all times satisfying the sliding condition. This is imposed to ensure that the added control effort forces the state trajectory to move opposite to the sign of s_i. In other words, if s_i is negative, the K_i term should be negative and this is only guaranteed if K_i is always positive. Combining the summation terms results in the final form of the equation

$$\left[\sum_{j=1}^{m} T_{ij}B_{ji}\right] K_i \geq \sum_{j=1}^{m} |T_{ij}|\, \tilde{f}_j + \left|[T_{ij} - \Delta_{ij}](\hat{f}_j + \lambda_{jj}\tilde{x}_j - \dot{x}_{dj})\right| + \eta_i \tag{2.24}$$

If the system is chosen to have 2 states and one actuator then Equation 2.24 reduces to

$$\mathbf{K} \geq |(\mathbf{TB})^{-1}\mathbf{T}|\tilde{\mathbf{f}} + \left|(\mathbf{TB})^{-1}\right| \eta + |(\mathbf{TB})^{-1}\mathbf{T} - (\mathbf{T}\hat{\mathbf{B}})^{-1}\mathbf{T}||\hat{\mathbf{f}} + \lambda\tilde{\mathbf{x}} - \dot{\mathbf{x}}_{\mathbf{d}}| \tag{2.25}$$

Comparisions to the SISO controller can be drawn by assuming $\mathbf{T}$ to be the transpose of the $\mathbf{B}$ matrix when $\mathbf{B}$ is square. Equation 2.26 demostrates the result of these assumptions.

$$\mathbf{K} \geq |(\mathbf{B})^{-1}|\tilde{\mathbf{f}} + \left|(\mathbf{B})^{-1}\right| \eta + |(\mathbf{B})^{-1} - (\hat{\mathbf{B}})^{-1}||\hat{\mathbf{f}} + \lambda\tilde{\mathbf{x}} - \dot{\mathbf{x}}_{\mathbf{d}}| \tag{2.26}$$

Comparing equation 2.26 to equation 2.8 it is obvious that they are of very similar form. The next step in deriving the controller is to determine the values for the plant parameters. Inaccuracies in the input influence matrix $\mathbf{B}$ should be considered in multiplicative form

$$\mathbf{B} = (\mathbf{I} + \mathbf{\Delta})\hat{\mathbf{B}} = \hat{\mathbf{B}} + \mathbf{\Delta}\hat{\mathbf{B}} \tag{2.27}$$

where $\mathbf{\Delta}$ is an upper bound limit of the uncertainties in $\mathbf{B}$. The resulting form of the control law is

$$\mathbf{u} = (\mathbf{T}\hat{\mathbf{B}})^{-1}\mathbf{T}\left[\dot{\mathbf{x}}_{\mathbf{d}} - \lambda\tilde{\mathbf{x}} - \hat{\mathbf{f}}\right] - \mathbf{K}\mathbf{sgn}\,(\mathbf{s}) \tag{2.28}$$

Due to the sign term in the above equation the control law will chatter significantly and could command unrealistic control effort and excite higher order unmodeled dynamics which could be detrimental to the system that is being controlled. To smooth out the discontinuity inherent to 2.28, a saturation term replaces the signum function. The saturation term will create a more continuous type of control effort which is more desirable

for real world control applications. Equation 2.28 takes the form

$$\mathbf{u} = (\mathbf{T}\hat{\mathbf{B}})^{-1}\mathbf{T}\left[\dot{\mathbf{x}}_\mathbf{d} - \lambda\tilde{\mathbf{x}} - \hat{\mathbf{f}}\right] - \mathbf{Ksat}\left(\frac{\mathbf{s}}{\phi}\right) \tag{2.29}$$

where ϕ is a mx1 vector of positive constants. Comparing the result in equation 2.29 to equation 2.9, it is easily derived that, if $\mathbf{T} = \hat{\mathbf{B}}^T$ and $\mathbf{B}$ is square then the two equations match as shown in Schkoda. In other words, if there are the same number of states and actuators in the system then the solution is the same as the SISO case derived in section 2.2.

Chapter 3

Anode Fuel Cell Model

Preface

Fuel cells are a good example of a highly nonlinear system that has tight control tolerances and fast dynamics. For this reason the anode portion of a fuel cell will be used as the plant model to test the viability of the proposed SMC algorithm.

The anode subsystem is responsible for providing hydrogen to support the fuel cell reaction. This is accomplished by controlling two parameters, system pressure (P) and the number of moles of nitrogen (n_{N_2}) in the system. The pressure is important because the fuel cells voltage is dependant on the hydrogen partial pressure. The hydrogen partial pressure is difficult to measure so using the total pressure becomes more practical in a real world application. Since the hydrogen partial pressure is unknown it is important to ensure that the nitrogen content doesn't increase to a point where the nitrogen becomes the majority of the gas stream. If this were to happen hydrogen starvation could occur which would cause permanent damage to the fuel cell stack [7]. A number of excellent resources are available for more detail into fuel cell system modeling. A book by Pukrushpan et al [5] is an example of one of many recent books written about fuel cell modeling and control.

The system to be evaluated in this paper is similar to the system presented by Karnik et al [1] and Zhu et al [16]. It consists of a hydrogen supply source with an upstream supply pressure (P_{sup}) and temperature (T_{sup}), a fuel cell stack, a volume (V_{an}), and an exhaust orifice. The system schematic can be seen in Figure 3.1. In automotive applications it is typical to use an injector to meter the fuel flow. For that reason an injector is used for this system.

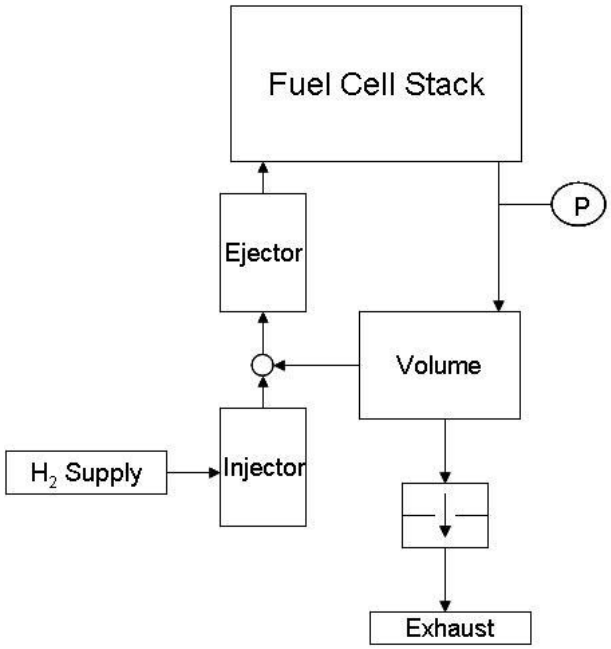

Figure 3.1: Anode System Mechanization

3.1 Pressure Model

The overall dynamic system pressure can be derived from the ideal gas law.

$$PV = nRT$$

Taking the derivative with respect to time leads to

$$\dot{P} = \frac{\dot{n}RT}{V}$$

The change in temperature and volume with respect to time are negligible compared to the change in pressure and flow rates. Making this assumption the change in pressure is equal to the sum of the flow rates into the system minus the sum of the flow rates out of the system.

$$\dot{P} = \frac{(\sum \dot{n}_{in} - \sum \dot{n}_{out})RT}{V} \tag{3.1}$$

The inflows of the system are the injector flow of hydrogen, and the permeation of nitrogen and water. From Figure 3.2 the outflows of the system are the exhaust flow and the consumption due to the fuel cell reaction.

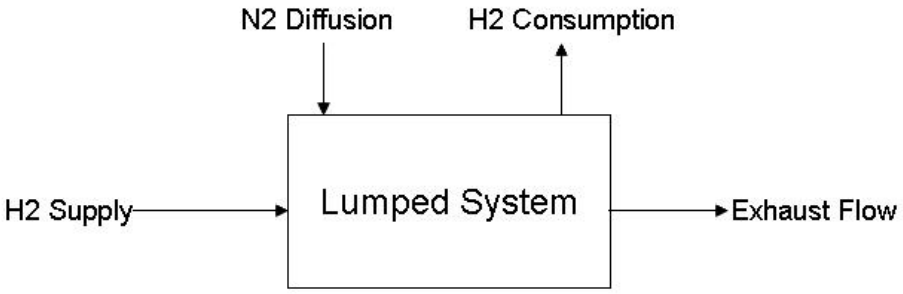

Figure 3.2: Lumped System Flow Diagram

Since fuel cells are made up of a porous membrane separating the cathode and anode species, over time diffusion through the membrane will try to equalize the two streams [4]. Therefore, because the cathode side consists of mostly nitrogen that nitrogen will slowly diffuse to the anode side until equilibrium is reached. The equation for the permeation rate of nitrogen from the cathode to the anode is given by

$$\dot{n}_{perm} = H(pp_{Ca} - pp_{An}) \tag{3.2}$$

where H is the diffusion rate and pp is the partial pressure of nitrogen. The partial pressure of nitrogen on the cathode side is proportional to cathode pressure and nitrogen concentration. In air the average nitrogen concentration is 0.79. The cathode pressure varies with air flow and is given for a given set of conditions. The anode partial pressure of nitrogen is also proportional to the anode pressure and the concentration of nitrogen on the anode side. For the purposes of this model the incoming hydrogen is assumed to be pure. Therefore, the only nitrogen in the anode side is the amount that has diffused from the cathode. Equation 3.2 can be rewritten as

$$\dot{n}_{perm} = H\left(0.79P_{Ca} - \frac{n_{N_2}RT}{V}\right) \tag{3.3}$$

During the fuel cell reaction water is produced on the cathode side of the membrane and also diffuses to the anode side. This process is much more difficult to model because of the potential for phase change from vapor to liquid. For this reason the fuel cell exhaust stream is assumed to be fully saturated with water vapor. This simplifies the model and makes water a function of temperature only. For a more complete analysis of the water transport phenomenon see [8]. Curve fitting the water saturation pressure

data gives the following equation [2].

$$pp_{h_2osat} = 0.000149(T - 273)^3 - 0.00732(T - 273)^2 + 0.233(T - 273) - 0.117 \quad (3.4)$$

where T is the temperature of the gas stream in Kelvin and pp_{h_2osat} is the saturation pressure of water in kPa. The moles of water are then given by

$$n_{h_2o} = \frac{RH \cdot pp_{h_2osat}}{P} \quad (3.5)$$

where RH is the relative humidity of the gas stream. From our earlier assumption that the stream is always saturated then $RH = 1$.

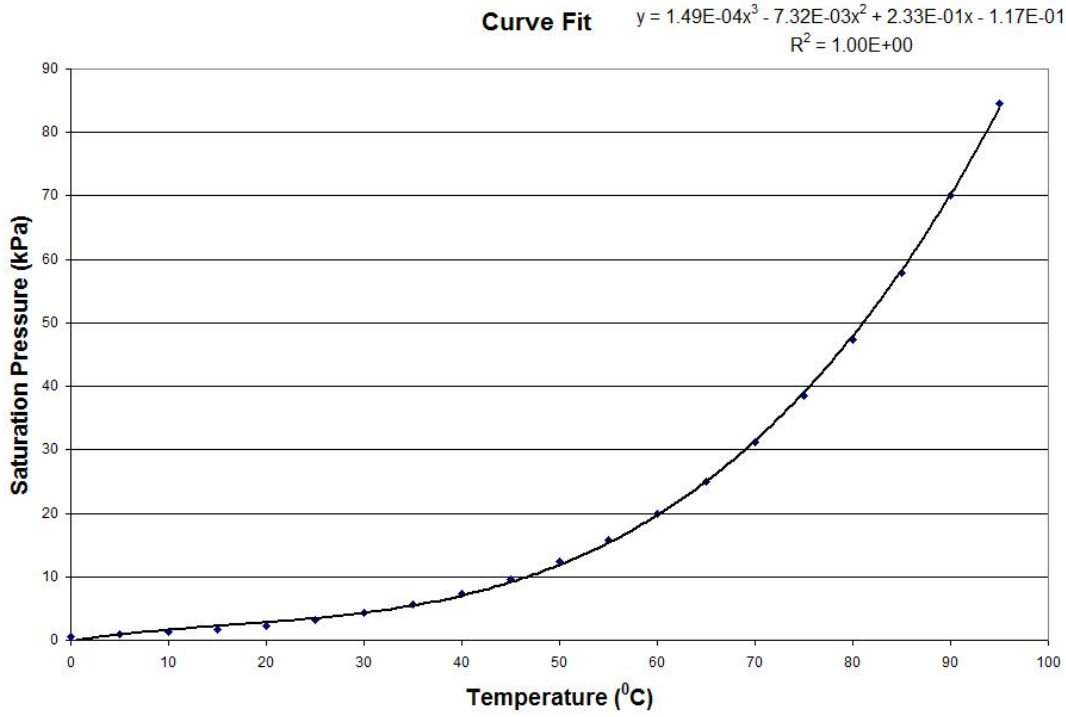

Figure 3.3: Saturation Pressure Curve Fit using Equation 3.4

The final flow source for the pressure model is the injector flow. The injector flow is needed to provide hydrogen to the fuel cell stack to support the reaction. There is an upstream pressure (P_{supply}) which effects the flow rate through the injector that is provided by the hydrogen storage tank. For this derivation that pressure will be assumed

to be constant. The resulting equation to determine the injector flow is given by

$$\dot{n}_{inj} = \frac{\dot{m}_{max} DC}{M_W} \tag{3.6}$$

where $\dot{m}_{max}$ is the maximum flow through the injector at a given upstream temperature and pressure, M_W is the molecular weight of hydrogen, and DC is the injector duty cycle. This equation assumes the injector is linear across its operating range which is a valid assumption if the duty cycle is above a certain threshold which depends of the hardware. The maximum flow rate of the injector can be derived using an isentropic sonic nozzle flow equation that is adapted to account for compressibility [4].

$$\dot{m}_{max} = P_{supply} A_{eff} \sqrt{\left(\frac{2}{k+1}\right)^{(k+1)/(k-1)} \left(\frac{k M_W}{RT}\right)}$$

where k is the ratio of specific heats, which for an ideal gas is 1.4, and A_{eff} is the effective area of the injector.

The system outflows are given by the fuel cell consumption and exhaust flow equations. The fuel cell consumption is an electrochemical reaction which, when current is drawn takes hydrogen and oxygen and produces water. During this process voltage is generated and therefore power is produced. The consumption of hydrogen to support the reaction is given by the following equation

$$\dot{n}_{cons} = \frac{I N_{cell}}{2F} \tag{3.7}$$

where I is the current drawn in amps, N_{cell} is the number of cells in the fuel cell stack, and F is Faraday's constant.

The exhaust flow can be modeled by a compressible orifice flow equation. The volume flow through an orifice is given by

$$Q = vA = C_d A_{or} \sqrt{\frac{2(P_1 - P_2)}{\rho(1 - A_{or}/A_{pipe})[1 - (A_{or}/A_{pipe})^2]}}$$

where Q is the volume flow of gas, C_d is the coefficient of discharge which is between 0.6 and 0.7, P_1 is the upstream pressure, P_2 is the down stream pressure, and ρ is the density of the gas. In this system the flow rate needed to maintain a nitrogen level is proportional to the nitrogen diffusion rate. Diffusion is a very slow process so the orifice

size is relatively small. That said the term $\frac{A_{or}}{A_{pipe}}$ is very small and can be ignored. Solving for the mass flow rate

$$\dot{m} = \rho Q = C_d A_{or} \sqrt{2\rho(P_1 - P_2)}$$

Adding a compressibility term to account for the expanding gas leads to the final form of the equation

$$\dot{n}_{or} = \frac{C_d A_{or}}{M_W} \sqrt{2\rho_{an} P_{an} \left(\frac{k}{k-1}\right) \left[(P_{ca}/P_{an})^{2/k} - (P_{ca}/P_{an})^{(k+1)/k}\right]} \tag{3.8}$$

where ρ is the density of the upstream gas which can be calculated from the ideal gas law as

$$\rho = \frac{m}{V} = \frac{P_{an} M_W}{RT}$$

and M_W is the molecular weight of the gas stream. The anode gas stream consists of three gases, hydrogen, nitrogen, and water vapor. Using molecular weight constants the equation is given by [2]

$$M_W = 2.016 x_{H_2} + 28.013 x_{N_2} + 18.015 x_{H_2O} \quad = \frac{25.984 n_{N_2} RT}{P_1 V} + 15.984 \frac{H_2O_{sat}}{P_1} + 2.016$$

where x is the concentration within the gas stream. The concentration is given by

$$x_{H_2} = \frac{n_{H_2} RT}{P_{an} V}$$

The sum of all the concentration must add to 1.

All the in and out flows have been derived. Rewriting equation 3.1 and substituting in equations 3.2, 3.6, 3.7, and 3.8 leads to

$$\dot{P} = \left[\frac{\dot{m}_{max} DC}{M_W} + H\left(0.79 P_{Ca} - \frac{n_{N_2} RT}{V}\right) - \frac{I N_{cell}}{2F} - \dot{n}_{or}\right] \frac{RT}{V} \tag{3.9}$$

3.2 Nitrogen Model

Deriving the change in nitrogen in the system uses similar equation to the ones derived above only now the nitrogen species is the only important parameter. From a mass

balance the change in nitrogen in the system is given as

$$\dot{n}_{N_2} = \sum \dot{n}_{in} - \sum \dot{n}_{out} \tag{3.10}$$

where, the inflows into the system are the permeation from the cathode to the anode and the outflows are the amount of nitrogen exhausted through the outlet orifice. The permeation equation is given by equation 3.2 where the exhaust flow equation is a slight deviation on equation 3.8. The nitrogen leaving the system is given by

$$\dot{n}_{or}^{N_2} = \dot{n}_{or} x_{N_2} \tag{3.11}$$

where x_{N_2} is the concentration of nitrogen in that point in the system and is given by

$$x_{N_2} = \frac{n_{N_2}}{n_{H_2} + n_{H20} + n_{N_2}} = \frac{n_{N_2} RT}{PV}$$

Substituting 3.2 and 3.11 into 3.10 leads to

$$\dot{n}_{N_2} = H \left(0.79 P_{Ca} - \frac{n_{N_2} RT}{V} \right) - \frac{C_d A_{or} x_{N_2}}{M_W} \sqrt{2 \rho_{an} P_{an} \left(\frac{k}{k-1} \right) \left[(P_{ca}/P_{an})^{2/k} - (P_{ca}/P_{an})^{(k+1)/k} \right]}$$

It is important for SMC that all the system states are measurable. The anode pressure is easily measured using a pressure sensor. Pressure sensors are commercially available and are currently used in automotive applications to measure the intake manifold pressure. Measuring the nitrogen content is more difficult. There are many ways to measure nitrogen content of a gas; two methods will be detailed here. The first and more accurate way is using a mass spectrometer which tends to be a more expensive option. The second method is using the speed of sound through the gas to infer the nitrogen content. This is more difficult because the speed of sound is not a direct measure of the nitrogen content it is more a measure of the gas molecular weight. However by making an assumption about the water vapor content a decent measure of nitrogen is possible using this technique.

3.3 Matrix Form

To be able to use the equations derived in Chapter 2, the model needs to be in the form of equation 2.10.

$$\dot{\mathbf{x}} = \mathbf{f} + \mathbf{B}\mathbf{u}$$

In this system the control parameter is the injector duty cycle so $\mathbf{u} = [DC]$. The system states are pressure and the moles of nitrogen.

$$\mathbf{x} = \begin{bmatrix} P_{an} \\ n_{N_2} \end{bmatrix}$$

The input influence matrix, $\mathbf{B}$, comes from equation 3.6 and is given by

$$\mathbf{B} = \begin{bmatrix} \frac{P_{supply} A_{eff}}{M_W} \sqrt{\left(\frac{2}{k+1}\right)^{(k+1)/(k-1)} \left(\frac{kM_W}{RT}\right)} \\ 0 \end{bmatrix} \tag{3.12}$$

Assuming ideal gas behavior for the supply hydrogen equation 3.12 reduces to

$$\mathbf{B} = \begin{bmatrix} 0.0098 P_{supply} A_{eff} \\ 0 \end{bmatrix} \tag{3.13}$$

To get the model in the proper form to use the sliding mode controller derived in Chapter 2, the form of $\mathbf{f}$ needs to be determined. The anode model is a system of two equations therefore $\mathbf{f}$ is a 2x1 vector. All the terms not captured in the input influece matrix need to be accounted for in $\mathbf{f}$. $\mathbf{f}$ takes the form

$$\mathbf{f} = \begin{bmatrix} \frac{(\dot{n}_{perm} - \dot{n}_{cons} - \dot{n}_{or})RT}{V} \\ \dot{n}_{perm} - \dot{n}_{or} x_{N_2} \end{bmatrix} \tag{3.14}$$

Combinding equations 3.12 and 3.14 the full nonlinear model in matrix form is given by

$$\begin{bmatrix} \dot{P}_{an} \\ \dot{n}_{N_2} \end{bmatrix} = \begin{bmatrix} \frac{(\dot{n}_{perm} - \dot{n}_{cons} - \dot{n}_{or})RT}{V} \\ \dot{n}_{perm} - \dot{n}_{or} x_{N_2} \end{bmatrix} + \begin{bmatrix} C_1 \\ 0 \end{bmatrix} [DC] \tag{3.15}$$

Chapter 4

SMC Applied to the Fuel Cell Model

Preface

In this chapter the fuel cell model will be applied to the augmented sliding mode controller developed in Chapter 2. Once applied modeling uncertainties will be accounted for to ensure system tracking stability. Finally, a method for determining the magnitude of the switching gain will be developed.

4.1 Applied Sliding Mode Controller

The system model given in equation 3.15 is of the form

$$\dot{\mathbf{x}} = \mathbf{f} + \mathbf{Bu}$$

The system's input influence matrix is $\Re^{2x1}$ so a transformation matrix must be applied to the system to force it square. The transformation matrix is a $\Re^{1x2}$ vector. The resulting intermediate variable y becomes

$$y = \mathbf{Tx}$$

The above transform makes the new control variable y a scalar. Using the result from 2.29 and applying the system model the control law is given by

$$u = (\mathbf{T}\hat{\mathbf{B}})^{-1}\mathbf{T}\left[\dot{\mathbf{x}}_\mathbf{d} - \lambda\tilde{\mathbf{x}} - \hat{\mathbf{f}}\right] - K\mathbf{sat}\left(\frac{s}{\phi}\right) \tag{4.1}$$

where K, s, and ϕ are scalar, and the rest of the terms are 2x1 vectors. The K term is given by 2.25

$$K \geq |(\mathbf{TB})^{-1}\mathbf{T}|\tilde{\mathbf{f}} + |(\mathbf{TB})^{-1}|\eta + |(\mathbf{TB})^{-1}\mathbf{T} - (\mathbf{T}\hat{\mathbf{B}})^{-1}\mathbf{T}||\hat{\mathbf{f}} + \lambda\tilde{\mathbf{x}} - \dot{\mathbf{x}}_{\mathbf{d}}|$$

4.2 Handling Modeling Uncertainties

The K term is a dynamic term accounting for the maximum possible model error for a given state. The question then arises, how do we determine the maximum error for a given state? First, all unknown modeling parameters need to be determined from the system model and bounds need to be applied to them. For this system the list of unknown parameters and there bounds are given by

$$\begin{aligned}
0.6 \leq \quad & C_d & \leq 0.7 \\
3.65 \times 10^{-6} \leq \quad & H & \leq 5.56 \times 10^{-6} \\
333 \leq \quad & T & \leq 363 \\
3.63 \times 10^{-7} \leq \quad & A_{or} & \leq 4.07 \times 10^{-7} \\
2.9 \leq \quad & V & \leq 3.1 \\
900 \leq \quad & P_{supply} & \leq 1100 \\
0.7 \leq \quad & RH & \leq 1
\end{aligned}$$

The best approximation of each parameter is one that will limit the maximum error based on the above bounds. Therefore the average of the upper and lower limits will be used as the best estimate for the system controller.

$$\hat{x} = \frac{x_{upper} + x_{lower}}{2}$$

The maximum error for any given term is

$$\epsilon = x_{upper} - \hat{x} = x_{upper} - \frac{x_{upper} + x_{lower}}{2} = \frac{x_{upper} - x_{lower}}{2}$$

If $x_{upper} = 100$ and $x_{lower} = 50$ then $\hat{x} = 75$ and the max error is 25, the lowest possible if there is an equal possibility for the parameter to be off in either direction. If for some reason it is known that the parameter tend to be closer to the upper bound, for

example, then a different approach should be used to take that information into account. By defining the best estimate in this way the switching gain K will be minimized. The controller terms become

$$\begin{aligned}
\hat{C}_d &= 0.65 \\
\hat{H} &= 4.61 \times 10^{-6} \\
\hat{T} &= 348 \\
\hat{A}_{or} &= 3.85 \times 10^{-7} \\
\hat{V} &= 3 \\
\hat{P}_{supply} &= 1000 \\
\hat{RH} &= 0.85
\end{aligned}$$

From the definition in Chapter 2 of $\tilde{\mathbf{f}}$ and Δ, lets determine the worst case scenario in which the maximum error is present. Due to the form of the model if all parameters are set to the maximum value it does not necessarily indicate that $\tilde{f}$ is at its maximum. To illustrate this point lets take the error equation to be

$$G = \frac{x_1}{x_2}$$

If x_1 and x_2 are bound by x_n^{upper} and x_n^{lower} and they are both set to there maximum value then

$$G = \frac{x_1^{upper}}{x_2^{upper}}$$

This is not the maximum value. The maximum value would be

$$G = \frac{x_1^{upper}}{x_2^{lower}}$$

With this in mind lets derive $\tilde{\mathbf{f}}$ and try to identify the maximum possible error. Restating $\tilde{\mathbf{f}}$ as

$$\tilde{\mathbf{f}} = |\mathbf{f} - \hat{\mathbf{f}}|$$

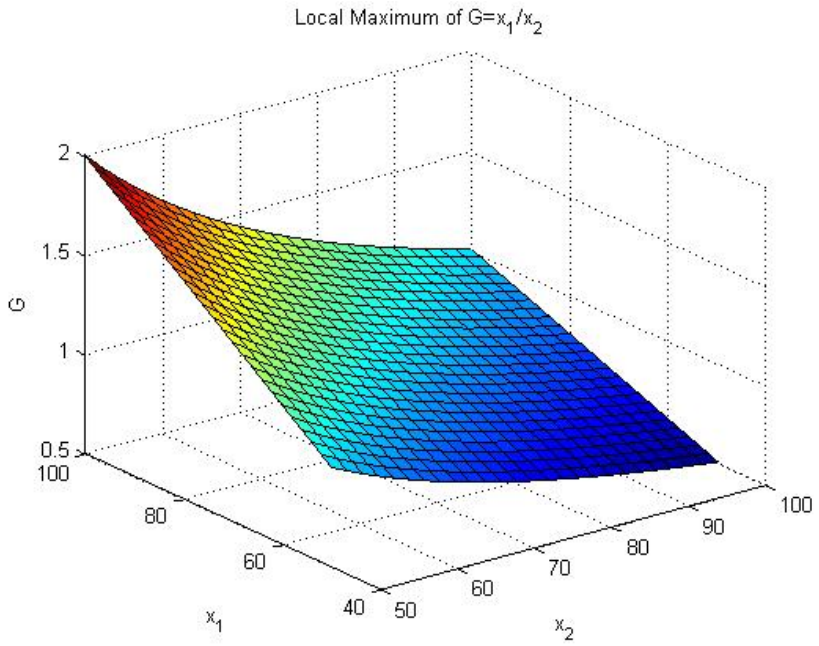

Figure 4.1: Example of Local Maximum

From 3.14 the previous equation can be rewritten as

$$\tilde{\mathbf{f}} = \left\| \begin{bmatrix} \frac{IN_{cell}RT}{2FV} - \frac{CAPRT}{VM_W}\sqrt{\frac{7M_W}{RT}\left[\left(\frac{P_2}{P_1}\right)^{1.43} - \left(\frac{P_2}{P_1}\right)^{1.71}\right]} \\ H\left(0.79P_{ca} - \frac{n_{N_2}RT}{V}\right) - \frac{CAn_{N_2}RT}{VM_W}\sqrt{\frac{7M_W}{RT}\left[\left(\frac{P_2}{P_1}\right)^{1.43} - \left(\frac{P_2}{P_1}\right)^{1.71}\right]} \end{bmatrix} \right.$$
$$\left. - \begin{bmatrix} \frac{IN_{cell}R\hat{T}}{2F\hat{V}} - \frac{\hat{C}\hat{A}PR\hat{T}}{\hat{V}\hat{M}_W}\sqrt{\frac{7\hat{M}_W}{R\hat{T}}\left[\left(\frac{P_2}{P_1}\right)^{1.43} - \left(\frac{P_2}{P_1}\right)^{1.71}\right]} \\ \hat{H}\left(0.79P_{ca} - \frac{n_{N_2}R\hat{T}}{\hat{V}}\right) - \frac{\hat{C}\hat{A}n_{N_2}R\hat{T}}{\hat{V}\hat{M}_W}\sqrt{\frac{7\hat{M}_W}{R\hat{T}}\left[\left(\frac{P_2}{P_1}\right)^{1.43} - \left(\frac{P_2}{P_1}\right)^{1.71}\right]} \end{bmatrix} \right\|$$

Simplifying the first equation above leads to

$$\tilde{f}_1 = \left| \frac{IN_{cell}R}{2F}\left(\frac{\hat{T}}{\hat{V}} - \frac{T}{V}\right) - 7.63P_1\sqrt{\left(\frac{P_2}{P_1}\right)^{1.43} - \left(\frac{P_2}{P_1}\right)^{1.71}}\left(\frac{\hat{C}\hat{A}\hat{T}}{\hat{V}\hat{M}_W} - \frac{CAT}{VM_W}\right) \right| \quad (4.2)$$

From this result it is clear that just setting all the terms to there maximum value is not

going to lead to the maximum value for the system. Taking a close look at equation 4.2 the same variables tend to be in the numerator and the denominator. For example, the volume always shows up in the denominator therefore it makes sense to set the volume to its lower limit to maximize that term. Lets look at the second equation to see if this theory holds up.

$$\tilde{f}_2 = \left| 0.79 P_{ca}(H - \hat{H}) - n_{N_2} R \left(\frac{\hat{H}\hat{T}}{\hat{V}} - \frac{HT}{V} \right) \right.$$
$$\left. - 63.43 n_{N_2} \sqrt{\left(\frac{P_2}{P_1}\right)^{1.43} - \left(\frac{P_2}{P_1}\right)^{1.71}} \left(\frac{\hat{A}\sqrt{\hat{T}}\hat{C}}{\hat{V}\sqrt{\hat{M}_W}} - \frac{A\sqrt{T}C}{V\sqrt{M_W}} \right) \right|$$

The same type of result is obtained in this equation. The volume term always shows up in the denominator while the orifice area is always in the numerator. The only difficult term to deal with is temperature. The temperature shows up in the numerator and also in the denominator because it affects the amount of water the gas stream can hold and therefore affects the molecular weight of the gas stream. Analyzing the effect of temperature on the $\tilde{\mathbf{f}}$ term shows that the hydrogen consumption term tends to dominate f_1 and because of the relative magnitude of f_1 compared to f_2 the molecular weight only becomes dominate for very large values of T_2. Applying this information set the following variables

$$\begin{aligned} C_d &= 0.7 \\ H &= 5.56 \times 10^{-6} \\ T &= 363 \\ A_{or} &= 4.07 \times 10^{-7} \\ V &= 2.9 \\ RH &= 70 \end{aligned}$$

The same type of analysis is necessary to determine the value of Δ. Δ is multiplied by the $\hat{\mathbf{B}}$ to determine the maximum error correction. Since Δ is multiplied into $\hat{\mathbf{B}}$ it must represent the maximum error ratio that will be seen by the system. The only parameter that is unknown in $\mathbf{B}$ is the hydrogen supply pressure. Therefore,

$$\Delta = \frac{\hat{P_{supply}}}{P_{supply}^{min}}$$

Defining Δ in this manner will lead to the maximum value of K for all bounded unknowns. Now that $\tilde{\mathbf{f}}$ and Δ have been defined for the parametric uncertainty in the control model the sliding mode controller can be simulated.

Chapter 5

Results

5.1 Choice of Transformation Matrix

The transformation matrix, $\mathbf{T}$, is used as a mapping function to force the systems $\mathbf{B}$ matrix to be square. The objective is achieved by choosing $\mathbf{T}$ to be the proper size. This concept was introduce in chapter 2. The question now is how to choose the values for each element in $\mathbf{T}$ and how will it affect the tracking of the system states? To understand the effect of the $\mathbf{T}$ matrix on system tracking, redefine the system model from 2.10

$$\dot{\mathbf{y}} = \mathbf{T}\dot{\mathbf{x}} = \begin{bmatrix} T_1 & T_2 \end{bmatrix} \begin{bmatrix} f_1 \\ f_2 \end{bmatrix} + \begin{bmatrix} T_1 & T_2 \end{bmatrix} \begin{bmatrix} f_1 \\ f_2 \end{bmatrix} u \tag{5.1}$$

Since there are two states to track in the fuel cell system and only one actuator the system is underactuated. Expanding equation 5.1 results in

$$\dot{\mathbf{y}} = T_1 f_1 + T_2 f_2 + (T_1 B_1 + 0 \cdot T_2) u \tag{5.2}$$

From this result it is obvious to see that T_1 is a multiplier on state one and T_2 is a multiplier on state two. It follows that to make state one dominate a high gain for T_1 is needed and to make state two dominate a high gain for T_2 is required. The term "high gain" is somewhat arbitrary. What is a "high gain"? To determine this, a good understanding of the system is needed. For the fuel cell system state one is system pressure in kPa and state two is the number of moles of nitrogen.

$$\begin{aligned} P &= 100 - 200 \quad kPa \\ n_{N_2} &= 0.1 - 0.2 \quad mol \end{aligned}$$

For the fuel cell system state one will have typical values in the 100-200 range while state two will have typical values in the 0.1 0.2 range. This means that if $T_1 = T_2$ then pressure will be heavily weighted by a factor of about 1000:1. Therefore, to make the controller weight the states evenly $T_2 \approx 1000T_1$. So for T_1 a high gain is achieved by setting $T_1 = T_2$, while for T_2 a high gain would be considered $1,000,000T_1$.

The magnitude of the gain for $\mathbf{T}$ is well understood from the previous discussion but what about the sign? What determines if T_1 and T_2 are positive or negative? The answer to that is found in the definition of the controller and some fundamental understanding of the system model. First, redefine the sliding mode controller from equation 2.29.

$$u = (\mathbf{T}\hat{\mathbf{B}})^{-1}\mathbf{T}\left[\dot{\mathbf{x}}_\mathbf{d} - \lambda\tilde{\mathbf{x}} - \hat{\mathbf{f}}\right] - K\mathbf{sgn}\,(s)$$

Where $\tilde{x}$ is defined by

$$\tilde{\mathbf{x}} = \begin{bmatrix} P \\ n_{N_2} \end{bmatrix} - \begin{bmatrix} P_{SP} \\ n_{N_2SP} \end{bmatrix} \tag{5.3}$$

Starting with pressure if $P > P_{SP}$ then $\tilde{x}_1$ is positive and because of the negative sign in front of that term u will be reduced if T_1 is positive. This is the correct result for this situation. To decrease the pressure in the system the injector duty cycle needs to decrease to supply less hydrogen flow and therefore reduce the pressure. Applying the same logic to the nitrogen term, if $n_{N_2} > n_{N_2SP}$ then $\tilde{x}_2$ is positive and if T_2 is positive it would say to decrease the injector duty cycle. This is the wrong result for this case. To reduce nitrogen it has to leave the exhaust orifice. To increase the flow rate through that orifice the pressure must to be increased, therefore the duty cycle must increase. To get the right dynamics out of the controller $T_1 > 0$ and $T_2 < 0$.

For this work, $\mathbf{T}$ will be chosen arbitrarily using the above methodology to show the effect that it has on the tracking performance of each state. More involved ways for choosing $\mathbf{T}$ could be developed using optimal control theory but these methods are beyond the scope of this work and are suggested as future work to make the choice of $\mathbf{T}$ for larger systems less tedious.

5.2 SMC with Sign Function

The augmented sliding mode controller was first tested using the pure signum function on the K term. The sliding mode controller used in the following analysis is given by

$$u = (\mathbf{T}\hat{\mathbf{B}})^{-1}\mathbf{T}\left[\dot{\mathbf{x}}_\mathbf{d} - \lambda\tilde{\mathbf{x}} - \hat{\mathbf{f}}\right] - K\mathbf{sgn}\,(s)$$

A full characterization of the controller is done using the following values to show the controllers robustness to modeling uncertainties and also its flexibility in tracking the desired states.

Table 5.1: Tested Operating Points

T_1	T_2	Δ_p
1	-1	0.5
1	-1000000	0.5
10	-10000	0.5
1	-6000	0.5
1	-1	1
1	-1000000	1
10	-10000	1
1	-6000	1
1	-1	0
1	-1000000	0
10	-10000	0
1	-6000	0
1	-1	0.25
1	-1000000	0.25
10	-10000	0.25
1	-6000	0.25
1	-1	0.75
1	-1000000	0.75
10	-10000	0.75
1	-6000	0.75

5.2.1 Varying T with a Perfect Plant Model

The analysis will start with the case where the plant and controller models are perfectly matched. This is an impractical case but should be the easiest to control. The response for the case where $\mathbf{T} = [1 \quad -1]$ is shown in Figure 5.1.

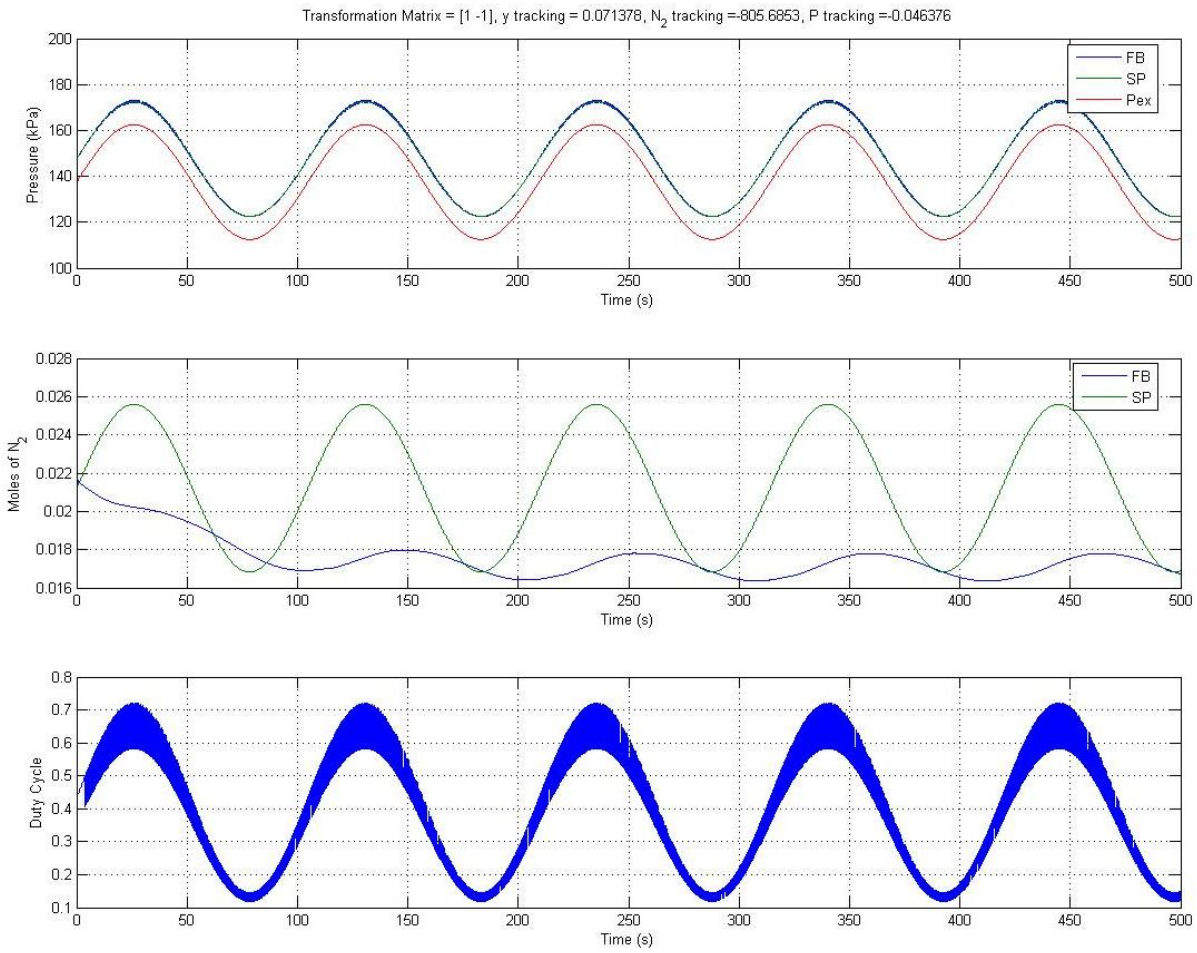

Figure 5.1: Tracking Performance for $\mathbf{T} = [1 \quad -1]$ and $\Delta_p = 0.5$

The first graph shows the system pressure tracking. Perfect pressure tracking is established for the reason given in section 5.1. However, the perfect pressure tracking comes at the expense of nitrogen control. The nitrogen tracking is shown in the second graph and is ignored by the controller in favor of pressure control. Finally, the control effort is shown in the third graph and the controller shows very noticeable chattering which is expected due to the signum function. The signum function forces the controller to switch between the maximum and minimum values of K in order to account for modeling uncertainties. Even in this case where there was no difference between the model and the controller there is significant chatter between the two states.

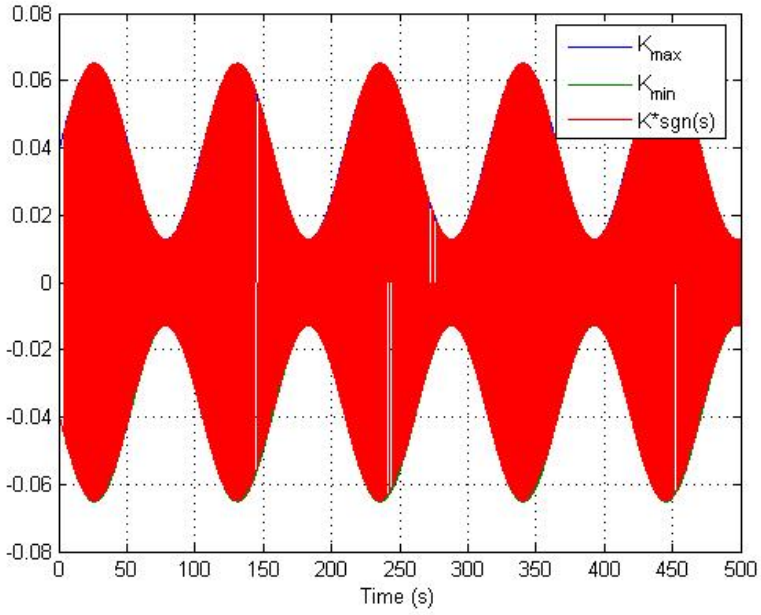

Figure 5.2: K Term for $\mathbf{T} = [1 \quad -1]$ and $\Delta_p = 0.5$

Figure 5.2 shows the response of the K term for the above simulation. The chattering in the control effort can be seen in this term which indicates that the signum function is causing the chattering. The next section will look at eliminating the chattering by modifying the K term.

Figure 5.1 shows the tracking of each individual state but the controller is not designed to track either of those states specifically. The controller is designed to perfectly track y which can correlate well to either state depending on how T is chosen. Figure 5.3 shows that y is perfectly controlled for these condition. This will always be the case as long as the controller has enough bandwidth to overcome the modeling uncertainties. To

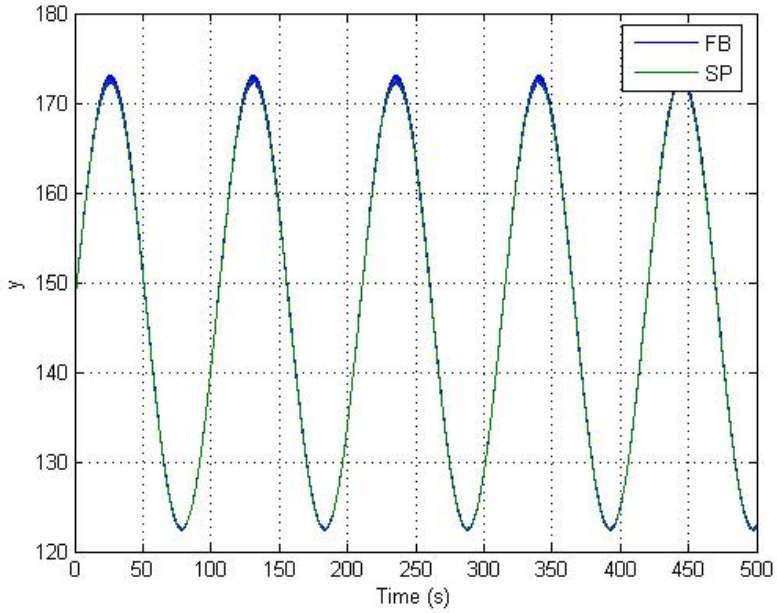

Figure 5.3: y Tracking for $\mathbf{T} = [1 \quad -1]$ and $\Delta_p = 0.5$

quantify the tracking error for each of the cases the following are calculated and displayed on the tracking graph for reference.

$$y_{error} = \int \left(\frac{y - y_d}{y_d} \right) dt \tag{5.4}$$

$$P_{error} = \int \left(\frac{P - P_{SP}}{P_{SP}} \right) dt \tag{5.5}$$

$$n_{N_2error} = \int \left(\frac{n_{N_2} - n_{N_2SP}}{n_{N_2SP}} \right) dt \tag{5.6}$$

The errors are normalized to eliminate scaling issues and give a better estimate of the tracking performance. Setting $\mathbf{T} = [1 - 1000000]$ is the next case that will be evaluated. From earlier discussion one would expect this case to provide perfect nitrogen tracking with little pressure control.

From Figure 5.4 it is obvious that the nitrogen control is greatly improved and perfect tracking is achieved. The pressure control has suffered with it varying from below setpoint, to build nitrogen, to above setpoint, to remove nitrogen from the system. The control law is modifying the pressure to control the nitrogen content. The third graph still demonstrates the control effort which shows significant chatter with this control law.

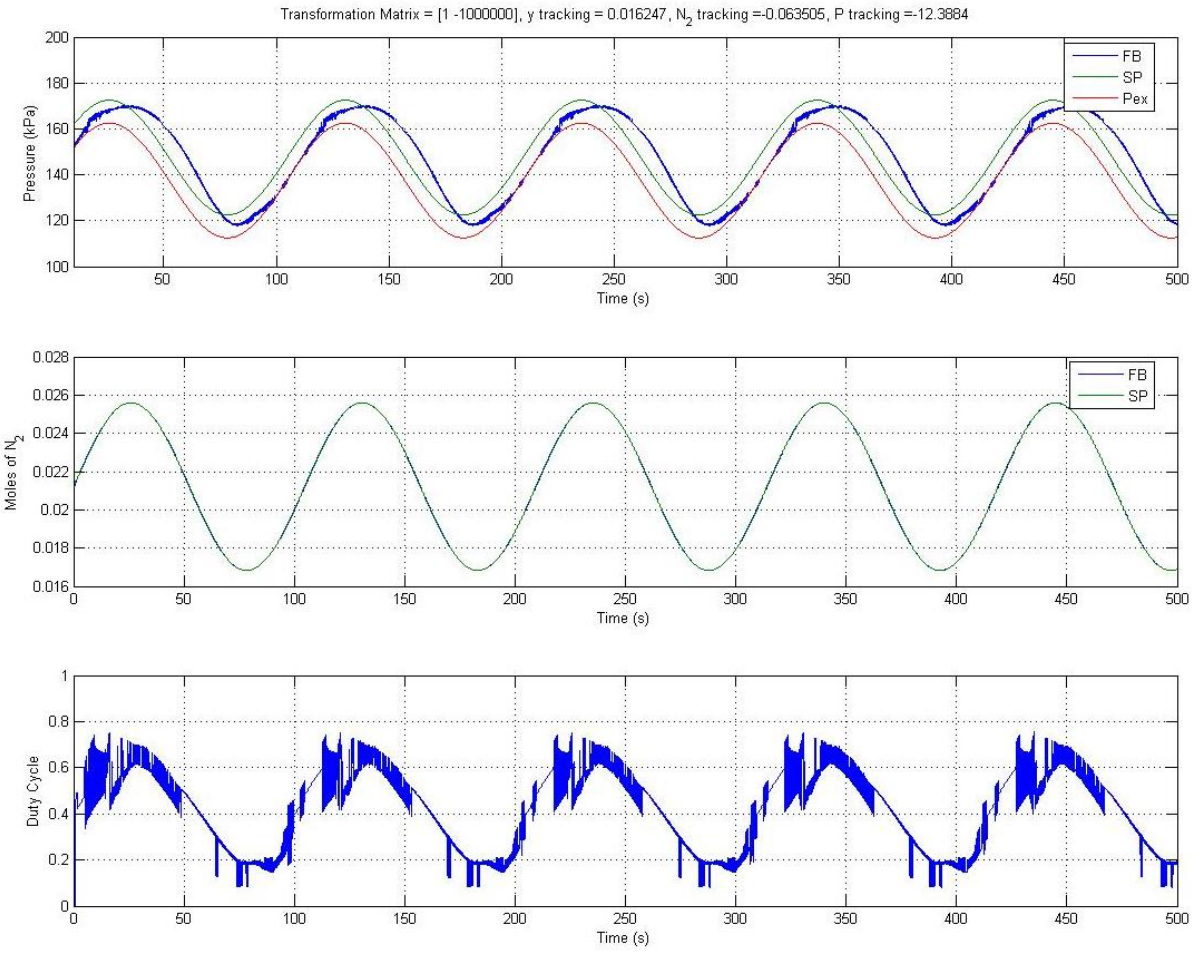

Figure 5.4: Tracking Performance for $\mathbf{T} = [1 \quad -1000000]$ and $\Delta_p = 0.5$

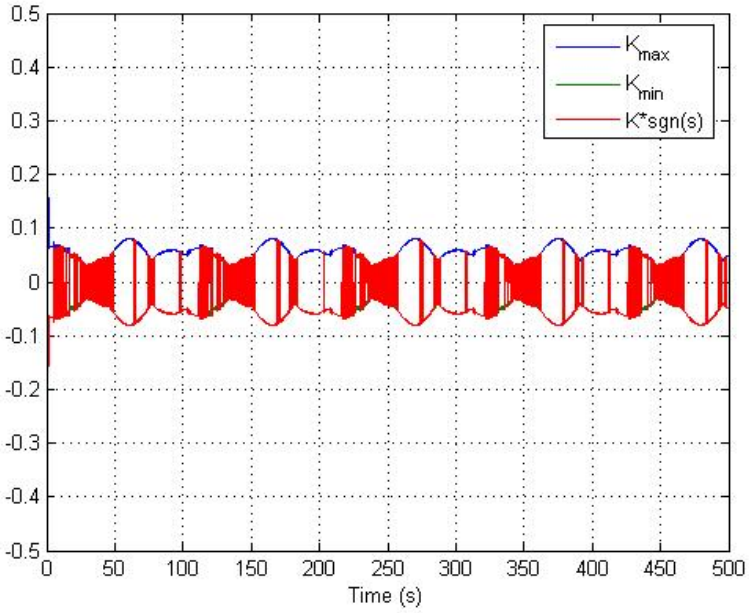

Figure 5.5: K Term for $\mathbf{T} = [1 \quad -1000000]$ and $\Delta_p = 0.5$

Figure 5.5 shows the response of the K term for the above simulation. Comparing Figure 5.2 and 5.5 there is a noticeable difference in the shape of the bounds between the two cases. Both cases were run with the same inputs the only difference is the weighting of each state. The current example shows how state dependent the robustness term is. Again a significant amount of chattering is observed which can be contributed to the signum function.

What does the controller response look like if each state is equally weighted? This case is demonstrated with $\mathbf{T} = [1 - 6000]$. Based on our previous discussion this should give similar error between the two states.

From Figure 5.6 setting the transformation matrix this way forces the controller into not tracking either state perfectly but tracking each state with similar error. This is quantified by the P_{error} and n_{N_2error} terms. For this simulation they are 4.03 and 4.05 respectively. The result is close to the one to one ratio that was expected. It is highly desirable to understand the interaction between setting values of $\mathbf{T}$ and how that effects the controller output. The following ratio function is proposed to give meaning to $\mathbf{T}$

$$T_{ratio} = \frac{C_1 T_1}{abs(T_2)} \tag{5.7}$$

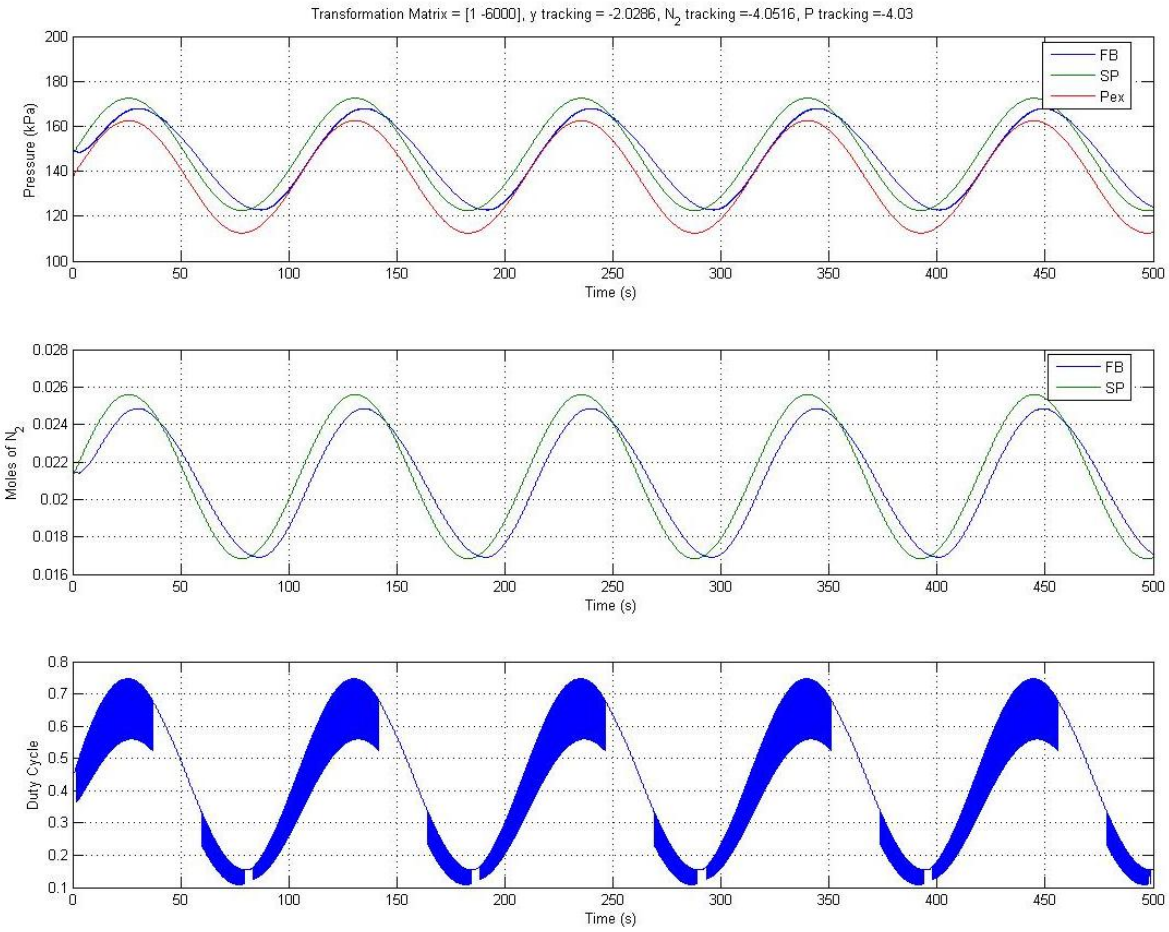

Figure 5.6: Tracking Performance for $\mathbf{T} = [1 \quad -6000]$ and $\Delta_p = 0.5$

where the C_1 is determined based on the given system. It is basically a ratio of the pressure over the moles of nitrogen at a given operating point.

$$C_1 = \frac{P}{n_{N_2}} \approx 6000$$

C_1 is a type a correction factor which is needed because the magnitude of the two states differ so significantly. If, for example, the system consisted of two separate pressure states then $C_1 = 1$ because the state magnitude would match up well. It is convenient to try to compare T_{ratio} to a ratio of the response errors given by

$$ResponseErrorRatio = \frac{n_{error}}{P_{error}} \tag{5.8}$$

where $n_{N2error}$ and P_{error} are given by equation 5.5 and 5.6 respectively. Figure 5.7 shows the actual simulation results compared to the ideal case. The main point to take away from this graph is that as the ratio of T_1 to T_2 is increased there is a predictable shift from controlling state two to state one. This result is an important point because it gives some guidelines for the engineer to be able to select gains and obtain a predictable result.

5.2.2 Varying Plant Parameters

The previous cases evaluated the controller performance for various transformation matrices when the controller and plant parameters matched perfectly. This section will evaluate the controllers stability when the plant and controller model differ. This is typically the case in any real world application and is the main reason for choosing SMC over other control algorithms. The following examples will be chosen at different parameter points. The parameter differences are chosen using the following equation.

$$PlantParameter = \Delta_p \cdot upperbound + (1 - \Delta_p) \cdot lowerbound \tag{5.9}$$

where Δ_p is the parameter difference and must be a value between 0 and 1. For the plant parameters to match the control parameter $\Delta_p = 0.5$. This is in line with the definition from Chapter 4 that the controller assumes all parameters are equal to the average of their upper and lower bound values. Table 5.2 shows the cases that will be run to assess the controller robustness to parameter variation.

The first case that will be evaluated is $\Delta_p = 0$. This is equivalent to setting all the

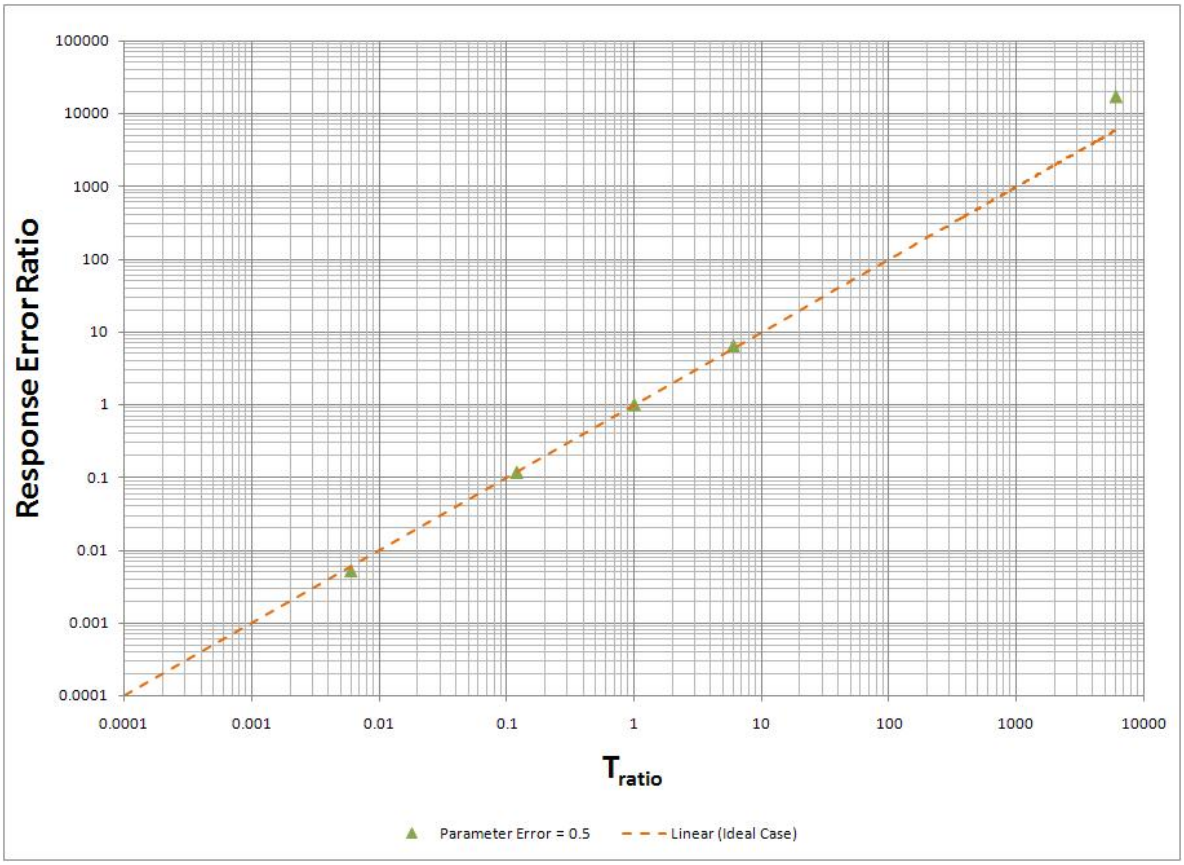

Figure 5.7: Effect of Varying $\mathbf{T}$ on System Response

Table 5.2: Tested Operating Points with Modeling Error

T_1	T_2	Δ_p
1	-1	1
1	-1000000	1
1	-1	0
1	-1000000	0
1	-1	0.25
1	-1000000	0.25
1	-1	0.75
1	-1000000	0.75

plant parameters to their minimum values. Setting $\Delta_p = 0$ is not a realistic case but it will test the limits of the controller. For each case perfect tracking of both nitrogen and pressure will be evaluated. If perfect tracking of both states is achievable then it is assumed that any combination in-between will also be achievable.

The system response for the example where $T = [1 \quad -1]$ with $\Delta_p = 0$ can be seen in Figure 5.8. Perfect tracking is again achieved for the pressure controller. Perfect tracking is the same result that was obtained when $\Delta_p = 0.5$. This result shows that the controller has adequate bandwidth to maintain pressure control as well as stability even with large modeling errors. One interesting note is that the chatter has been significantly reduced for this case. The reduced chatter can be explained because now that the plant parameters are at there minimum value the controller has to spend more time at its extremes to maintain proper tracking. This result indicated that if the plant parameters were decreased any further then the controller may not be able to provide the proper tracking. $\Delta_p = 0$ is the lower limit for the controller.

For the next example let $T = [1 \quad -1000000]$. This case should give perfect nitrogen control even with the modelling errors. The response for this case can be seen in Figure 5.9. Again perfect nitrogen control and system stability is achieved.

The next case that will be evaluated is the case where $\Delta_p = 1$. This is equivalent to setting all the plant parameters to their maximum values. This again is not a realistic case but it will test the limits of the controller. For each case perfect tracking of both nitrogen and pressure will be evaluated. If perfect tracking of both states is achievable then it is assumed that any combination in-between will also be achievable.

The system response for the example where $T = [1 \quad -1]$ with $\Delta_p = 1$ can be seen in Figure 5.10. Perfect tracking is again achieved for the pressure controller. Perfect

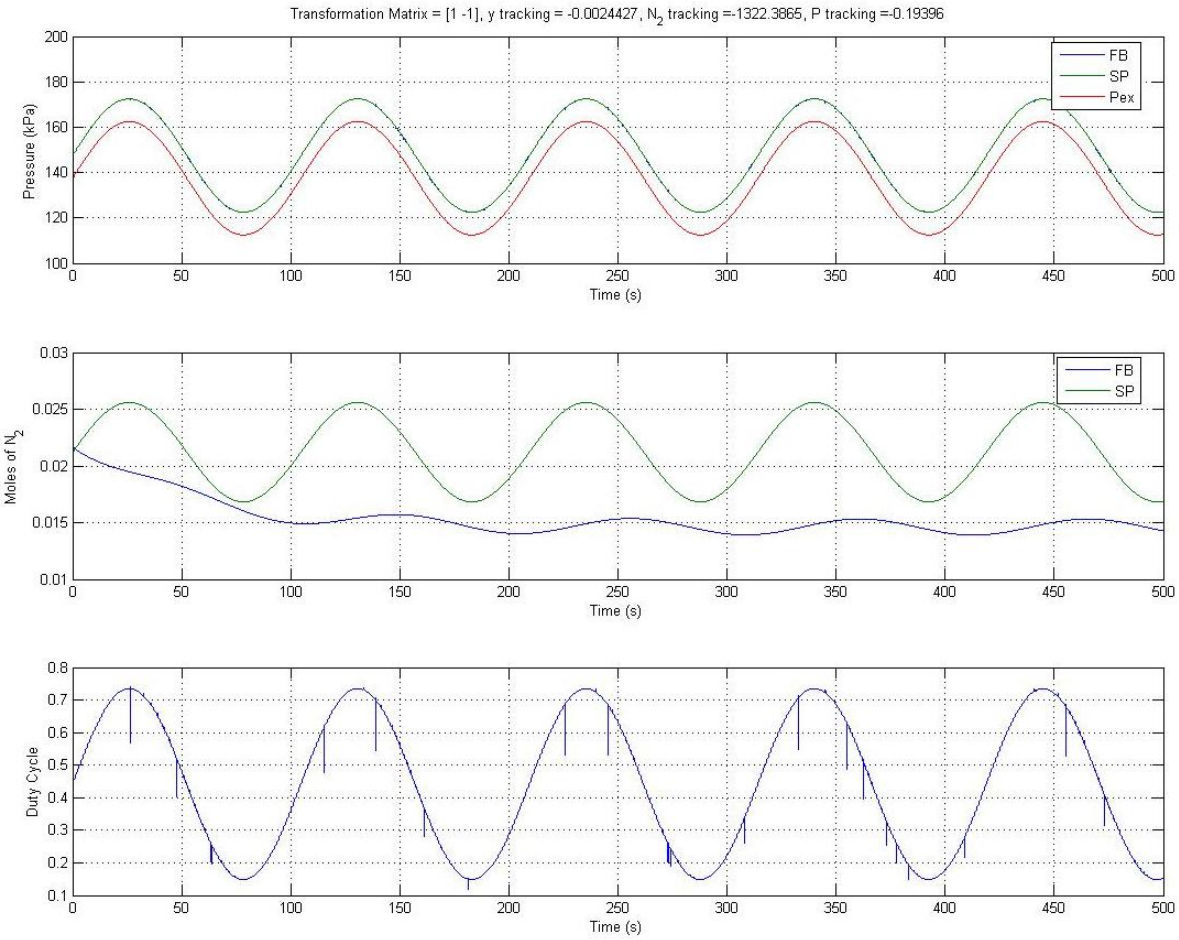

Figure 5.8: Tracking Performance for $\mathbf{T} = [1 \quad -1]$ and $\Delta_p = 0$

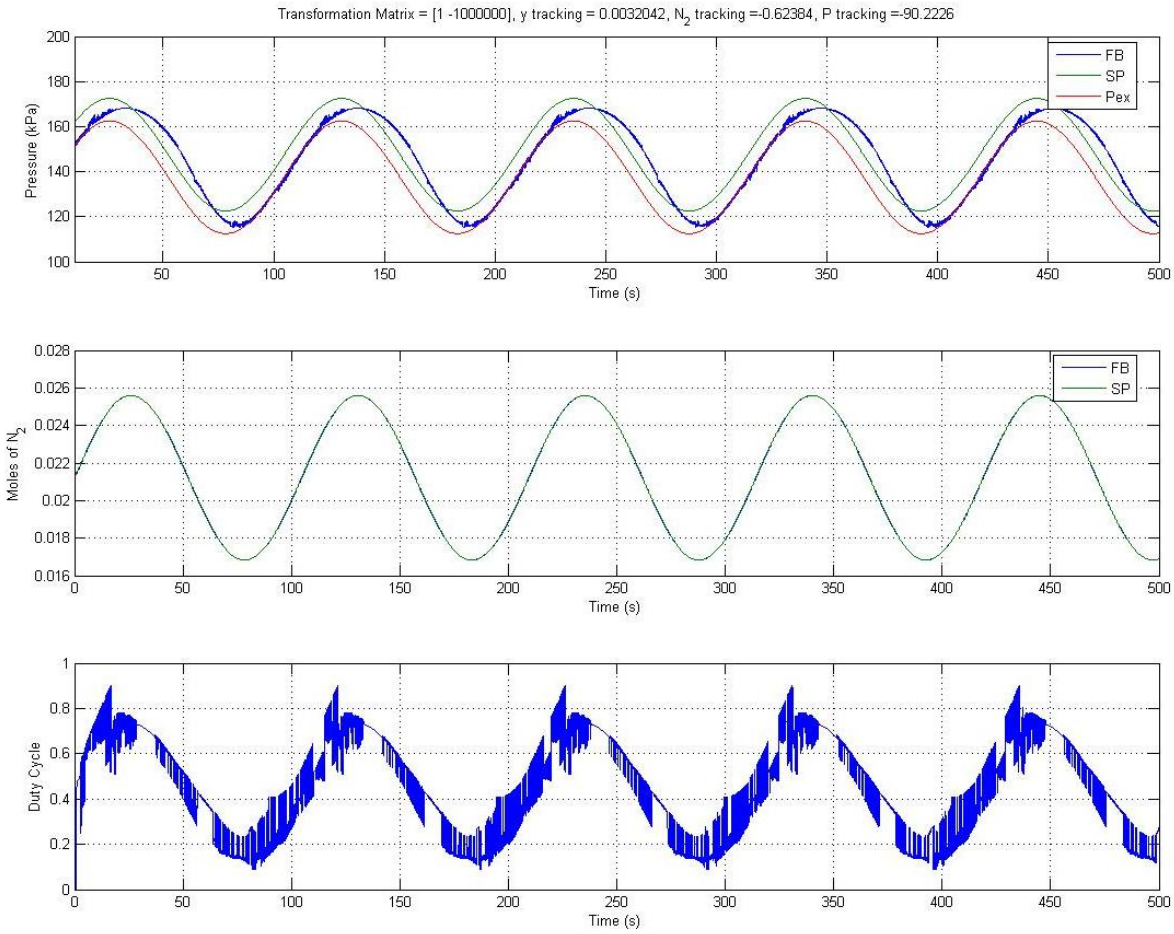

Figure 5.9: Tracking Performance for $\mathbf{T} = [1 \quad -1000000]$ and $\Delta_p = 0$

tracking is the same result that was obtained when $\Delta_p = 0.5$ and $\Delta_p = 0$. This shows that the controller has adequate bandwidth to maintain pressure control as well as stability. From the third graph, there is still a large amount of chatter within the control law which indicates that the controller has significant bandwidth left. The added bandwidth indicates that this case is not as extreme as the previous one. Setting $\Delta_p = 0$ is more difficult to control than setting $\Delta_p = 1$.

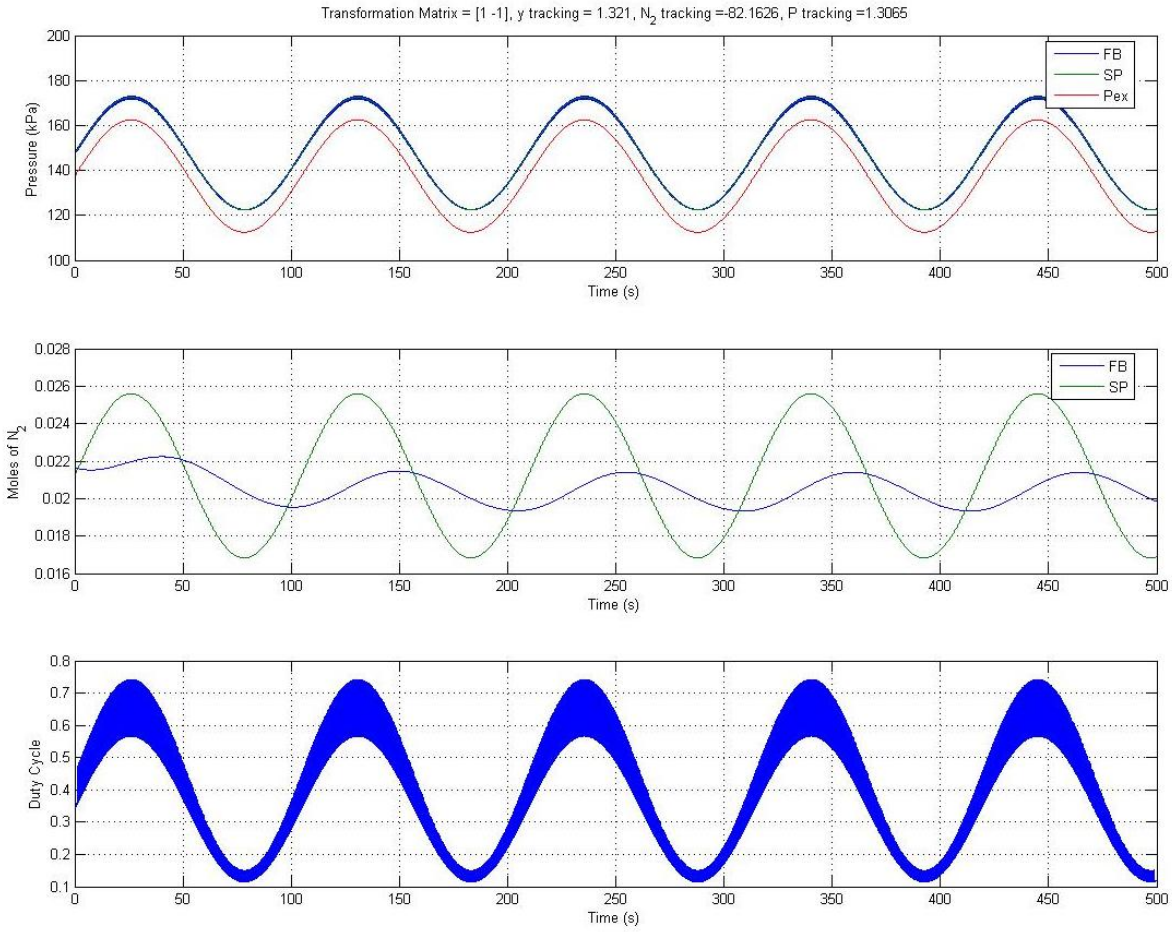

Figure 5.10: Tracking Performance for $\mathbf{T} = [1 \quad -1]$ and $\Delta_p = 1$

For the next example let $T = [1 \quad -1000000]$. This case should give perfect nitrogen control even with the modeling errors. The response for this case can be seen in Figure 5.11. Again perfect nitrogen control and system stability is achieved.

From the results of the previous two cases it is safe to say that within the limits that the controller was designed for it is able to maintain stability and tracking performance. A few other cases were run to prove this point and are given in Table 5.2. To summarize

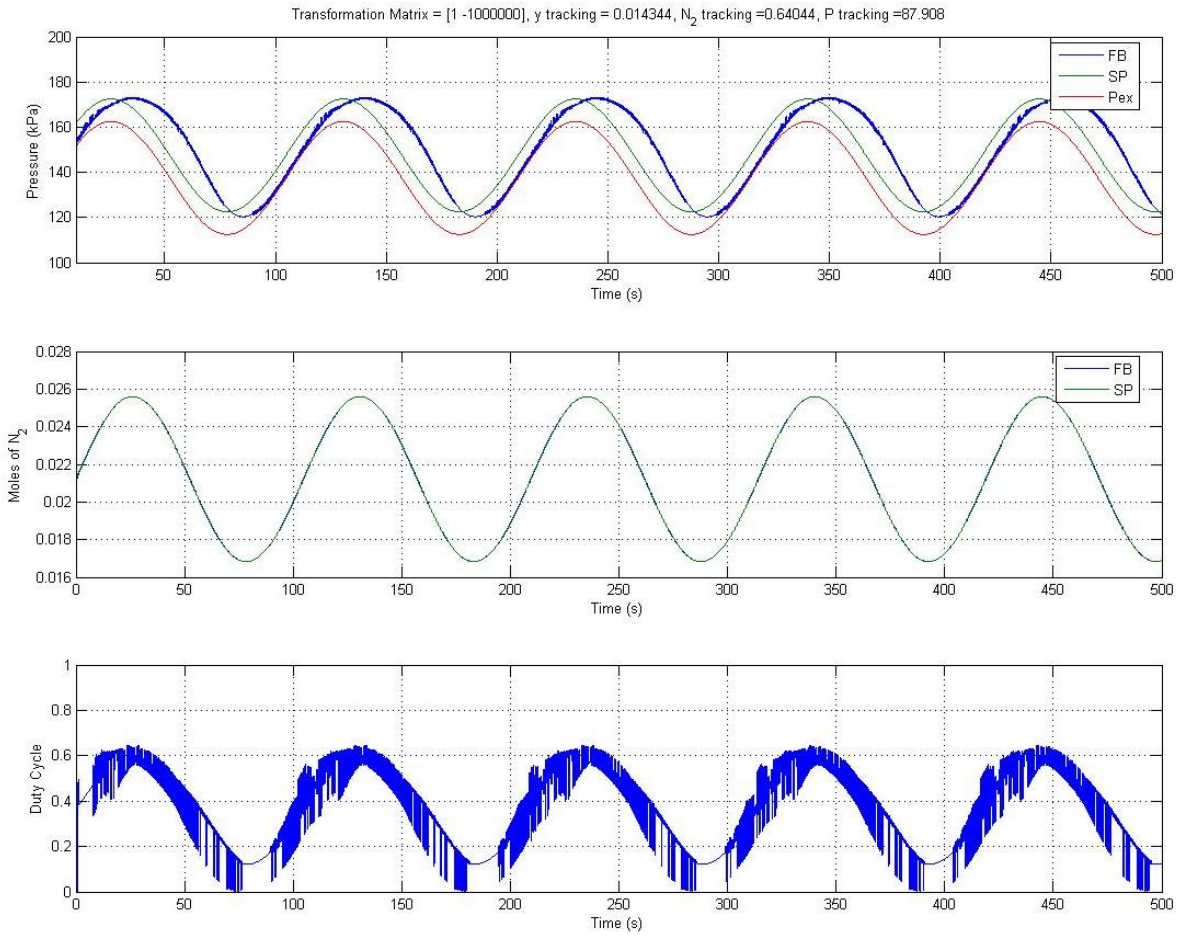

Figure 5.11: Tracking Performance for $\mathbf{T} = [1 \quad -1000000]$ and $\Delta_p = 1$

the results of these simulations in a compact manner a similar approach was taken as shown in Figure 5.7.

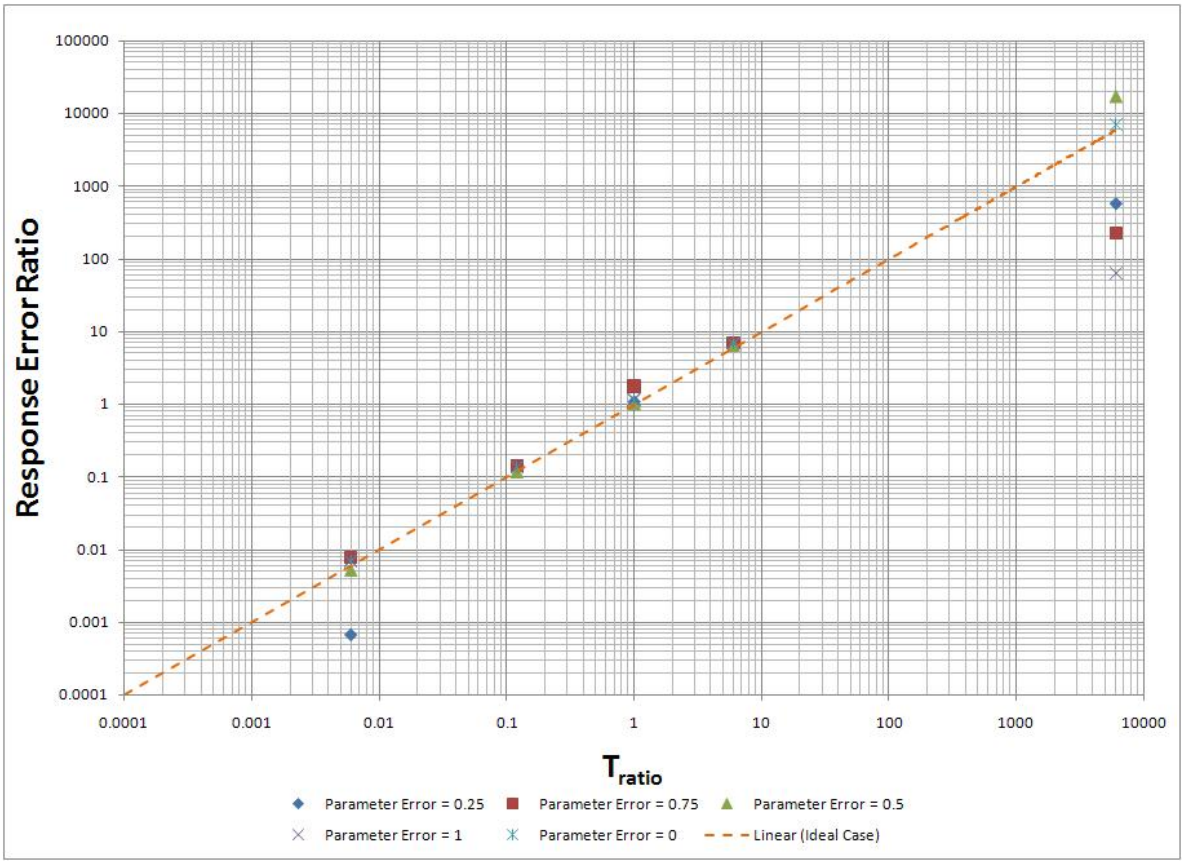

Figure 5.12: Effect of Varying **T** on System Response

Figure 5.12 shows all the cases overlaid and compared to the ideal case. For the most part all the cases agree well with the ideal case which means that the controller is acting as expected for those cases. On the extreme cases the error between runs becomes much more pronounced. This is an artifact of the method more than anything. For high accuracy pressure and nitrogen control one of the error terms becomes very small. Therefore the ratio becomes very sensitive to small changes in that parameter from run to run. When inspecting the actual tracking performance no difference is visible.

5.3 SMC with Saturation Function

In this section the sign term within the sliding mode controller will be replaced with a saturation term with boundary layer to try to reduce the unwanted high frequency

chattering that was observed in the previous section. The sliding mode controller used in the following analysis is given by

$$u = (\mathbf{T}\hat{\mathbf{B}})^{-1}\mathbf{T}\left[\dot{\mathbf{x}}_\mathbf{d} - \lambda\tilde{\mathbf{x}} - \hat{\mathbf{f}}\right] - K\mathbf{sat}\left(\frac{s}{\phi}\right)$$

where ϕ is a small positive number. For the following anaylsis ϕ was set equal to 0.00001.

5.3.1 Tracking Comparision

It is important to make sure that this modification to the control law does not adversely affect the tracking performance of the system. The first thing to check is that for the same transformation matrices the same tracking performance is achieved. This section will compare the tracking results for $\Delta_p = 0$ and 1 and the transformation matrix setup for perfect pressure and nitrogen control. The assumption here is that if the controller is capable of adequate performance at its limits then the performance will only get better as the conditions are brought closer to the average.

The first case that will be evaluated is $\Delta_p = 0$. This is equivalent to setting all the plant parameters to their minimum values. For each case perfect tracking of both nitrogen and pressure will be evaluated.

The system response for the example where $T = [1 \quad -1]$ with $\Delta_p = 0$ can be seen in Figure 5.15. Perfect tracking is again achieved for the pressure controller. This is the same result that was obtained when using the sign function. The control effort in the third graph is much smoother with no discontinuities. This will be evaluated more fully in the next section.

For the next example let $T = [1 \quad -1000000]$. This case should give perfect nitrogen control even with the modeling errors. The response for this case can be seen in Figure 5.14. Again perfect nitrogen control and system stability is achieved.

The next case that will be evaluated is the case where $\Delta_p = 1$. This is equivalent to setting all the plant parameters to their maximum values. For each case perfect tracking of both nitrogen and pressure will be evaluated.

The system response for the example where $T = [1 \quad -1]$ with $\Delta_p = 1$ can be seen in Figure 5.15. Perfect tracking is again achieved for the pressure controller. This again shows that the controller has adequate bandwidth to maintain pressure control as well as stability. The effect of changing the plant parameters is evident when comparing the second graph in Figure 5.13 to the second graph in Figure 5.15. In both examples perfect

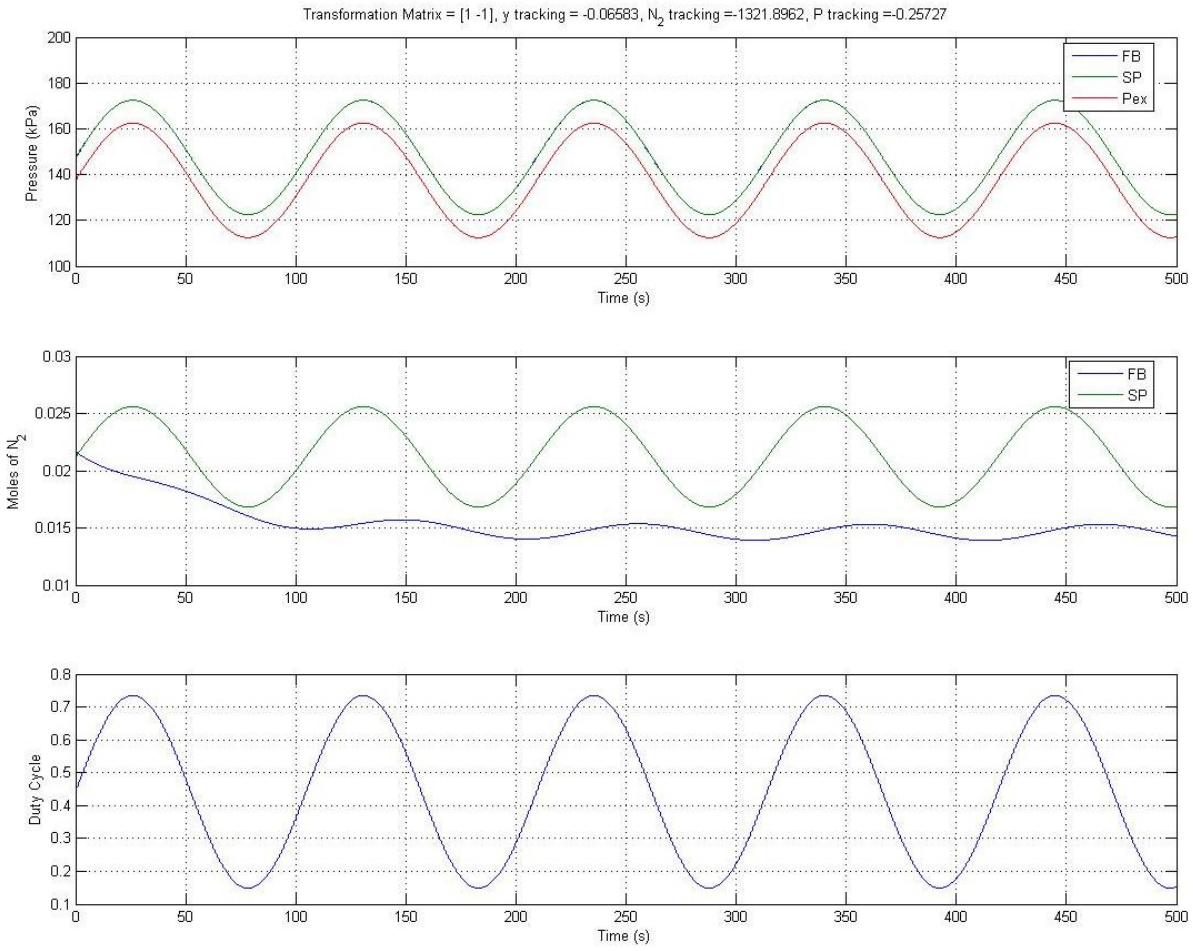

Figure 5.13: Saturation Tracking Performance for $\mathbf{T} = [1 \quad -1]$ and $\Delta_p = 0$

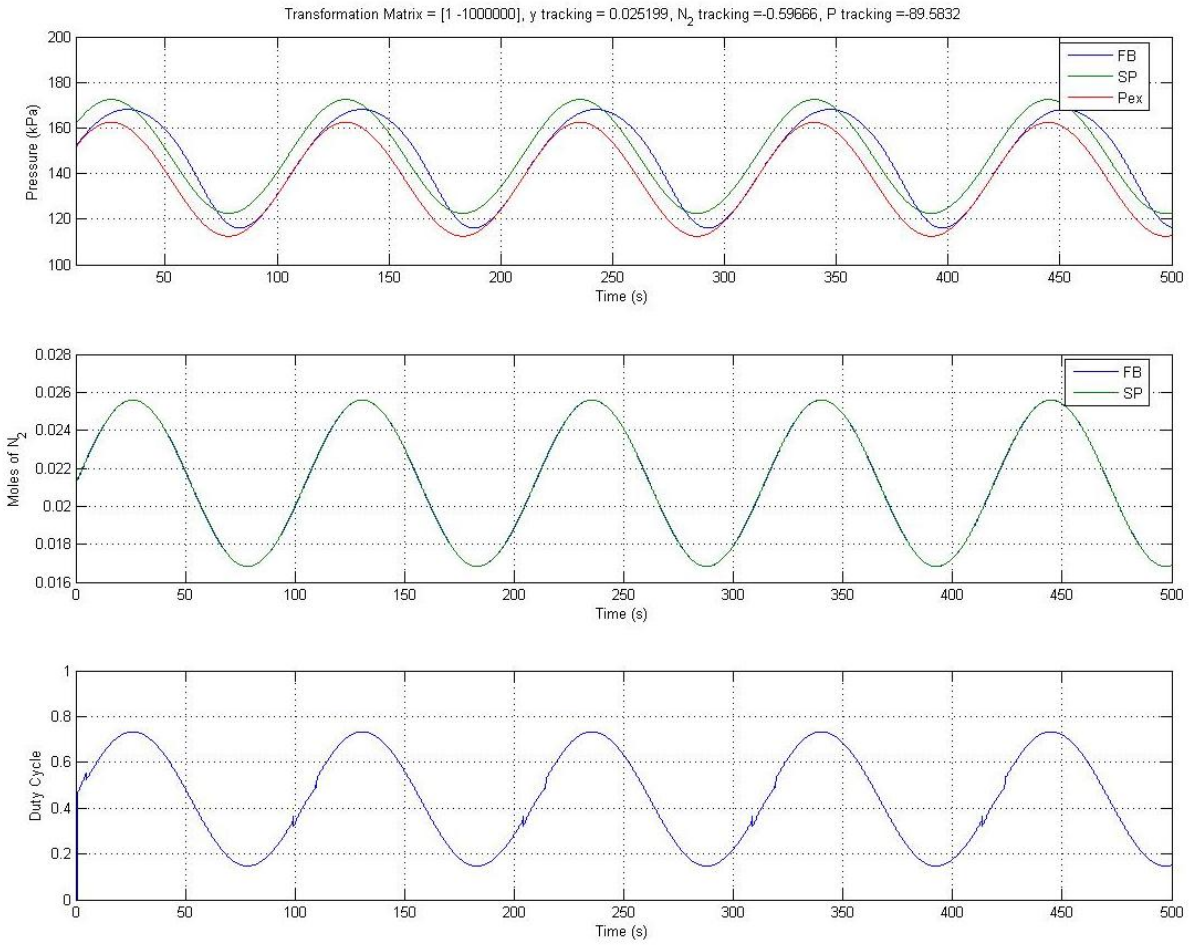

Figure 5.14: Saturation Tracking Performance for $\mathbf{T} = [1 \quad -1000000]$ and $\Delta_p = 0$

pressure control is achieved however and the setpoint is exactly the same. However the nitrogen content that the system settles out at is totally different. This is a direct effect of the plant parameters being varied.

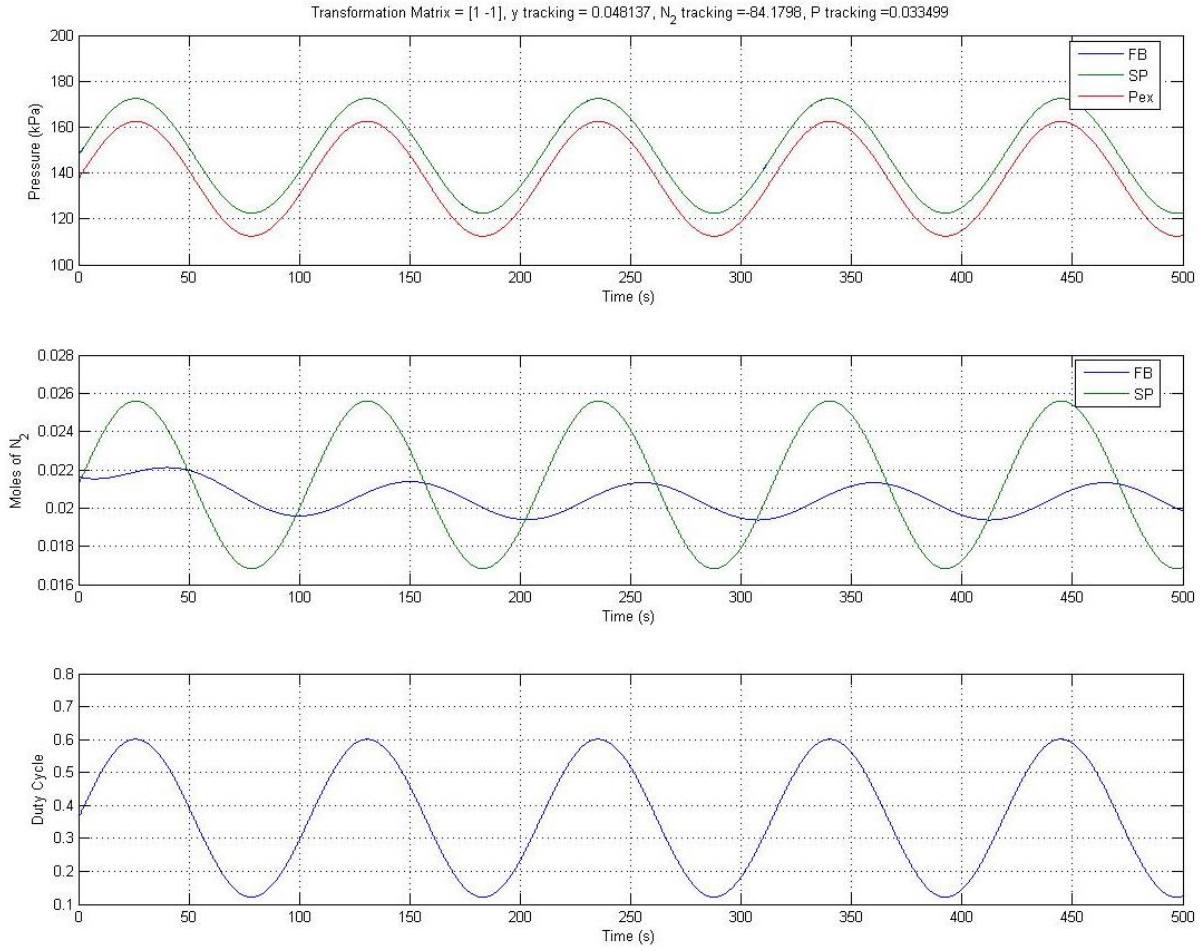

Figure 5.15: Saturation Tracking Performance for $\mathbf{T} = [1 \quad -1]$ and $\Delta_p = 1$

For the next example let $T = [1 \quad -1000000]$. This case should give perfect nitrogen control even with the modeling errors. The response for this case can be seen in Figure 5.16. Again perfect nitrogen control and system stability is achieved.

By using the same technique used in the previous section to quantify tracking performance a direct comparison can be drawn between the two controllers. Figure 5.17 shows the tracking performance for all the same cases that were run for the first controller. A very similar result is obtained from this type of analysis. This means that the saturation function can be used with little to no loss of controller performance.

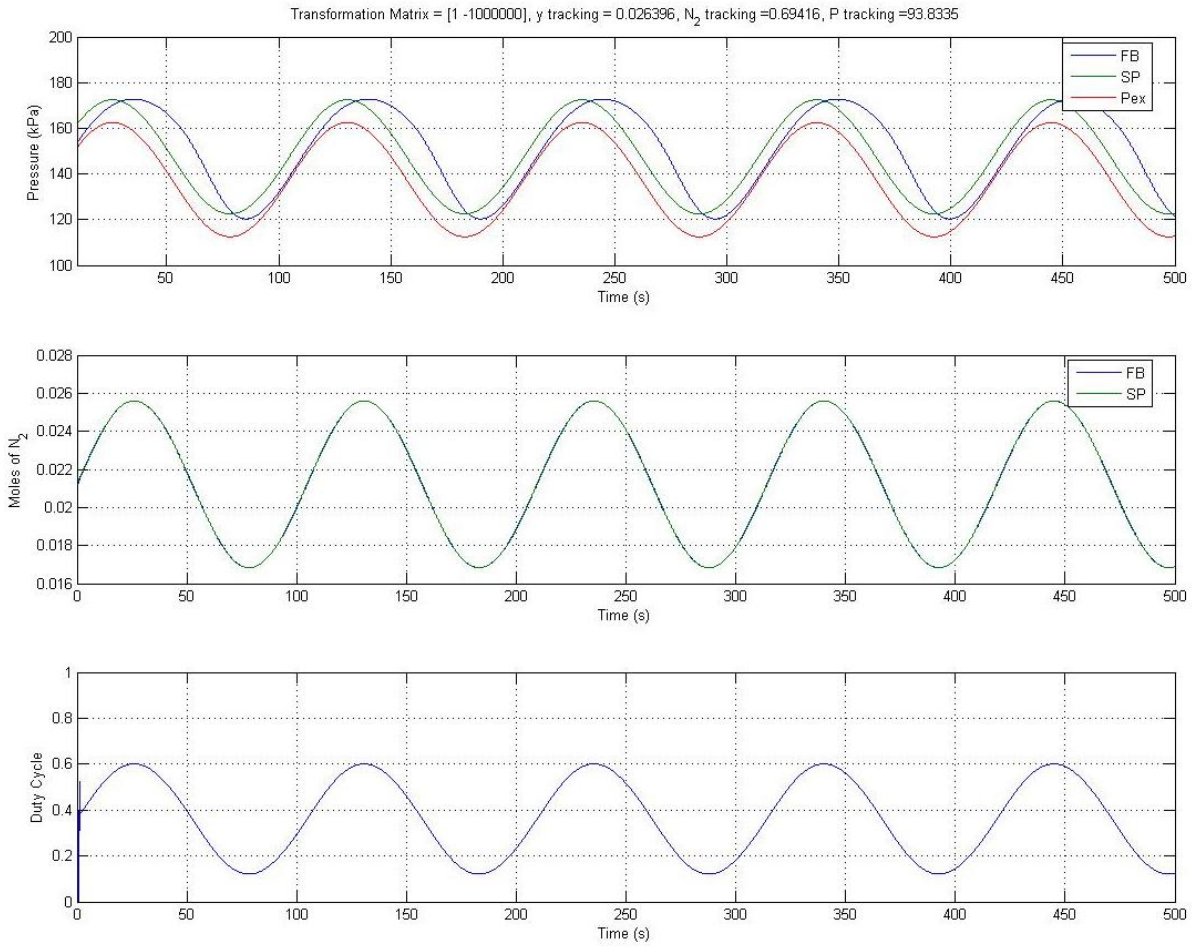

Figure 5.16: Saturation Tracking Performance for $\mathbf{T} = [1 \quad -1000000]$ and $\Delta_p = 1$

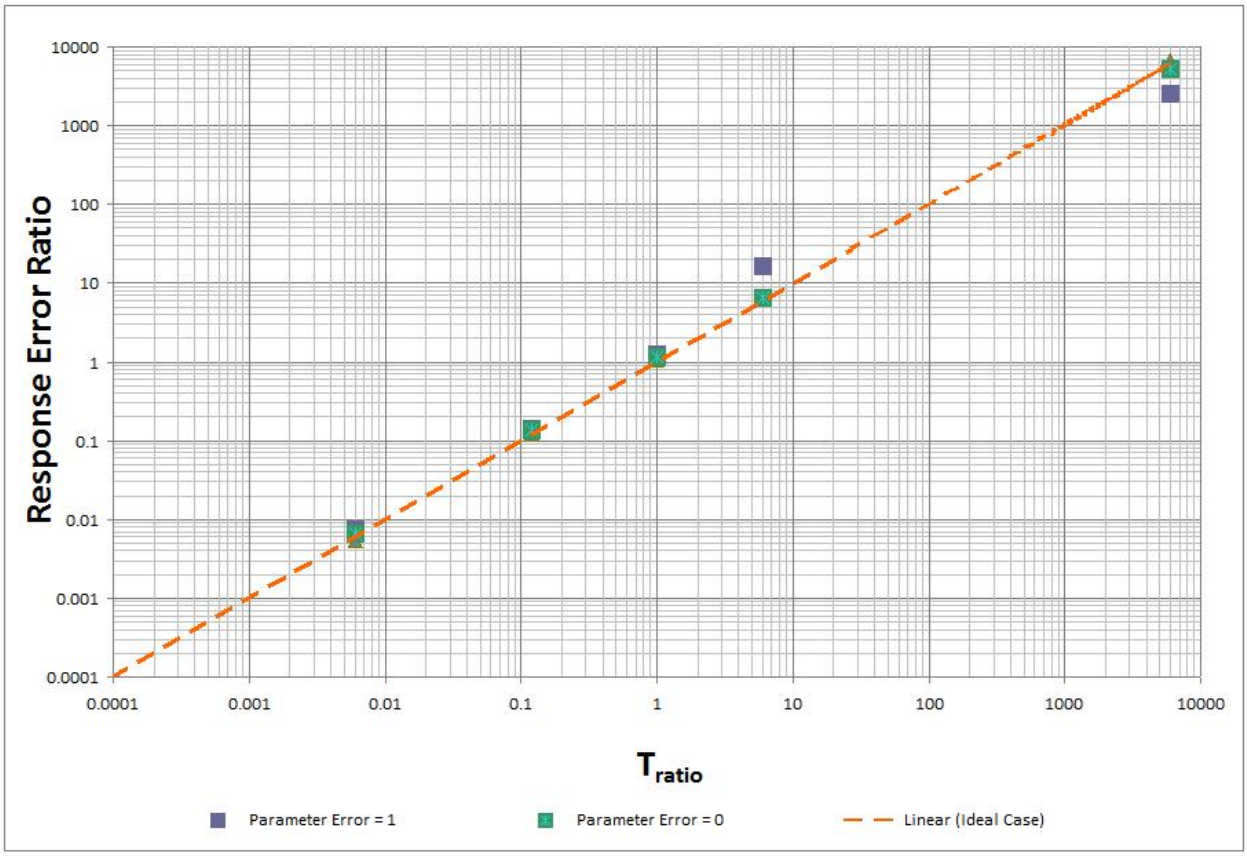

Figure 5.17: Effect of Varying **T** on System Response With Saturation Function

5.3.2 Control Effort Comparison

This section will focus on the control effort and the differences inherent to using the saturation term instead of the sign term. For this comparison the K terms response will be evaluated for the three major cases already discussed, $\Delta = 0$, 0.5, and 1. The responses are similar for different choices of $\mathbf{T}$ so for these simulations $T = [1 \quad -1000000]$.

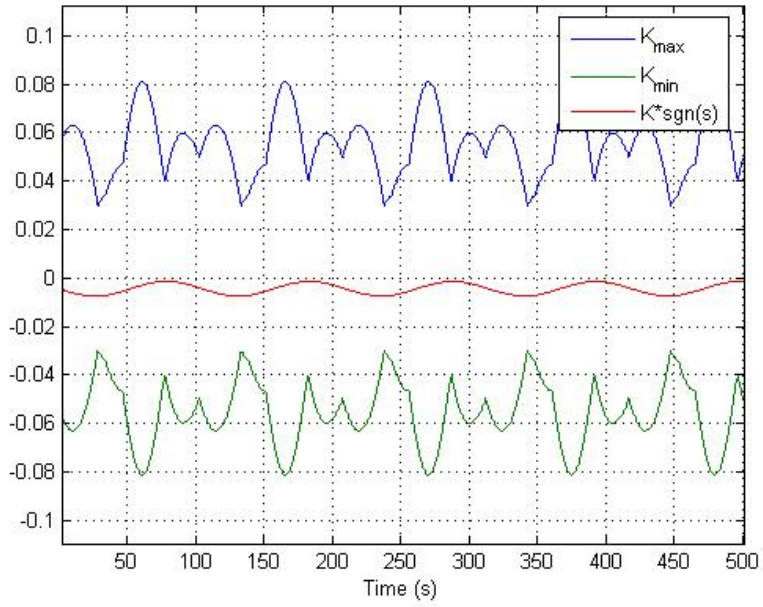

Figure 5.18: K Term with Sat Function $\mathbf{T} = [1 \quad -1000000]$ and $\Delta_p = 0.5$

The first case that will be evaluated is the case where $\Delta_p = 0.5$. Figure 5.18 shows the response of the K term and the upper and lower bounds of that term over the simulation time. Comparing the results from Figure 5.18 to that of Figure 5.5 shows the difference in the control approaches. By adding the saturation term to the control law the controller is able to control the system without oscillating between max and min values. Instead it stays around 0 and compensates slightly when necessary. This is expected because when $\Delta_p = 0.5$ there is no error between the plant model and the control model so the controller should be able to track perfectly without much error in the s term.

The next case that will be evaluated is the case where $\Delta_p = 0$. Figure 5.19 demonstrates the response for this case. There is significantly more control effort associated with this case. The K term tends toward the upper bound to maintain proper tracking. This is an expected result because, for these values of $\mathbf{T}$, nitrogen is the dominate state.

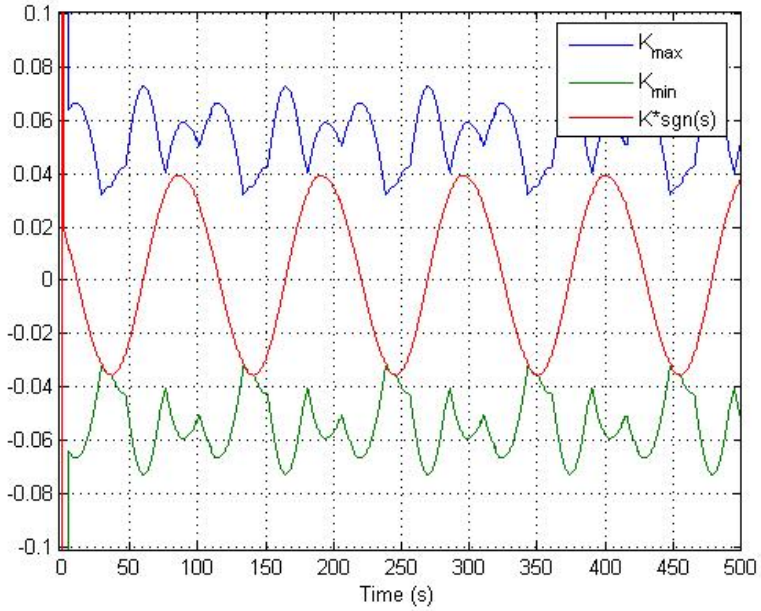

Figure 5.19: K Term with Sat Function $\mathbf{T} = [1 \quad -1000000]$ and $\Delta_p = 0$

The K term goes to the upper bound for the same reasons T_2 has to be less than zero.

The final case to be evaluated is the case where $\Delta_p = 1$. Figure 5.20 demonstrates the response for this case. Comparing Figure 5.20 to Figure 5.20 it is noticed that this case has the opposite effect that the last case had. In other words, to obtain proper tracking in this case the K term trended toward the lower bound value. Comparing both Figures 5.20 and 5.20 to Figure 5.19 there is a much higher control effort need for the cases where $\Delta_p \neq 0$. This is the expected result because of the increased modeling errors present in those cases.

If pressure control was dominated this trend would be reversed. Figure 5.21 demonstrates the difference in K terms when pressure control is dominate. For this case when the plant model is greater than the control model the K term tends toward the upper bound. This is a more intuitive result.

5.3.3 Evaluating Discrete Effects

For this sliding mode control strategy to be viable, in a real system, discrete effects need to be considered. Due to the complexity of sliding mode control and the current computing capabilities of modern processors, most control applications are implemented

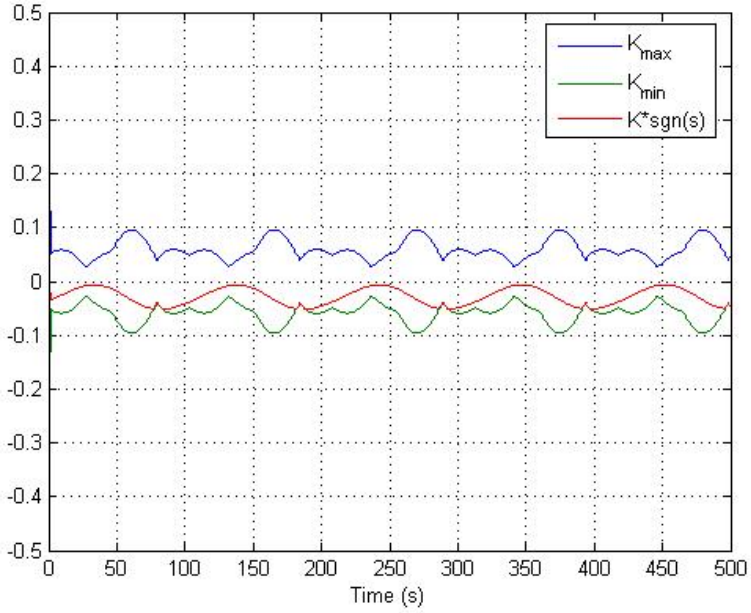

Figure 5.20: K Term with Sat Function $\mathbf{T} = [1 \quad -1000000]$ and $\Delta_p = 1$

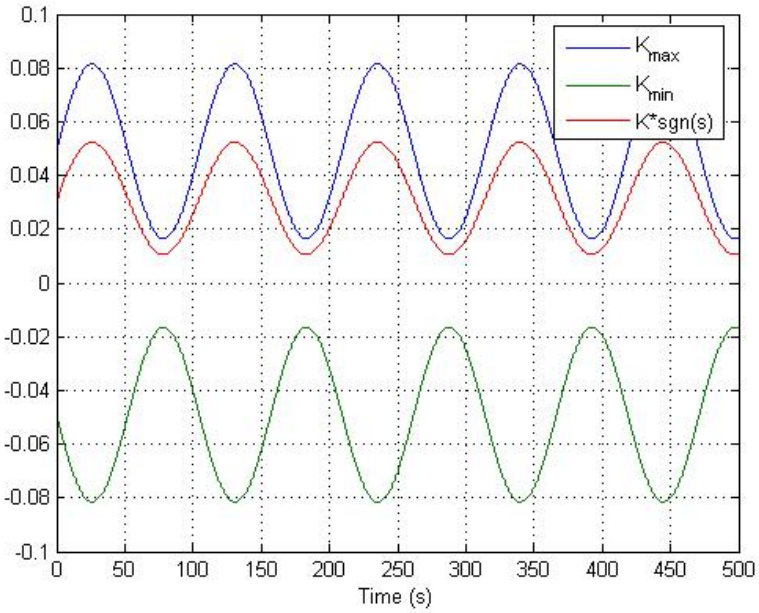

Figure 5.21: K Term with Sat Function $\mathbf{T} = [1 \quad -1]$ and $\Delta_p = 0$

on a digital computer. All the modeling and stability analysis performed in Chapters 2 and 3 were done assuming a continuous system. When the controller is implemented on a digital computer this assumption is no longer the case. This section will look at the effects of sample rate on the stability of the proposed controller.

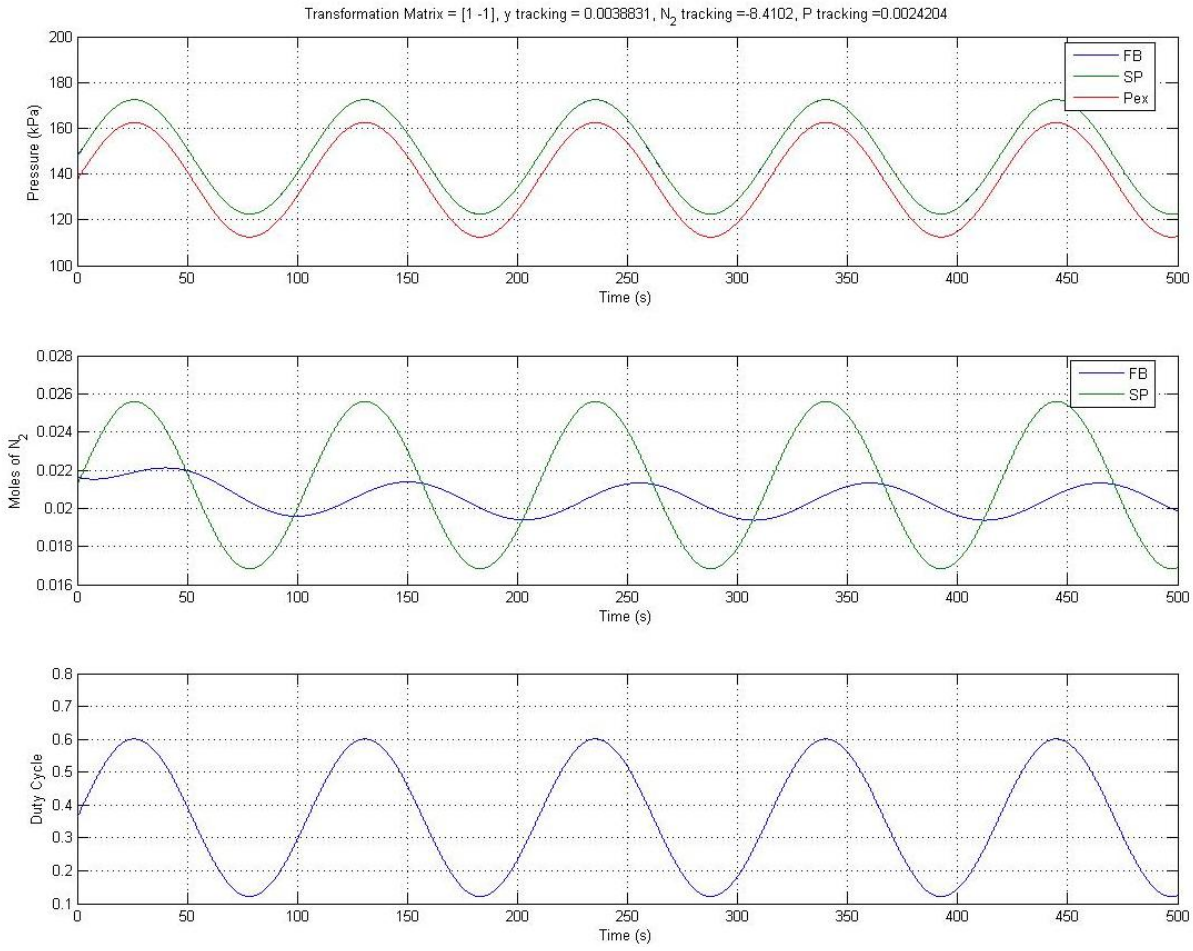

Figure 5.22: Tracking Performance for $\mathbf{T} = [1 \quad -1]$, $\Delta_p = 1$ and a 10ms Zero Order Hold

The first case that will be evaluated is the case where our sample rate is set at 10 milliseconds. This is a very conservative estimate but not out of the realm of possibility for a controller. Figure 5.22 shows almost no difference between that and the continuous case. This gives at least a potential solution in a real system.

The next case is one where the sample rate is set to 50ms. This is a much longer sample time and discrete effects will probably have an effect on the control effort. From Figure 5.23 it is obvious that this sample time is too long. The system is still stable but

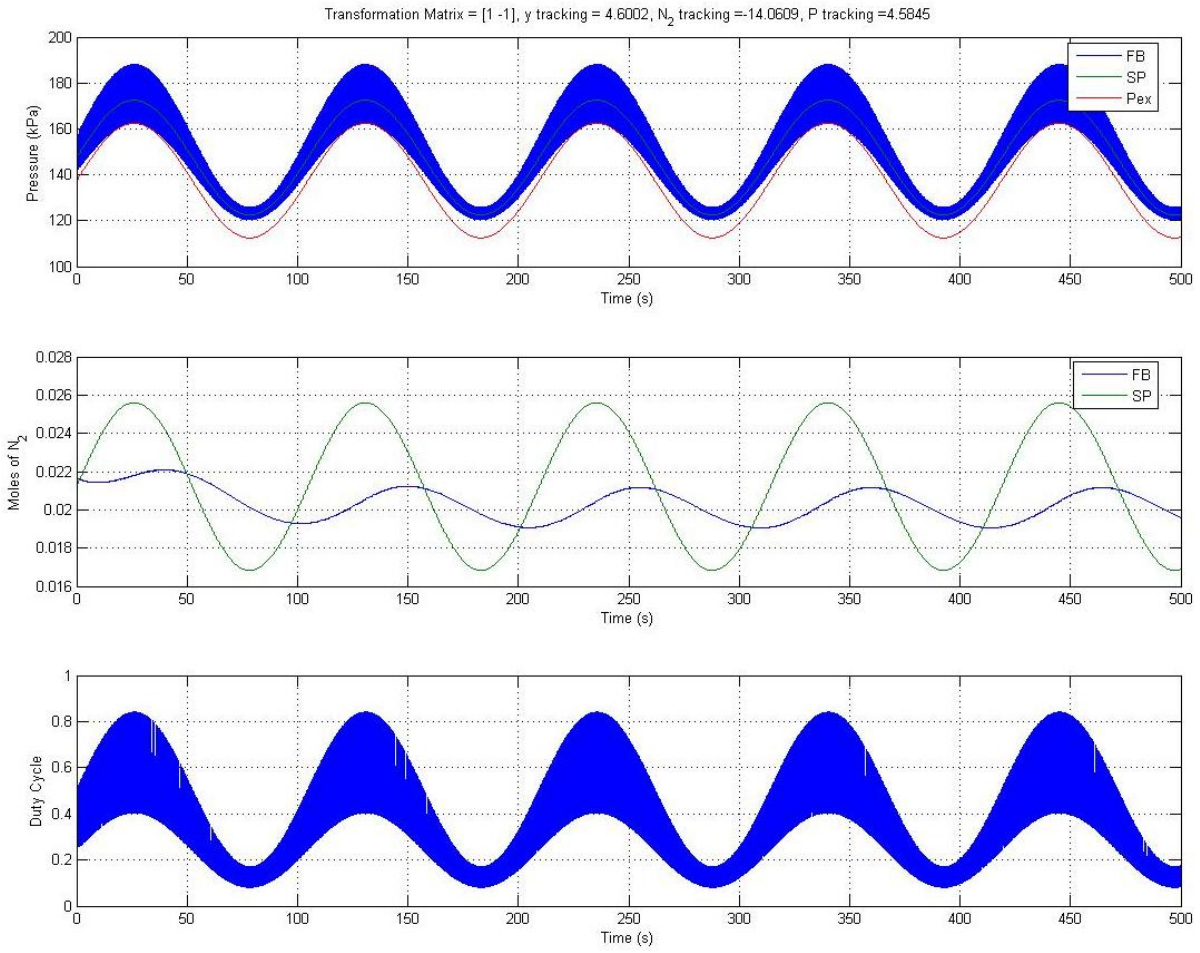

Figure 5.23: Tracking Performance for $\mathbf{T} = [1 \quad -1]$, $\Delta_p = 1$ and a 50ms Zero Order Hold

the magnitude of the pressure oscillations is unacceptable for any real system. This will be used as a limiting case.

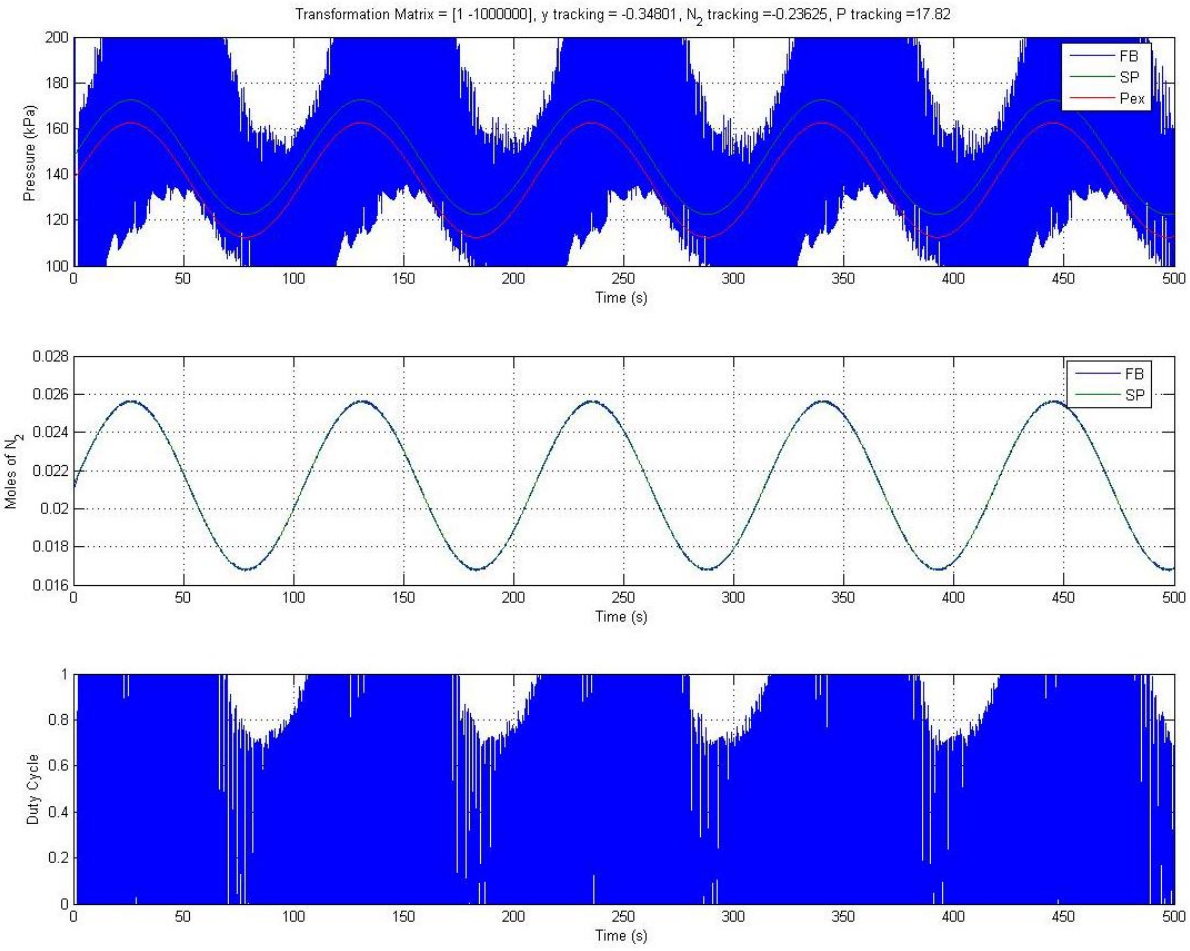

Figure 5.24: Tracking Performance for $\mathbf{T} = [1 \quad -1000000]$, $\Delta_p = 1$ and a 50ms Zero Order Hold

Figure 5.24 shows the effect of a 50ms sample rate on nitrogen control. Even with these long delays good nitrogen control is achieved however the control effort and pressure are unstable. This shows that nitrogen control is more sensitive to discrete effects than pressure control. This is mainly because the nitrogen control relies on pressure so the errors tend to add to each other.

The final case that was run is one where the sample rate is set to 20ms. This case will split the difference between the acceptable case and the unacceptable one. Figure 5.25 shows that the system is stable and the control effort has been minimized considerable form the last case but at the higher current values there is still substantial pressure

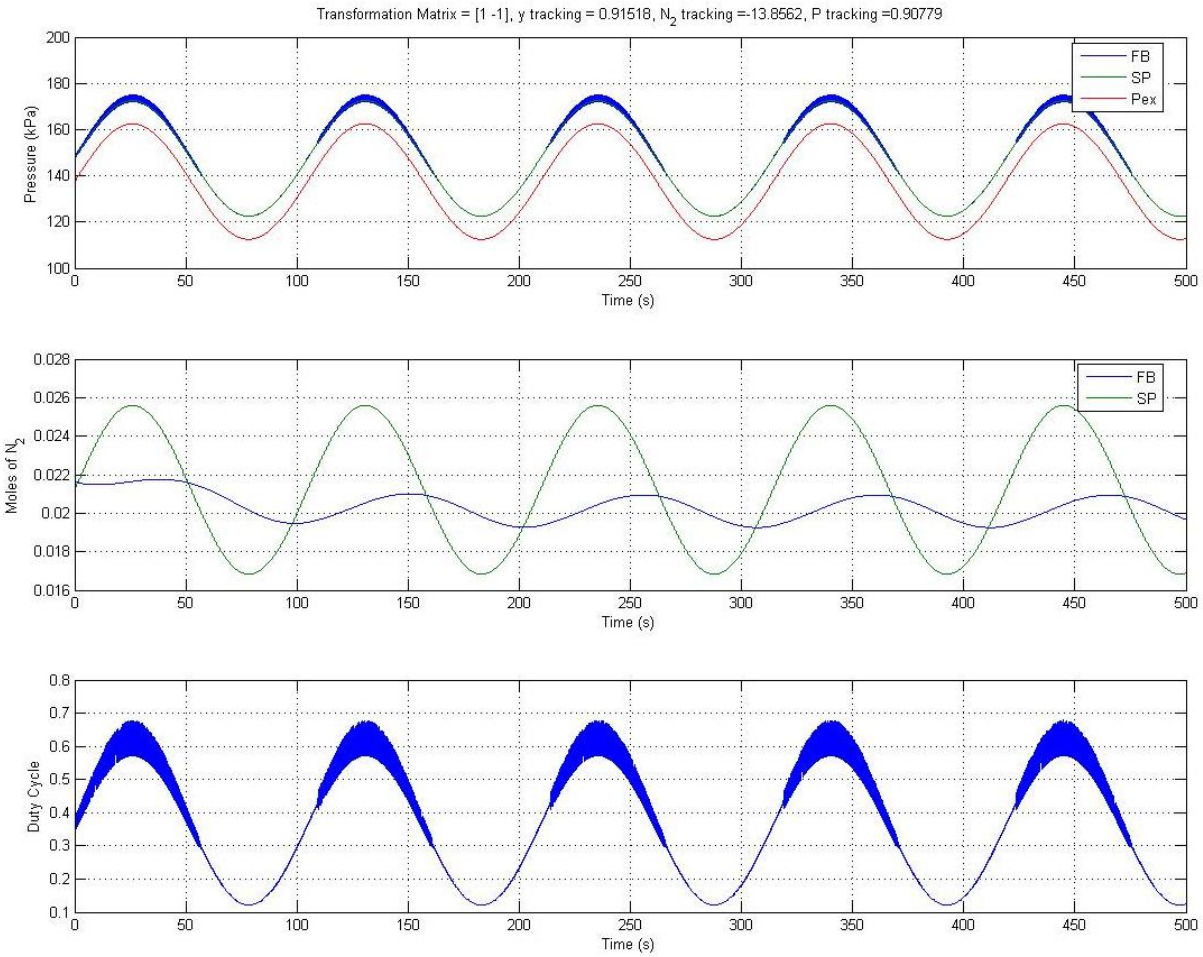

Figure 5.25: Tracking Performance for $\mathbf{T} = [1 \quad -1]$, $\Delta_p = 1$ and a 20ms Zero Order Hold

oscillations. This is expected because as the current increases the hydrogen consumption by the fuel cell will also increase so at the higher currents is where any issues with sample rate would first occur. From this result the 10ms case is chosen as the best option because of its feasibility and lack of effect on the controller.

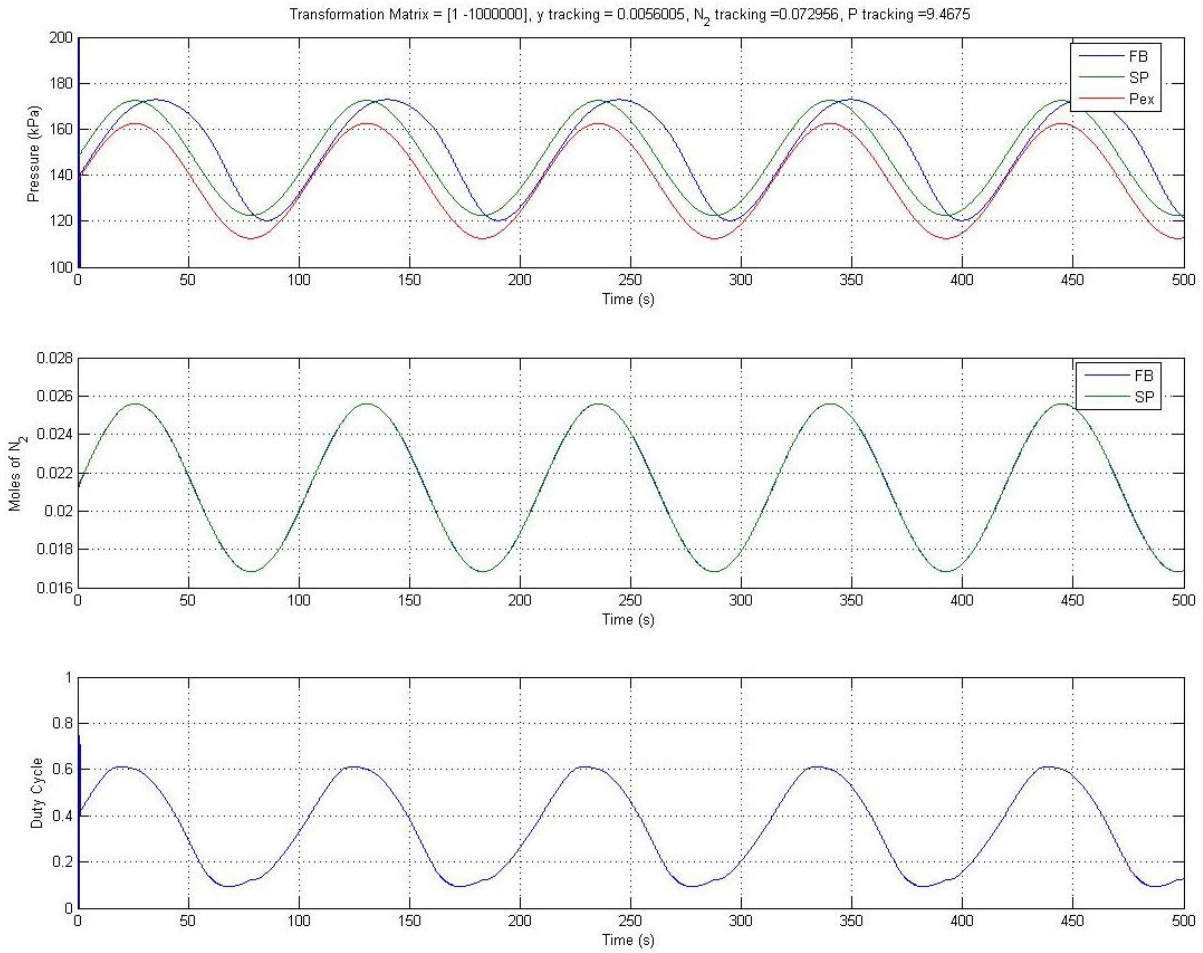

Figure 5.26: Tracking Performance for $\mathbf{T} = [1 \quad -1000000]$, $\Delta_p = 1$ and a 10ms Zero Order Hold

Figure 5.26 shows the effect of 10ms sample rate on nitrogen control. From the graph, there seems to be almost no effect on the controller compared to the continuous case. This makes the choice of sample rates fairly straightforward.

5.3.4 Robustness to Sensor Noise

In a real world system high frequency sensor noise will often affect the control effort and tracking performance. This section will focus on the sliding mode controller and its robustness to system noise. To simulate sensor noise a uniform random number generator was used with upper and lower bounds. For each state a reasonable amount of noise was added. For pressure the noise band was +-0.5kPa while for the nitrogen it was +-0.00001 moles. These values will be used for all the subsequent cases.

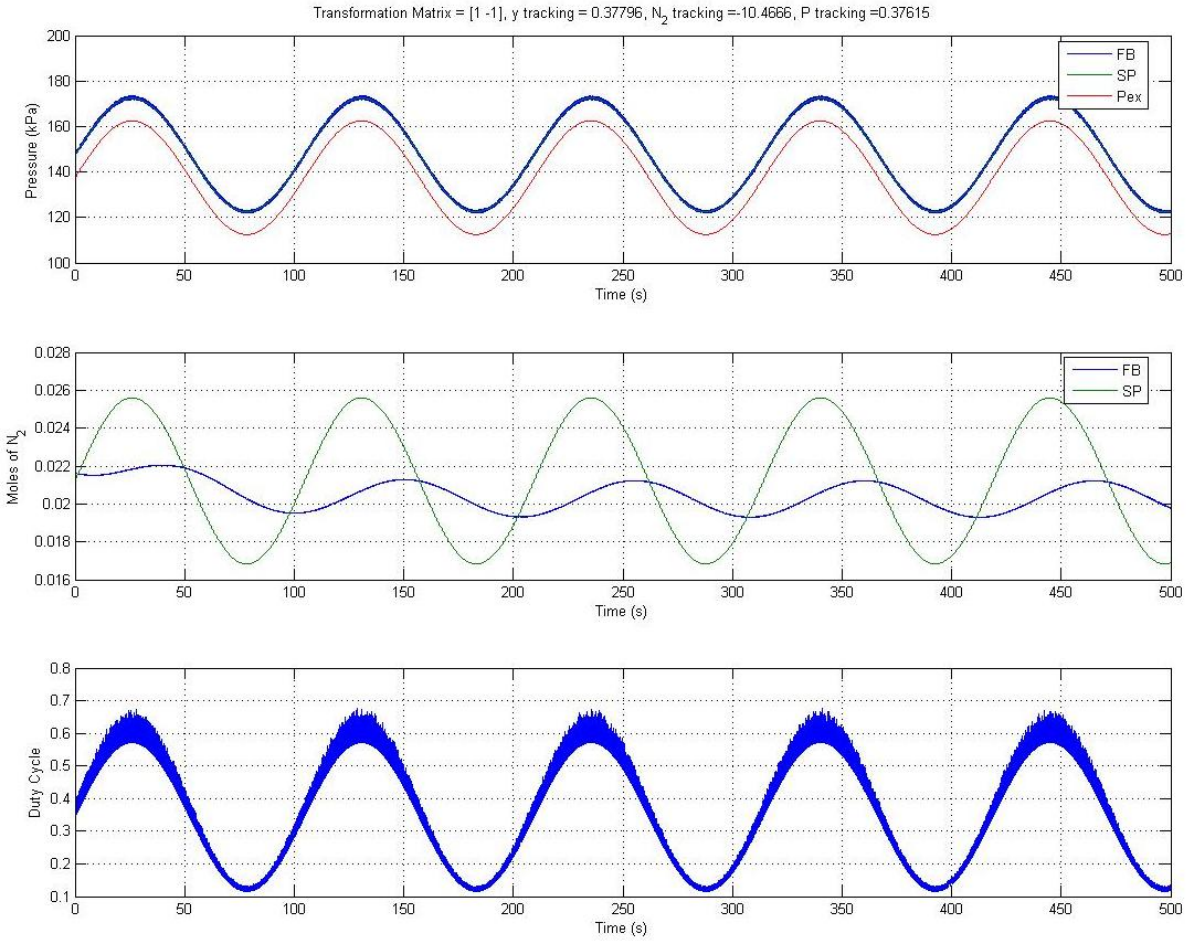

Figure 5.27: Tracking Performance for $\mathbf{T} = [1 \quad -1]$, $\Delta_p = 1$ and Sensor Noise

Figure 5.27 show the system response to noise with pressure control calibrations. From the first graph there seem to be a similar level of tracking compared to the Figure 5.15. The biggest difference in the two runs is the amount of control effort. This case needs a lot more control effort to negate the effect of the noise on the tracking performance.

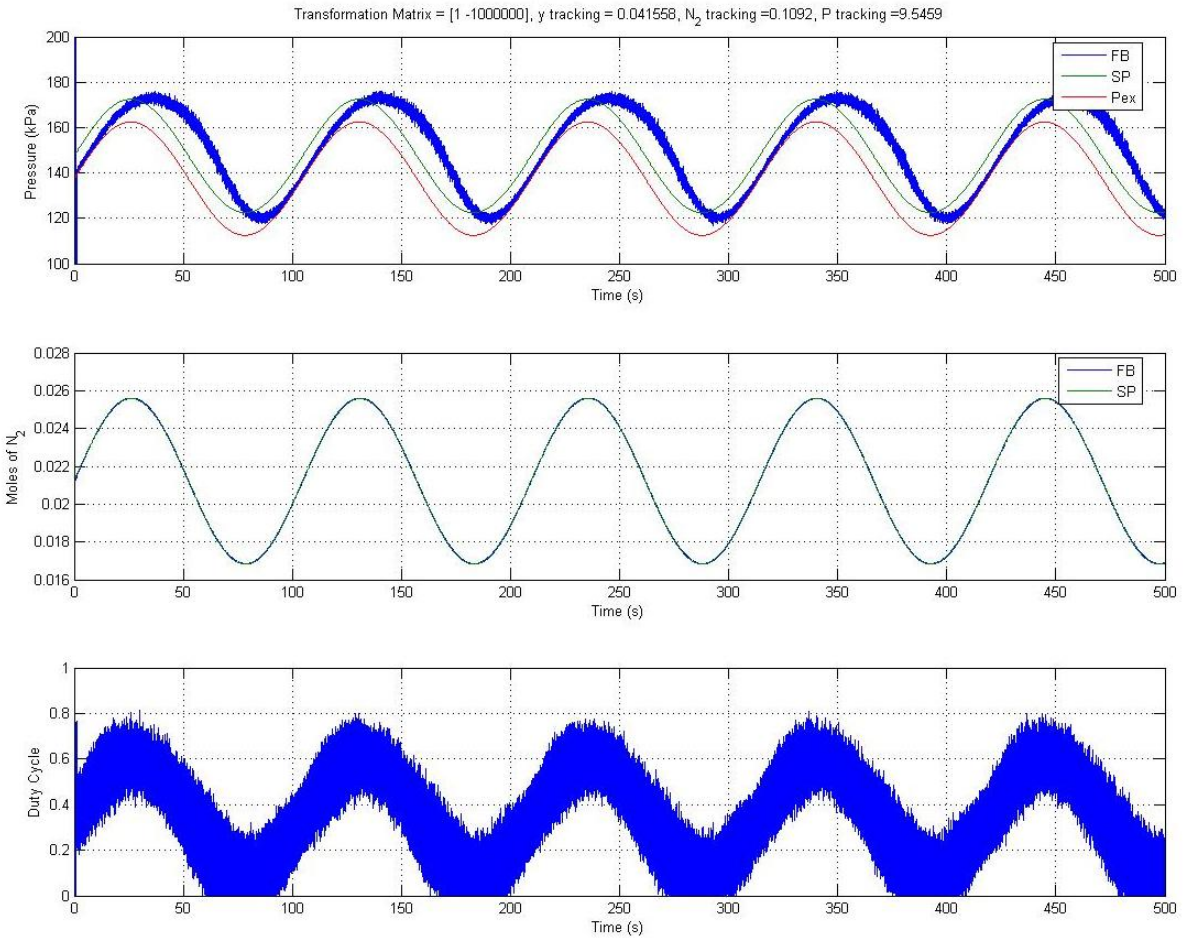

Figure 5.28: Tracking Performance for $\mathbf{T} = [1 \quad -1000000]$, $\Delta_p = 1$ and Sensor Noise

Figure 5.28 shows the system response to noise with nitrogen control calibrations. From the second graph a high level of tracking is achieved. However, compared to Figure 5.16 the control effort has significantly increased. Comparing the control effort between the two cases it is evident that noise is a bigger problem for nitrogen control than pressure control.

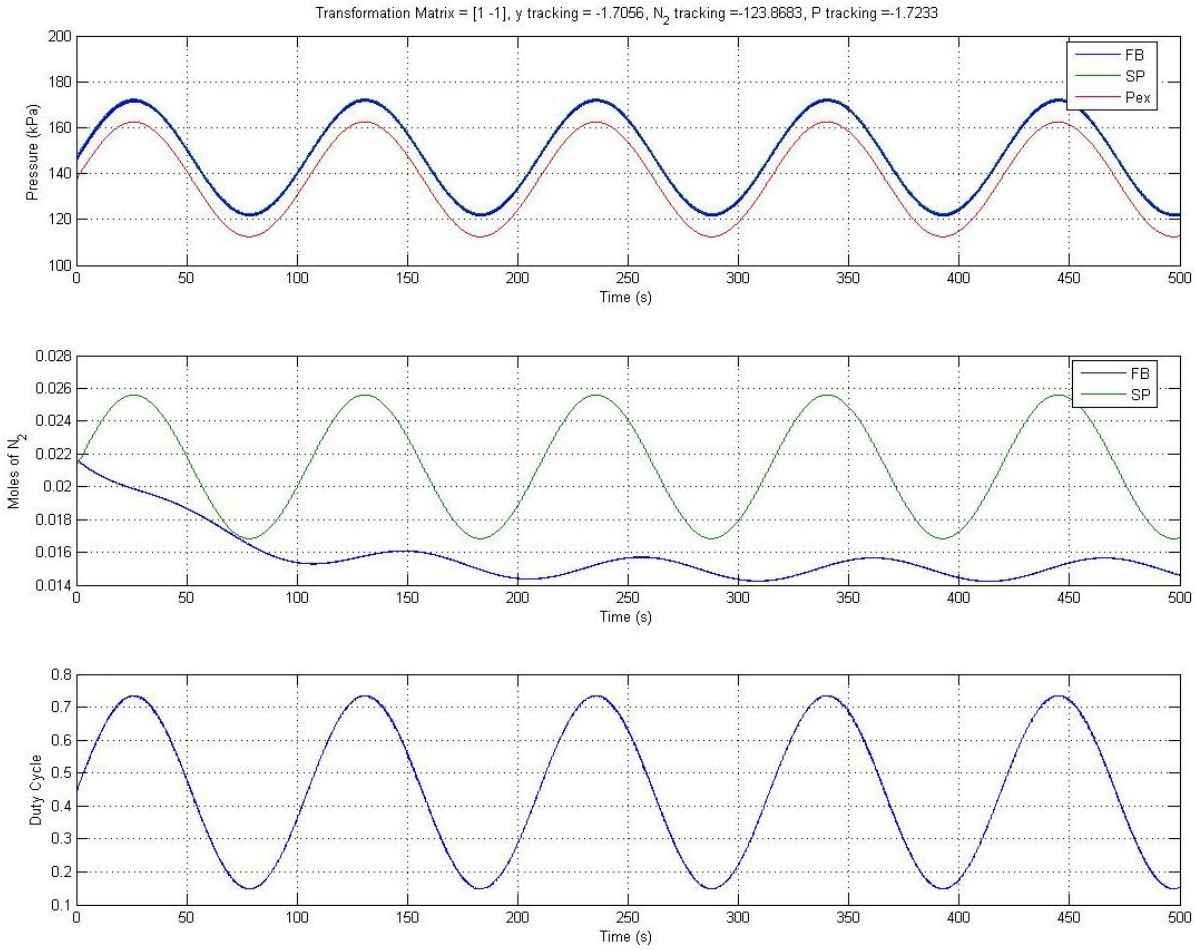

Figure 5.29: Tracking Performance for $\mathbf{T} = [1 \quad -1]$, $\Delta_p = 0$ and Sensor Noise

The previous two cases were run with $\Delta_p = 1$. This case will evaluate what happens when $\Delta_p = 0$. Figure 5.29 shows the similar control effort and tracking performance to the early cases. This means that there is no loss of stability with this level of sensor noise even with the most inaccurate model allowed. This is a promising result that this controls approach would work well in an actual system.

5.4 Comparing SMC and PI Control

This section will compare a more traditional control method to the sliding mode controller developed in Chapter 2. For linear systems Proportional Integral control is a well known and widely used control strategy. The results obtained in sections 5.3.3 and 5.3.4 are positive but how do they compare to more traditional methods as far as control effort and tracking? This is the question that will be addressed in this section.

PI control is a single input single output type of controller, therefore to control both desired states two controllers will have to be used. An in-depth discussion of linear control theory is given by [11].

The basic equation for a PI controller is given by

$$u = Kp \cdot \tilde{x} + Ki \int \tilde{x} dt$$

where Kp is the proportional gain and Ki is the integral gain. For this application because it is multiple input single output system the traditional PI controller needs to be modified. The proposed controller takes the form

$$u = Kp_p(P - P_{SP}) + Ki_p \int (P - P_{SP}) + Kp_N(n_{N_2} - n_{N_2SP}) + Ki_N \int (n_{N_2} - n_{N_2SP})$$

where the P and N represent pressure and nitrogen respectively. An optimization routine is used to determine appropriate gains for the proposed PI controller. The cost function used is given by

$$J = \int [R(P - P_{SP})^2 + Q(n_{N_2} - n_{N_2SP})^2 + Su] dt$$

By weighting the R and Q gains values for Ki_P, Kp_P, Ki_N, and Kp_N can be found that will give an optimal solution for that case. The hope is that by weighting R and Q similar to T_1 and T_2 a similar type of tracking can be obtained. The S term is added to limit the control effort as much as possible while still maintaining proper tracking. Upper and lower bounds are set for each gain in the optimization routine. This speeds convergence by limiting the search area and also guarantees that the gains have the right sign to maintain system stability. The bounds used during the optimization were

Figure 5.3 shows the two cases will be evaluated for comparison to the sliding mode controller and the resulting gains for each case.

Table 5.3: Upper and Lower Bounds

Upper Bound	Gain	Lower Bound
0	Kp_p	-100
0	Ki_p	-100
1000	Kp_N	0
1000	Ki_N	0

Table 5.4: Tested Cases with Gains

T_1	T_2	Kp_P	Ki_P	Kp_N	Ki_N
1	-1	-0.035028	-0.44992	2.0055	0.0905
1	-1000000	-0.00181	-0.00012	501.35	62.387

The first case that will be evaluated is the case where $R = Q = S = 1$. This case should be similar to the case in sliding mode control that gives perfect pressure control. The second case that will be evaluated is the case where $R = S = 1$ and $Q = 1000000$. This case should be similar to the case with the sliding mode controller that gives perfect nitrogen control. After the optimization the gains for both cases were obtained and are shown in table 5.4.

The major difference between a PI control law and sliding mode control is that sliding mode control uses an inverse model scheme to properly track states. This means that the controller knows how the states will react to a given condition and can compensate before any error occurs in the system tracking. This is a huge advantage over a PI scheme which relies solely on feedback error to adjust control effort. Therefore to obtain the same tracking with a PI controller that is obtainable with sliding mode control, one would expect much higher control effort for the PI controller.

Figure 5.30 compares the pressure control between the two control schemes. From Figure 5.30 the first graph shows the pressure tracking error in kPa. The second graph shows the nitrogen tracking error and the third graph compares the control effort for the two runs. An important note because ultimately these control schemes would be implemented into a real system sensor noise and discrete effects are present in all the comparison simulations.

From Figure 5.30, graph one shows the pressure control for both controllers is nearly perfect. The difference between the controls is evident in the control effort that it takes to maintain that level of tracking. The PI controller takes significantly more control effort than the sliding mode control case.

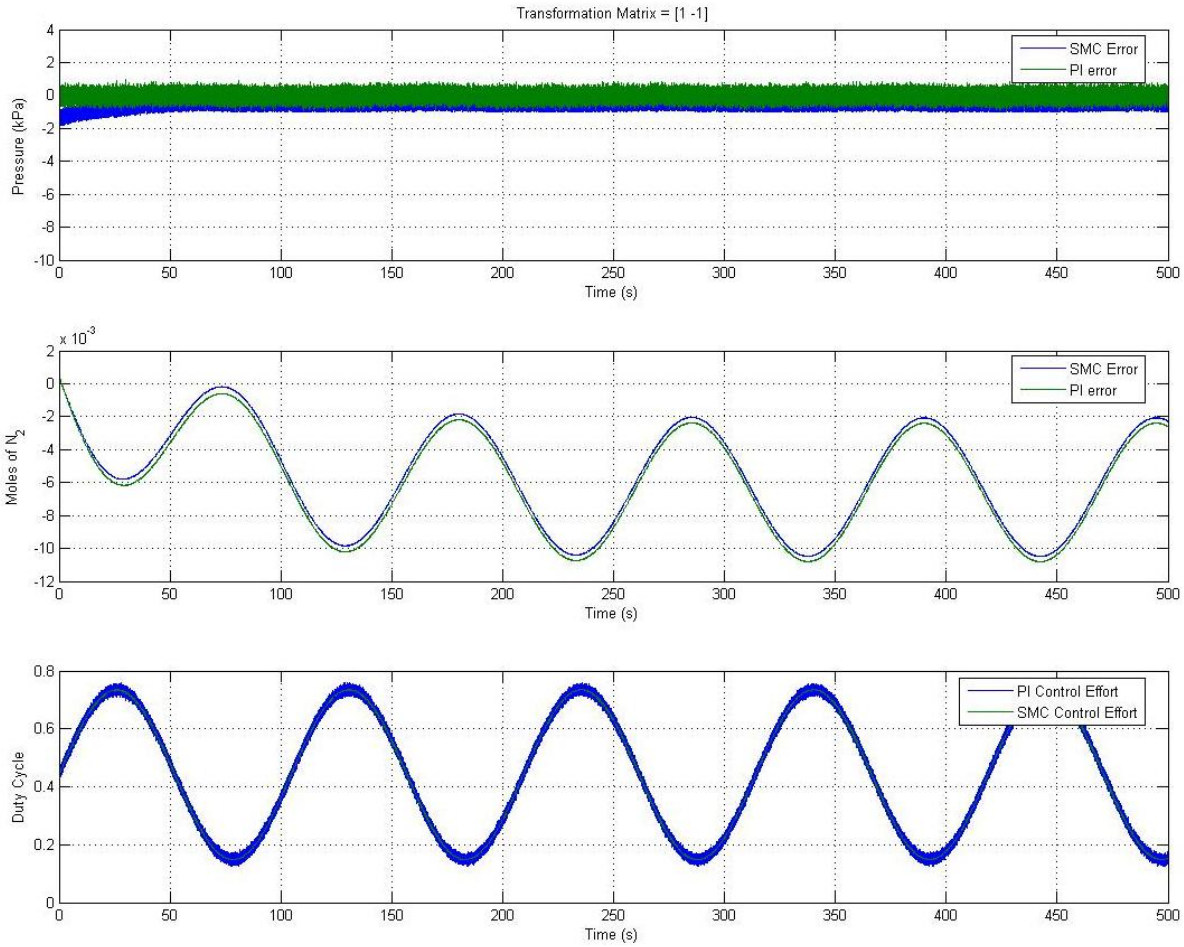

Figure 5.30: Pressure Control Comparision

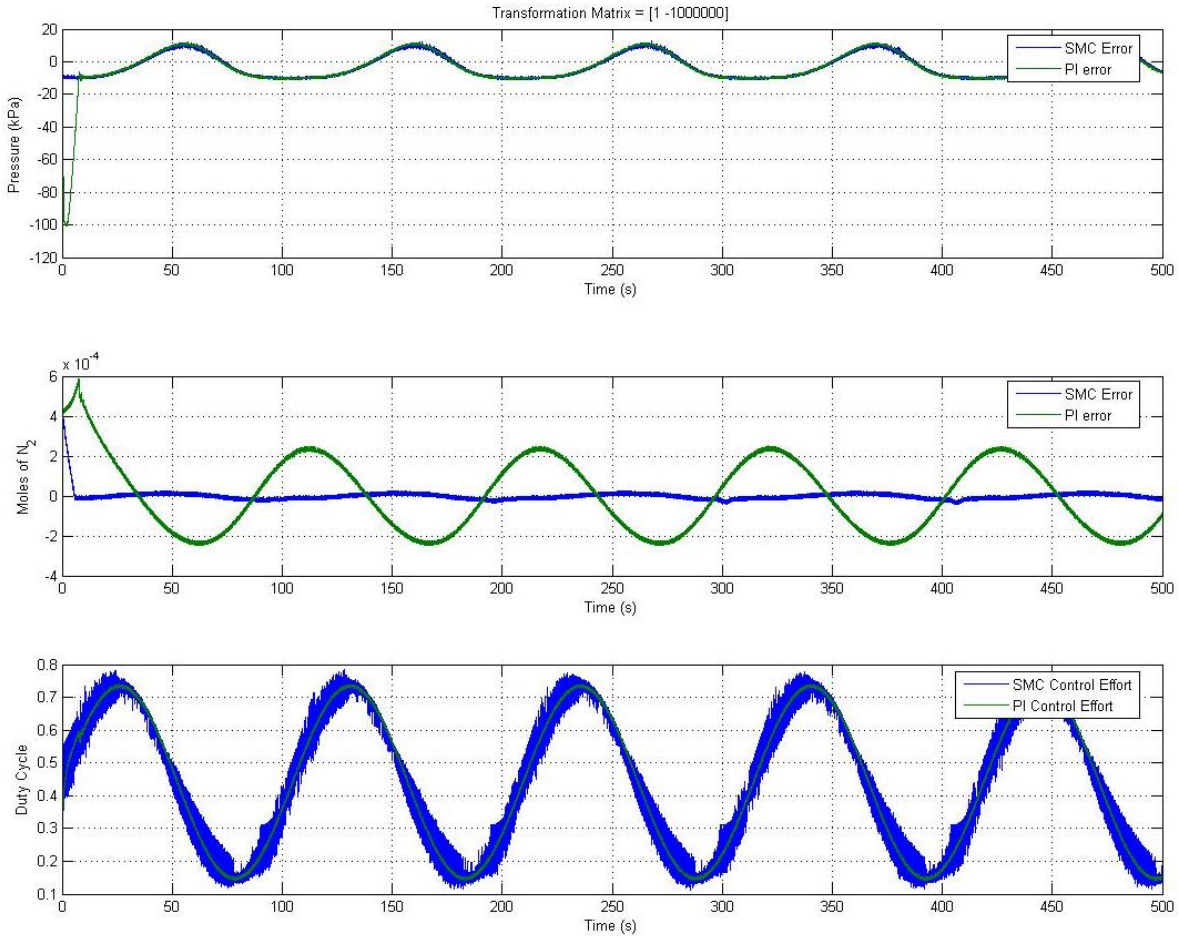

Figure 5.31: Nitrogen Control Comparision

The next case that will be examined is nitrogen control. Figure 5.31 shows that the sliding mode controller is capable of much higher tracking performance for the nitrogen control case. To accomplish this, higher control it does take more control effort. For a similar level of tracking between the two controllers the sliding mode controller will always have less control effort.

What happens when an input other than a sinusoid is used? The following examples will compare the control response for a step input case. The first case is pressure control. Figure 5.32 shows the SMC response to the step input. It is clear from the figure that the system responds the same as a first order system. That is the response is overdamped with no oscillation.

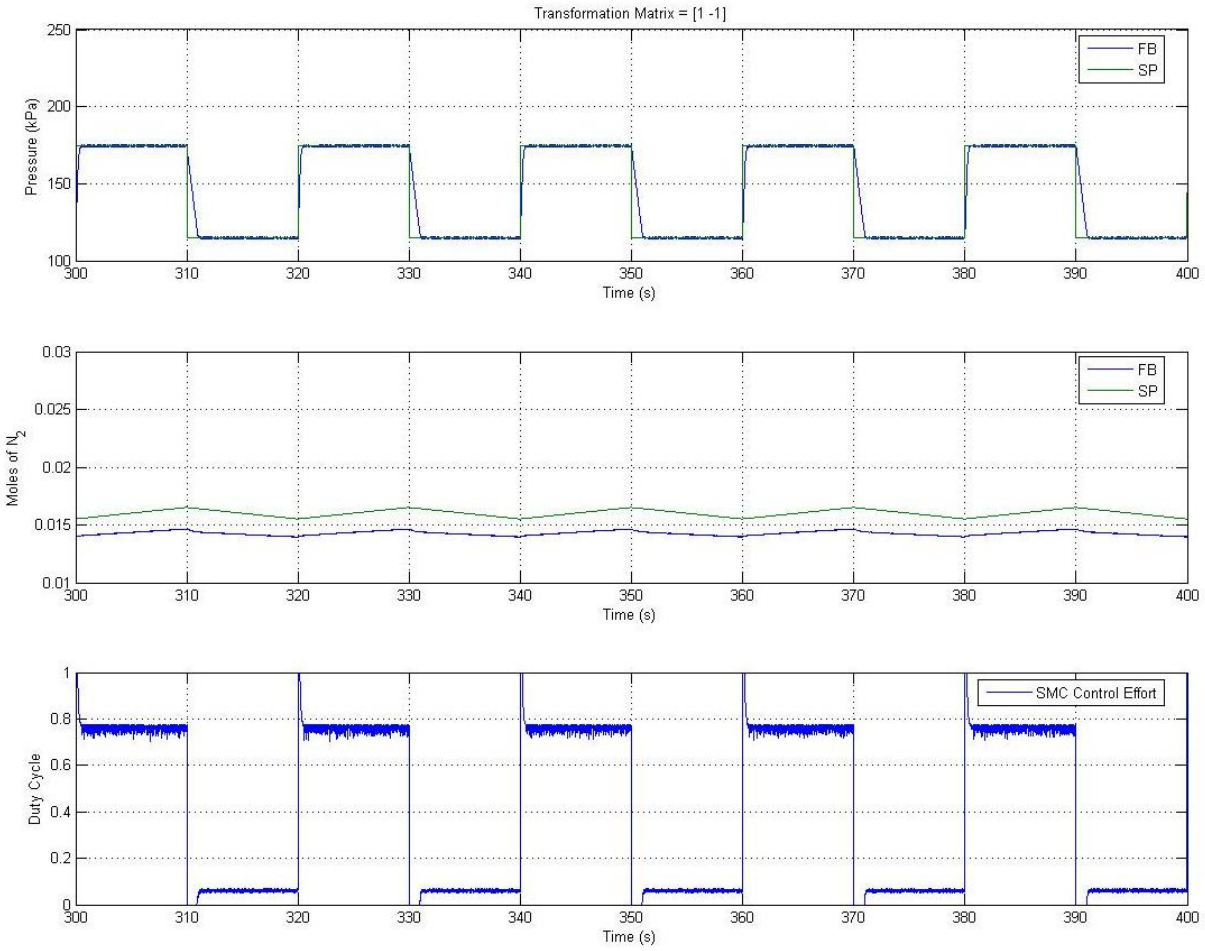

Figure 5.32: Tracking Performance for $\mathbf{T} = [1 \quad -1]$, $\Delta_p = 0$ and a Step Input

Figure 5.33 compares the responses for both controllers. The SMC response is more encouraging that the PI response. Figure 5.33 highlights one of the major advantages of

SMC, SMC is always overdamped. A major problem with PI control is to obtain fast tracking the control effort will tend to oscillate. SMC avoids this problem by canceling the nonlinear terms and forcing the system dynamics to be first order.

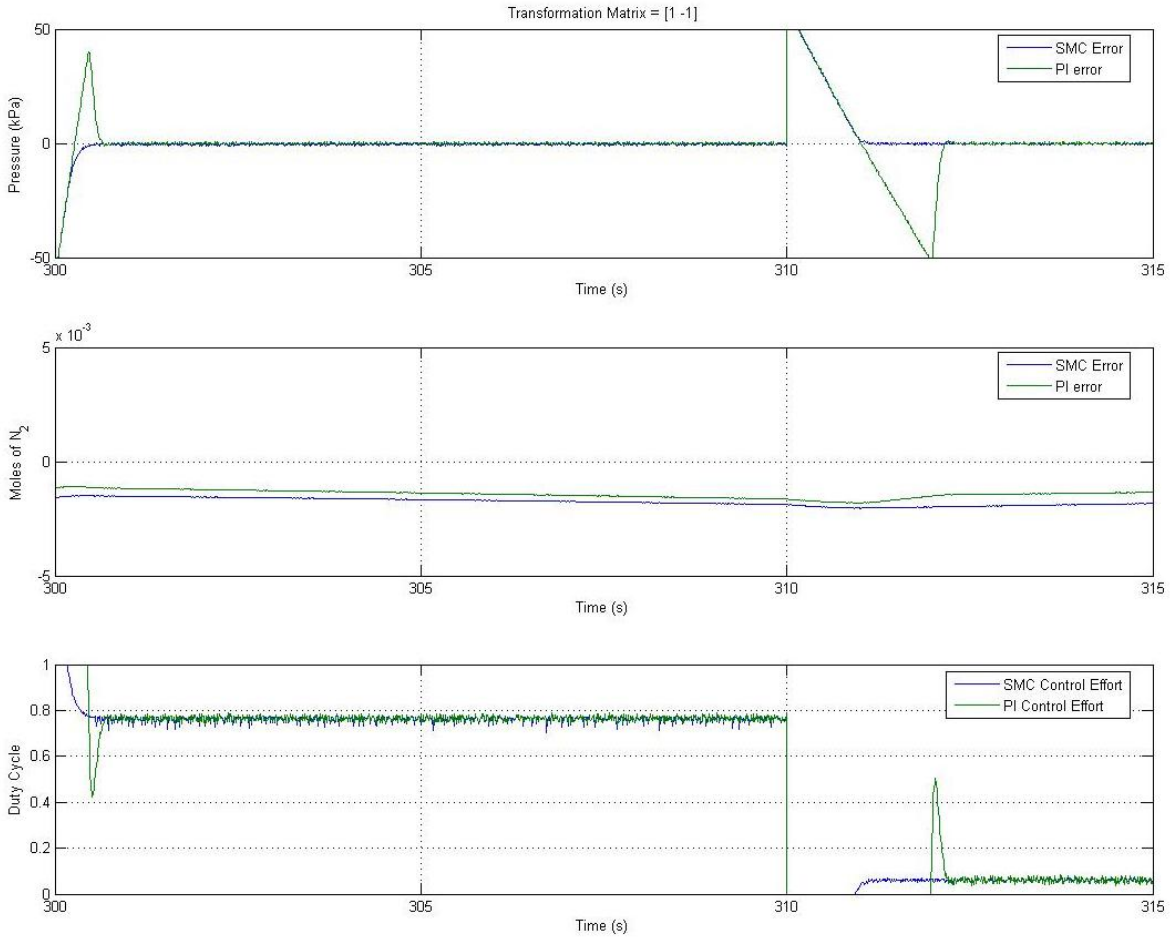

Figure 5.33: Pressure Control Comparision with Step Input

The next case to be examined is nitrogen control. Figure 5.34 verifies what was observed in Figure 5.31, that SMC is capable of much closer tracking than the PI control law. The higher tracking performance of SMC is offset by higher control effort. The higher control effort is not unreasonable for the added accuracy. Overall, the sliding mode controller delivers superior tracking performance with less control effort compared to a PI control law. This as well as its flexibility makes it an attractive option for multivariable control problems.

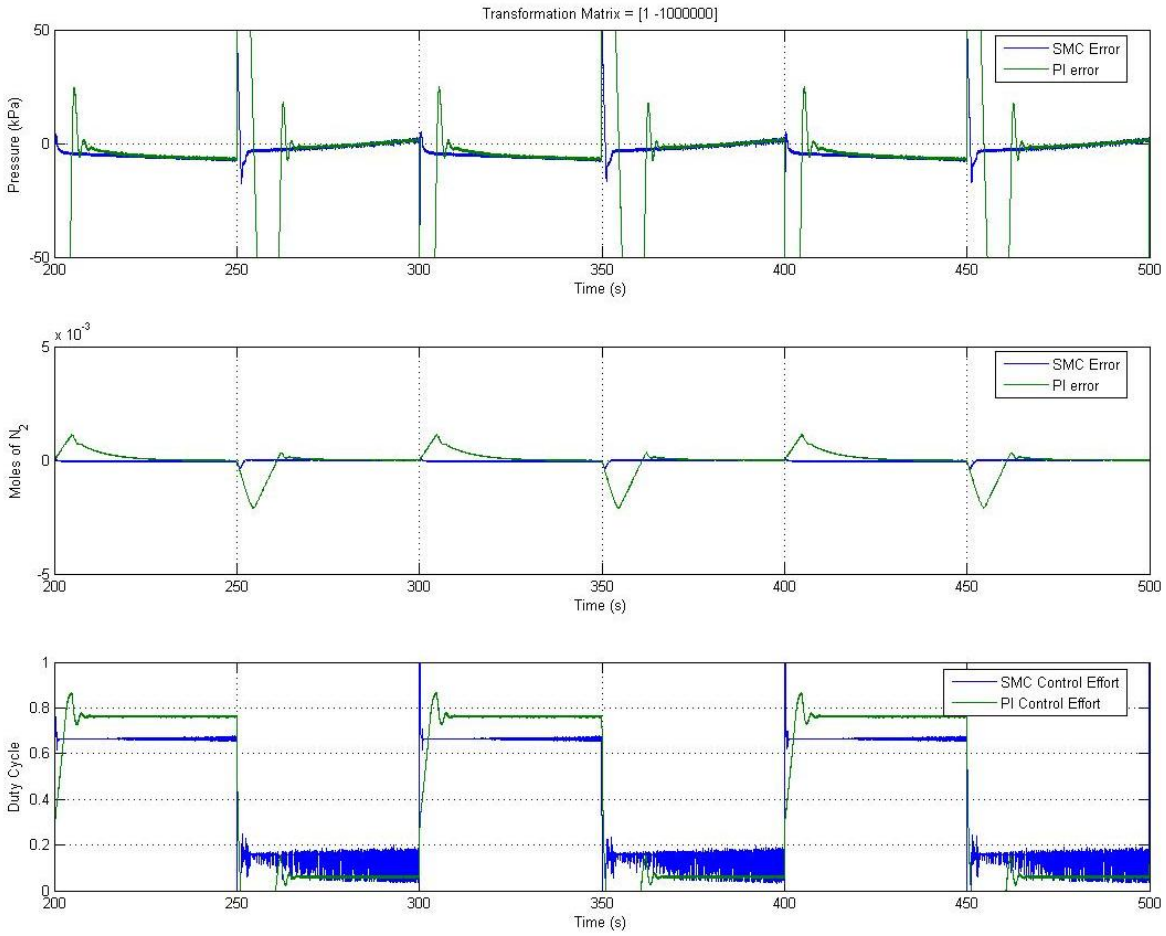

Figure 5.34: Nitrogen Control Comparision with Step Input

Chapter 6

Conclusion

6.1 Conclusion

A new control strategy was proposed to allow the use of SMC for nonsquare systems. The proposed approach allows for perfect control of any state variable or equal tracking of all states. The tracking is achieved by properly defining the transformation matrix $\mathbf{T}$. A number of simulations were run each generated a very different system tracking response. The controller was designed to track $\mathbf{y}$ and by changing $\mathbf{T}$ the weighting of each state into $\mathbf{y}$ was modified. The modified weighting allowed for perfect tracking of the chosen state in $\mathbf{x}$.

First, the controller was verified using a sign function for the robustness term. The plant model parameters were modified to show the robustness of the SMC controller and to verify stability at the system extremes. The controller was able to maintain excellent tracking and stability for all plant parameter values within the designed space. As the parameter error increased the SMC algorithm used more control effort and bandwidth to compensate.

The signum function induced high frequency chatter in the control effort which is undesirable in a real system. The signum function was then replaced with a saturation function to reduce the chattering. A similar analysis was performed to test system tracking and stability over the operating range of system parameters. The analysis showed there was no change in performance between the two algorithms other than a reduction in chattering for the saturation case.

The sliding mode controller was then tested in real world conditions by the addition of sensor noise and discrete effects. The proposed controller was unaffected by discrete

effect with sampling times up to 10 milliseconds. However, when the sampling time increased to over 20ms the controller was unable to maintain adequate control. From this result, it is proposed to use a sampling time of less then 20ms to generate proper tracking. The controller was able to negate the effects of signal noise on the state output, however increased control effort was observed to maintain the tracking performance. The added control effort was expected and overall the controller performs to expectation when it came to disturbance rejection.

Finally, SMC was compared to a more traditional linear approach. Both algorithms were tested under real world conditions with the sliding mode controller shown to out perform the PI control algorithm in tracking response and control effort. The added performance verifies what was expected out of the augmented sliding mode control approach. SMC is a superior algorithm for MIMO nonlinear systems compared to a classical linear control approach. The added flexibility of the SMC algorithm to be able to control each state with one controller is an added benefit not commonly observed in other architectures .

6.2 Recommendations

The research done is this work was rather specific to underactuated nonlinear system. A number of enhancements could be made to this work to expand the range of its application.

The first area that should be investigated is applying the linear quadratic regulator problem to the augmented sliding mode controller. The current research focused on adding the robustness terms and gave some insight into choosing values of $\mathbf{T}$. Since the system had only two inputs and one output it was fairly easy to choose values that gave the desired tracking. However, as the number of states and actuators increase, choosing $\mathbf{T}$ by trail and error no longer becomes an option. The LQR problem solves these issues by optimally choosing $\mathbf{T}$ to minimize a cost function. To apply this method to a nonlinear system, linearization techniques need to be evaluated.

The second suggestion for future work is the application of this method to an overactuated system. Overactuated systems add the problem of control allocation to choosing $\mathbf{T}$. The problem is no longer which state should be controlled, instead the problem becomes how do the states get controlled to optimize efficiency.

Another area that could be investigated is modifying the plant model to a “plugged

flow model". The "plugged flow model" would account for multiple volumes and would potentially be more representative of the actual system. The recommendation would be to keep the lumped system model control law developed in this work and implement the "plugged flow model" as the plant model in the simulations. By implementing the alternate plant model, the control law's robustness to unmodeled dynamics could be tested.

Bibliography

[1] Jin Sun Amey Y. Karnik and Julia H. Buckland. Control analysis of an ejector based fuel cell anode recirculation system. In *Proceedings of the 2006 American Control Conference*, June 2006.

[2] Yunus A. Cengel and Robert H. Turner. *Fundamentals of Thermal Fluid Sciences*. McGraw-Hill, 2001.

[3] Miguel A. Mayosky Cristian Kunusch, Paul F. Puleston and Jordi Riera. Sliding mode strategy for pem fuel cells stacks breathing control using a super-twisting algorithm. *Transactions on Control Systems Technology*, 2008.

[4] Don W. Green and Robert H. Perry. *Perry's Chemical Engineers' Handbook*. McGraw-Hill, 8th edition, 2008.

[5] A. G. Stefanopoulou J. T. Pukrushpan and H. Peng. *Control of Fuel Cell Power Systems Principles, Modeling, Analysis and Feedback Design*. Springer Verlag, 2004.

[6] Erwin Kreyszig. *Advanced Engineering Mathematics*. Willey, 8th edition, 1999.

[7] James Larminie and Andrew Dicks. *Fuel Cell Systems Explained*. John Wiley Sons, 2nd edition, 2003.

[8] S. Rael M. Hinaje, D. Nguyen and B. Davat. Modelling of the proton exchange membrane fuel cell in steady state. *Groupe de Recherche en Electrotechnique et Electronique de Nancy*, 2008.

[9] Hashem Ashrafiuon Mehdi Nikkhah and Kenneth R. Muske. Optimal sliding mode control for underactuated systems. In *Proceedings of the 2006 American Control Conference*, 2006.

[10] Suk-Kyo Hong Mun-Soo Park, DongKyoung Chwa. Decoupling control of a class of underactuated mechanical systems based on sliding mode control. In *International Joint Conference*, 2006.

[11] Norman S. Nise. *Control Systems Engineering*. John Wiley Sons, 3rd edition, 2000.

[12] Ryan F. Schkoda. Dynamic inversion of underactuated systems via squaring transformation matrix. Master's thesis, Rochester Institute of Technonlogy, 2007.

[13] Jean-Jacques E. Slotine and Weiping Li. *Applied Nonlinear Control*. Prentice Hall, 1991.

[14] Dong-Bin Zhoa Wei Wang, Jian-Qiang Yi and Xiao-Jing Liu. Adaptive sliding mode controller for an underactuated manipulator. In *Third International Conference on Machine Learning and Cybernetics*, 2004.

[15] Dongbin Zhao Yinxing Hao, Jianqiang Yi and Dianwei Quin. Robust control using incremental sliding mode for underactuated systems with mismatched uncertainties. In *Proceedings of the 2008 American Control Conference*, 2008.

[16] Yinhai Zhu and Yanzhong Li. New theoretical model for convergent nozzle ejector in the proton exchange membrane fuel cell system. *Journal of Power Sources*, 2009.

Appendix A

Matlab Code

```
% Run Nonlinear SMC Control

% Model Constants
Ncell=251;
V=2.53;
AA=360;
R=8.314;
CaDiff=10;
F=96485;

% Model Uncertainties
n_inj_max_max=1; n_inj_max_min=0.8;
C_max=0.75; C_min=0.6;
T_min=273+60; T_max=273+80;
V_min=2.4; V_max=2.6;
D2_min=0.00068; D2_max=0.00072;
RH_min=0.7; RH_max=1;
H_min=3.65e-6; H_max=5.56e-6;

%Best Approximations
n_inj_max_hat=(n_inj_max_max+n_inj_max_min)/2;
C_hat=(C_max+C_min)/2;
T_hat=(T_min+T_max)/2;
V_hat=(V_min+V_max)/2;
RH_hat=(RH_min+RH_max)/2;
H_hat=(H_min+H_max)/2;
```

```
D2_hat=(D2_min+D2_max)/2;
A2_hat=3.14*(D2_hat)^2/4;
B_hat=[n_inj_max_hat*R*T_hat/V_hat;0];
h2o_sat_hat=RH_hat*(9.6E-7*(T_hat-273)^4-3.3E-5*(T_hat-273)^3+ ...
    0.0036*(T_hat-273)^2+0.016*(T_hat-273)+0.67);

% n_inj_max_hat=n_inj_max_max;
% C_hat=C_max;
% T_hat=T_max;
% V_hat=V_max;
% RH_hat=RH_max;
% H_hat=H_max;
% D2_hat=D2_max;
% A2_hat=3.14*(D2_hat)^2/4;
% B_hat=[n_inj_max_hat*R*T_hat/V_hat;0];
% h2o_sat_hat=RH_hat*(9.6E-7*(T_hat-273)^4-3.3E-5*(T_hat-273)^3+ ...
    %0.0036*(T_hat-273)^2+0.016*(T_hat-273)+0.67);

%Worst Case Values
n_inj_max=n_inj_max_min;
C=C_min;
T=T_min;
V=V_min;
H=H_min;
RH=RH_min;
D2=D2_min;
A2=3.14*(D2)^2/4;
B=[n_inj_max*R*T/V;0];
h2o_sat=RH*(9.6E-7*(T-273)^4-3.3E-5*(T-273)^3+0.0036*(T-273)^2+ ...
    0.016*(T-273)+0.67);

% Plant Values
n_inj_max_plant=(0)*(n_inj_max_max-n_inj_max_min)+n_inj_max_min;
C_plant=(0)*(C_max-C_min)+C_min;
T_plant=(0)*(T_max-T_min)+T_min;
V_plant=(0)*(V_max-V_min)+V_min;
H_plant=(0)*(H_max-H_min)+H_min;
RH_plant=(0)*(RH_max-RH_min)+RH_min;
D2_plant=(0)*(D2_max-D2_min)+D2_min;
A2_plant=3.14*(D2_plant)^2/4;
B_plant=[n_inj_max_plant*R*T_plant/V_plant;0];
```

```
h2o_sat_plant=RH_plant*(9.6E-7*(T_plant-273)^4-3.3E-5*(T_plant-273)^3 ...
    +0.0036*(T_plant-273)^2+0.016*(T_plant-273)+0.67);

%CC=K*pinv(K*B);

%Controller Parameters
K=[1 -1];
gamma=[10 0;0 10];
fe=1;
eta=[0.00000001];

% Kp_P=-0.0018094;
% Ki_P=-0.0001204;
% Kp_N=501.35;
% Ki_N=62.387;

Kp_P=-0.035028;
Ki_P=-0.44992;
Kp_N=2.0055;
Ki_N=0.0905;

%Simulation Initialization
Beta=K*B_hat*inv(K*B);
P0=150;
n0=P0*V_hat/(R*T_hat);
h2o_0=h2o_sat_hat/P0*n0;
%n2_0=(n0-h2o_0)*0.2;
n2_0=0.0001;

%Simulation Parameters
tf=500;
ts=0.01;

% Simulate System
sim('NonlinearSMCwithPI')

% y_tracting=trapz((y-yd)./yd.*ts)
% n2_tracking=trapz(((x(:,2)-xd(:,2)))./xd(:,2).*ts)
% P_tracking=trapz(((x(:,1)-xd(:,1)))./xd(:,1).*ts)

%Plot results
```

```
figure(1),subplot(311),plot(Time,x(:,1)-xd(:,1),Time,x_errorPI(:,1)),grid
legend('SMC Error','PI error')
xlabel('Time (s)')
ylabel('Pressure (kPa)')
axis([300 315 -50 50])
title(['Transformation Matrix = [',num2str(K(1)),' ',num2str(K(2)),']'])

subplot(312),plot(Time,x(:,2)-xd(:,2),Time,x_errorPI(:,2)),grid
legend('SMC Error','PI error')
xlabel('Time (s)')
axis([300 315 -0.005 0.005])
ylabel('Moles of N_2')

subplot(313),plot(Time,DC,Time,uPI),grid
legend('SMC Control Effort','PI Control Effort')
xlabel('Time (s)')
axis([300 315 0 1])
ylabel('Duty Cycle')

figure(2),subplot(311),plot(Time,x(:,1),Time,xd(:,1)),grid
legend('FB','SP')
xlabel('Time (s)')
ylabel('Pressure (kPa)')
axis([300 400 100 250])
title(['Transformation Matrix = [',num2str(K(1)),' ',num2str(K(2)),']'])

subplot(312),plot(Time,x(:,2),Time,xd(:,2)),grid
legend('FB','SP')
xlabel('Time (s)')
axis([300 400 0.01 0.03])
ylabel('Moles of N_2')

subplot(313),plot(Time,DC),grid
legend('SMC Control Effort')
xlabel('Time (s)')
ylabel('Duty Cycle')
axis([300 400 0 1])

% figure(2),plot(x(:,1)-(xd(:,1)-CaDiff),ndot_vlv,x(:,1)- ...
    %(xd(:,1)-CaDiff),ndot_vlv_act),grid
% xlabel('Valve Pressure Differential (kPa)')
```

```
150 % ylabel('Valve Flow (mol/s)')
151 % legend('Estimate','Actual')
152 %
153 % figure(3),plot(Time,y,Time,yd)
154 % legend('FB','SP')
155 % xlabel('Time (s)')
156 % ylabel('y')
157 % grid
158
159 % figure(4),subplot(311),plot(Time,xd_dot(:,1),Time,gamma_xd(:,1) ...
160     %,Time,f(:,1))
161 % legend('x_d dot','x_d','f')
162 % ylabel('P')
163 % grid
164 %
165 % subplot(312),plot(Time,xd_dot(:,2),Time,gamma_xd(:,2),Time,f(:,2))
166 % legend('x_d dot','x_d','f')
167 % ylabel('N2')
168 % grid
169 %
170 % subplot(313),plot(Time,CC(2)*(xd_dot(:,2)-gamma_xd(:,2)-f(:,2)) ...
171 %,Time,CC(1)*(xd_dot(:,1)-gamma_xd(:,1)-f(:,1)))
172 % legend('n_N_2','P')
173 % grid
174 %
175 % figure(6),plot(Time,Ksg(:,1),Time,-Ksg(:,1),Time,Ksg_term(:,1))
176 % legend('K_m_a_x','K_m_i_n','K*sgn(s)')
177 % xlabel('Time (s)')
178 % grid
```

Appendix B

Simulink Diagrams

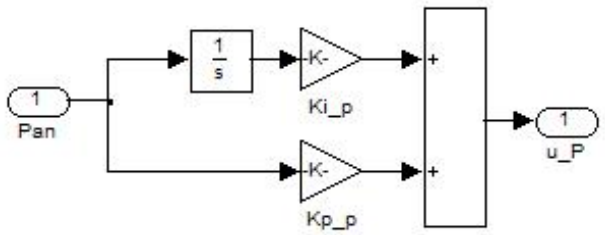

Figure B.1: PI Block Diagram

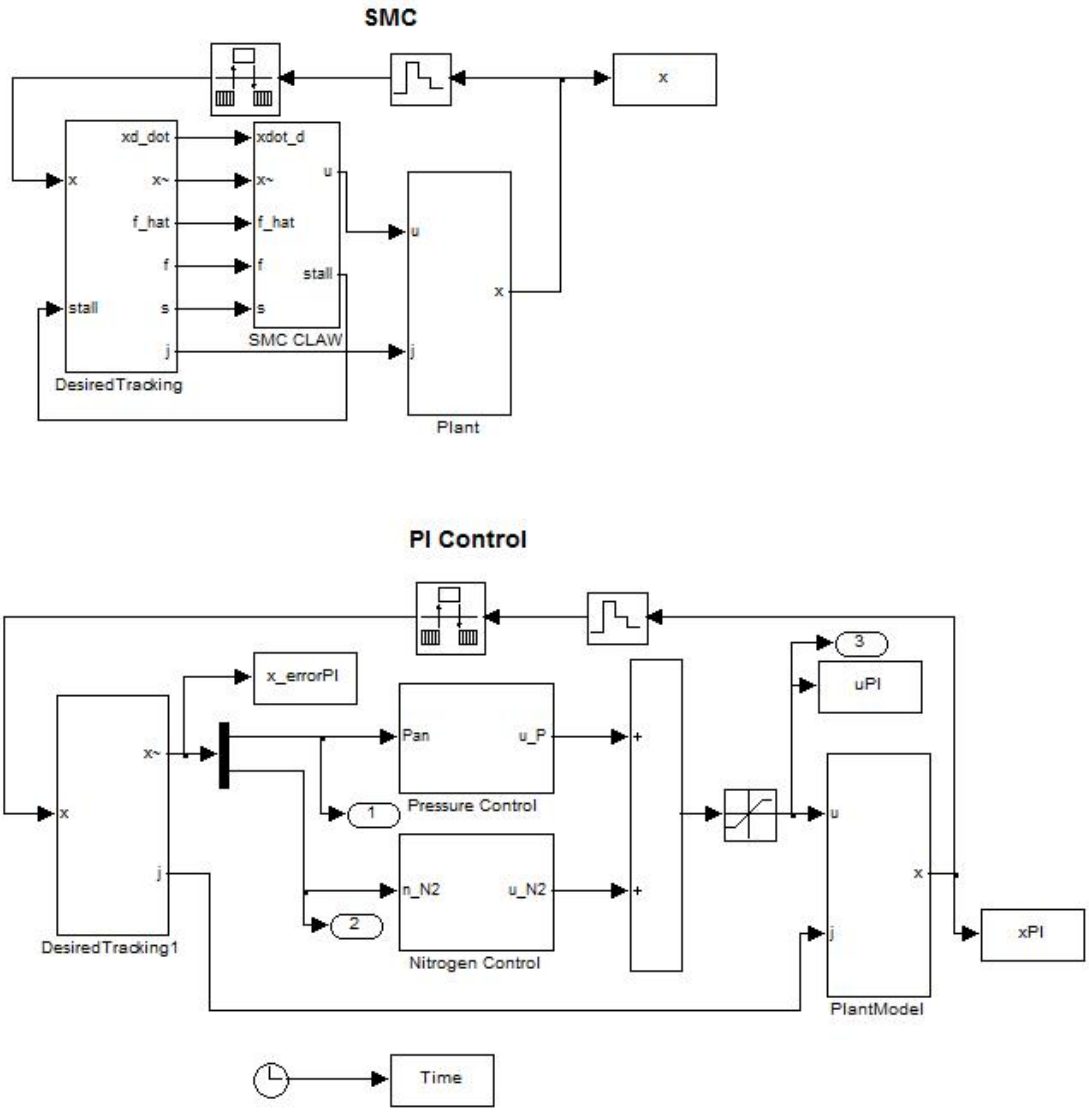

Figure B.2: Top Level Model

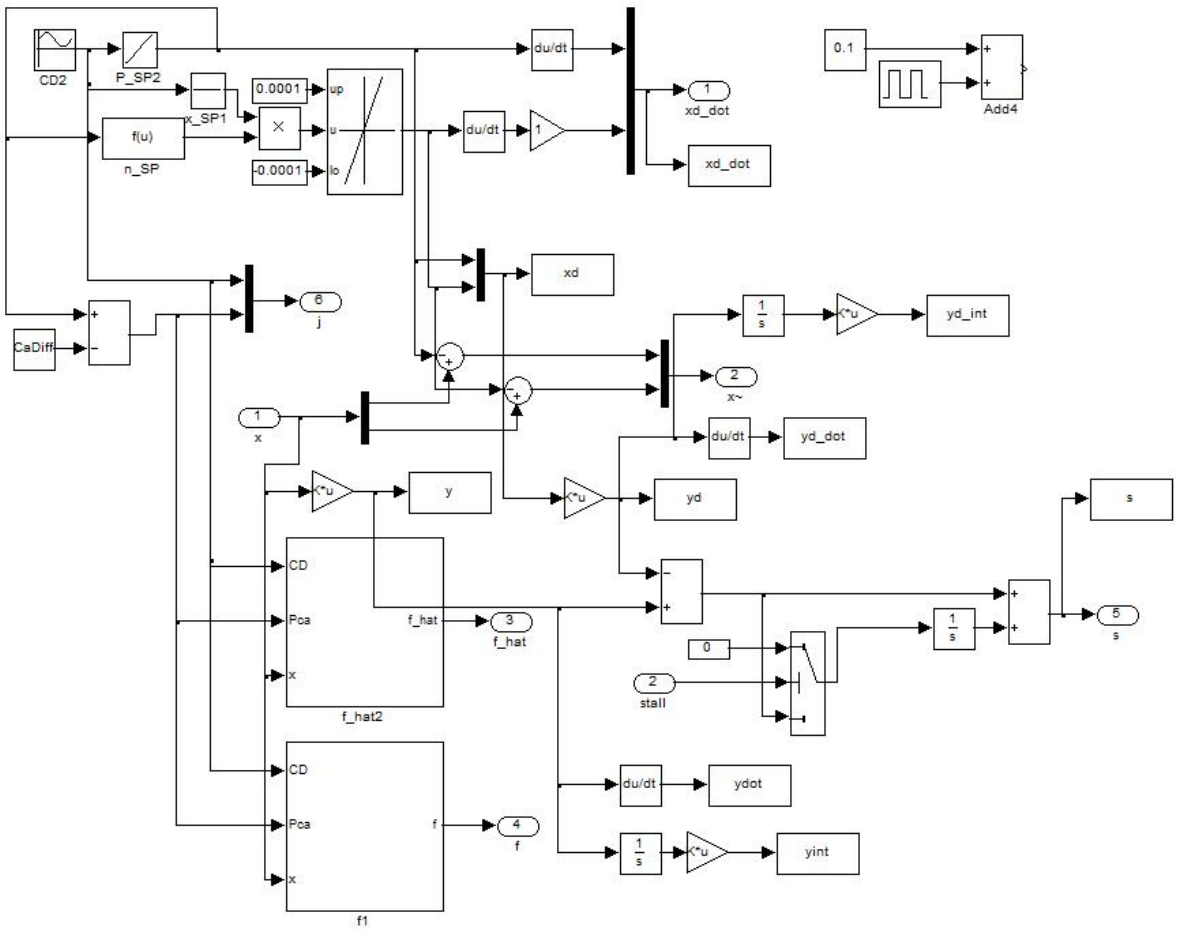

Figure B.3: Desired Tracking Block

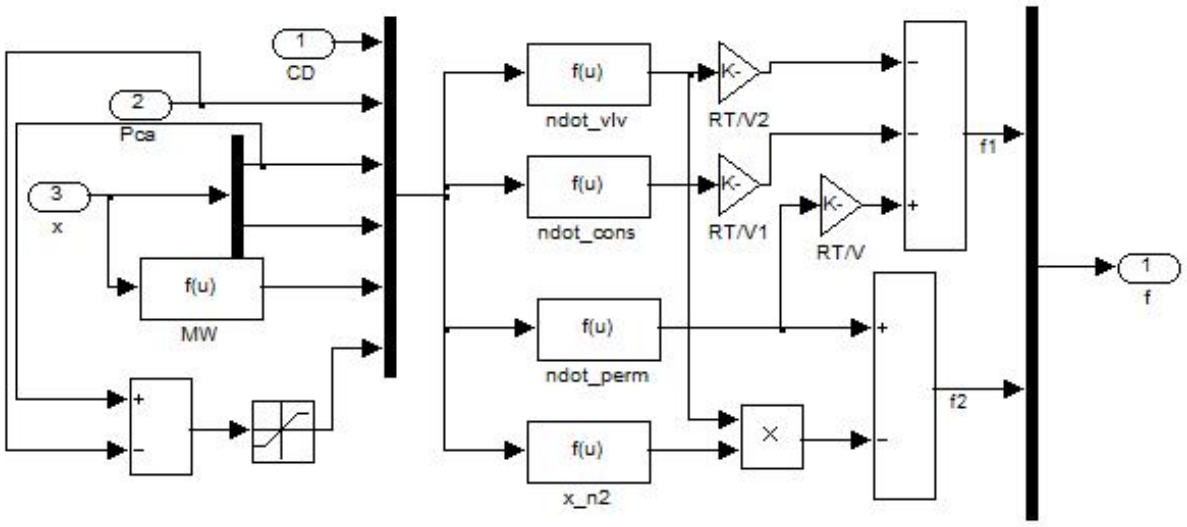

Figure B.4: Simulink Representation of Nonlinear Terms

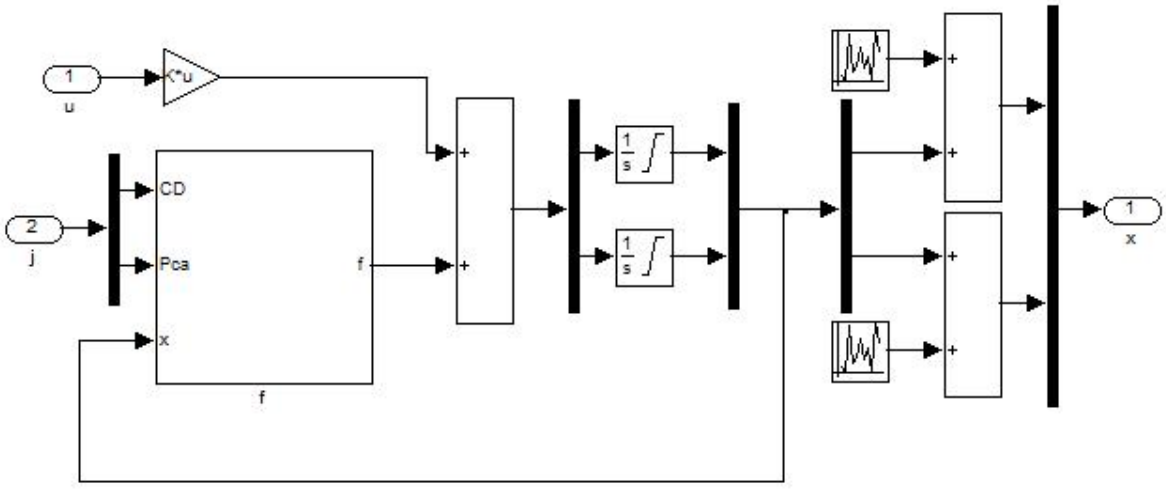

Figure B.5: Plant Model Block Diagram

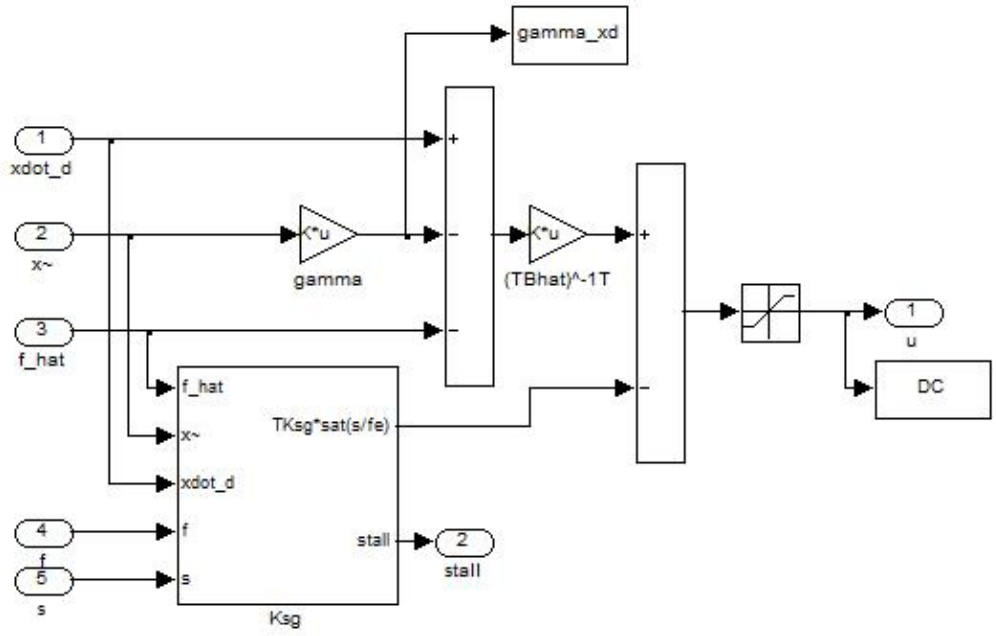

Figure B.6: SMC Block Diagram

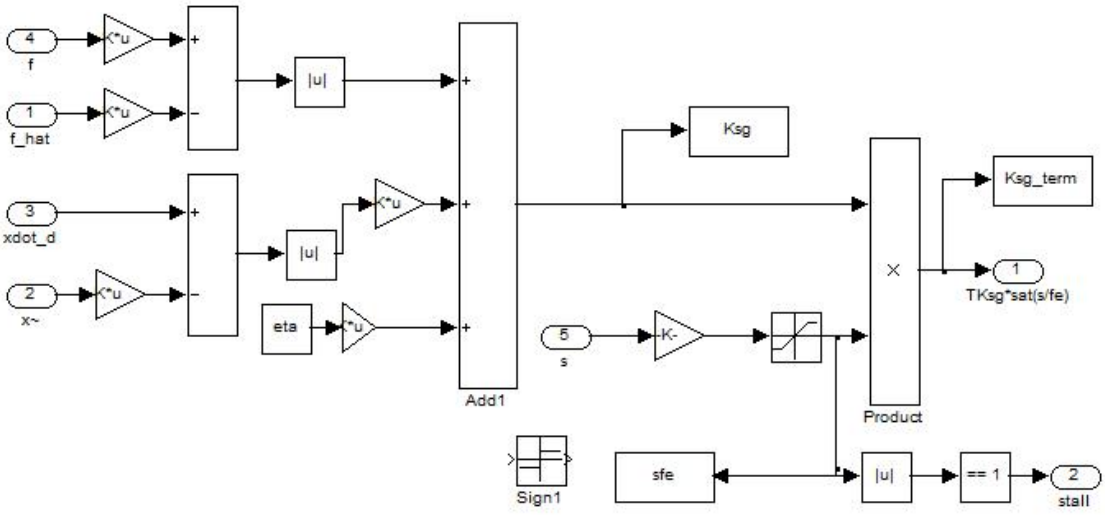

Figure B.7: Robustness Term Block Diagram